LUND UNIVERSITY

Single-Proton Irradiation of Living Cells - Development of New Tools for Low-Dose Radiation Research

Arteaga, Natalia

2010

Thesis for the Degree of Doctor of Philosophy in Engineering

Single-Proton Irradiation of Living Cells

Development of New Tools for Low-Dose Radiation Research

Natalia Arteaga Marrero

Lunds universitet
Lunds Tekniska Högskola

Division of Nuclear Physics
Department of Physics

2010

Organization LUND UNIVERSITY Department of Physics PO Box 118 SE-221 00 Lund Sweden	Document name DOCTORAL DISSERTATION Date of issue April 12, 2010 Sponsoring organization
Author(s) Natalia Arteaga Marrero	

Title and subtitle

Single-Proton Irradiation of Living Cells - Development of New Tools for Low-Dose Radiation Research

Abstract

A Single-Ion Hit Facility (SIHF) consists of a custom-build facility based in particle accelerators which offers irradiation controlling the number of delivered particles with a precise targeting localization. The irradiation spot can be confined down to the nanometre scale allowing the irradiation of subcellular compartments with a single particle. Therefore, these facilities have become a very powerful tool for biological applications specifically to study low-dose radiation effects on living cells.

A SIHF has been created at the Lund Nuclear Microprobe (LNM-SIHF) and, in order to make it operational, several tools were fabricated. These tools included the necessary software for cell recognition, custom-designed Petri-type dishes suitable for cell culture and irradiation, and other tools which allow the evaluation of the system. Additionally, the importance of reactive oxygen species (ROS) in bystander cells after non-targeted proton irradiation was investigated on the human hepatoma cell line (HepG2).

In-house implemented software, SeACell, provides on-line cell recognition and localization in a short time and high efficiency without the use of cell-staining dyes. The program was developed using IDL 6.2 language, and includes automated and manual targeting selection through a user-friendly interface. In addition, table colour display and filter drop-down menus were added to improve the quality of the input image if required.

Custom-designed irradiation dishes permit controlling the cells growth position by confining them through limiting structures on the floor of the dish and therefore, facilitating repeated access to the cell position. The epoxy-based photopolymer SU-8 was patterned by UV lithography technique producing irradiation dishes, with a supporting layer of approximately 5 microns thick where 5 microns height walls were used to form the limiting structure. The entire structure contains 400 squares that can be located by a row letter and column number printed outside the grid.

Other tools were manufactured by UV large exposure and the SU-8 photoresist: an artificial cell sample, which offered a semi-realistic scenario to test the system's capability, and a calibration sample used to establish the coordinates of the irradiation point in all the microscopes in which the cells were inspected. Also, two Ni dot arrays were fabricated using electron beam lithography to test the targeting accuracy of the system.

Key words: Single-Ion Hit Facility, low-dose, cell irradiation, cell recognition, SU-8, lithography, UVL, EBL, SeACell, human hepatoma cells (HepG2), bystander effect, reactive oxygen species (ROS)

Classification system and/or index termes (if any):

Supplementary bibliographical information:		Language English
ISSN and key title:		ISBN 978-91-628-8088-0
Recipient's notes	Number of pages 133	Price
	Security classification	

Thesis for the Degree of Doctor of Philosophy in Engineering

Single-Proton Irradiation of Living Cells

Development of New Tools for Low-Dose Radiation Research

Natalia Arteaga Marrero

Division of Nuclear Physics
LTH, Lund University
Sweden
2010

Faculty Opponent: Professor Philippe Moretto
Centre d'Etudes Nucléaires de Bordeaux Gradignan, Gradignan, France

Academic dissertation which, by due permission of the Faculty of Engineering at Lund University, will be publicly defended on Friday, the 21^{st} of May 2010, at 10.15 in lecture hall B, at the Department of Physics, Sölvegatan 14A, Lund.

Single-Proton Irradiation of Living Cells
Development of New Tools for Low-Dose Radiation Research

Printed in Sweden by Mediatryck, Lund, 2010

Division of Nuclear Physics
Department of Physics
Lund University
PO Box 118
SE-221 00 Lund
Sweden

ISBN 978-91-628-8088-0
ISRN LUTFD2/(TFKF-1039)/1 - 133/(2010)

The picture on the front cover shows the oxidation produced by non-targeted proton irradiation on human hepatoma cells.

To my family

Never give up, never surrender!

List of Publications

This thesis is based on the following peer-reviewed publications and submitted manuscripts, which are appended at the end of this thesis. The author′s contribution is described below each article.

Paper I: **The New Cell Irradiation Facility at the Lund Nuclear Probe**
N. Arteaga-Marrero, J. Pallon, M.G. Olsson, V. Auzelyte, M. Elfman, P. Kristiansson, K. Malmqvist, C. Nilsson and M. Wegdén.
Nuclear Instruments and Methods in Physics Research B **260** (2007) 91. Proceedings of the 10^{th} International Conference on Nuclear Microprobe Technology and Applications.

The design of the experimental part, the data acquisition, software development, data analysis and manuscript writing were performed by the author.

Paper II: **A SU-8 Dish for Cell Irradiation**
N. Arteaga-Marrero, V. Auzelyte, M.G. Olsson and J. Pallon.
Nuclear Instruments and Methods in Physics Research B **263** (2007) 523.

The design of the dish and the experimental part, sample preparation and evaluation, data acquisition and manuscript writing were performed by the author.

Paper III: **Applications of SU-8 in the Development of a Single-Ion Hit Facility**
N. Arteaga-Marrero, G. Astromskas, M.G. Olsson, M. Elfman, P. Kristiansson, C. Nilsson, E.J.C. Nilsson and J. Pallon.
Nuclear Instruments and Methods in Physics Research B **267** (2009) 2117. Proceedings of the 11^{th} International Conference on Nuclear Microprobe Technology and Applications.

The preparation and fabrication of the samples, data acquisition and

analysis, and manuscript writing were performed by the author.

Paper IV: **SeACell: Cell Recognition Software for a Single-Ion Hit Facility**
N. Arteaga-Marrero, M.G. Olsson, P. Kristiansson and J. Pallon.
Submitted to Review of Scientific Instruments

The software implementation, testing, data acquisition and analysis, and manuscript writing were performed by the author.

Paper V: **Oxidative Effects Studies and Updated Technical Description of the Lund Nuclear Microprobe Single-Ion Hit Facility**
N. Arteaga-Marrero, P. Kristiansson, M.G. Olsson, S. Rutardóttir, C. Nilsson, J. Pallon and Bo Åkerström
Manuscript

The data acquisition and analysis as well as the manuscript writing were performed by the author.

Related publications not included in this thesis

Peer-reviewed International Scientific Journals

1. ***A pre-sample charge measurement system for quantitative NMP-analysis***

   P. Kristiansson, M. Borysiuk, N. Arteaga-Marrero, M. Elfman, E.J.C. Nilsson, C. Nilsson and J. Pallon.
   Nuclear Instruments and Methods in Physics Research B - Article in Press doi:10.1016/j.nimb.2010.02.119.
   Proceedings of the 19^{th} International Conference on Ion Beam Analysis.

2. ***At the Tip of an MeV Beam: Provoking Cells and Performing Tomographic Imaging***

   J. Pallon, N. Arteaga-Marrero, Ch. Nilsson, M. Elfman, P. Kristiansson, C. Nilsson, M. Wegdén, M.G. Olsson and B. Åkerström.
   Acta Physica Polonica A **115** (2009) 501.
   Proceedings of the 42^{nd} Zakopane School of Physics International Symposium Breaking Frontiers.

3. ***Using microdispensing to manufacture a customized cell dish for microbeam irradiation of single, living cells***

   E.J.C. Nilsson, M.G. Olsson, J. Nilsson, J. Pallon, A. Masternak, J. Paczesny, N. Arteaga-Marrero, M. Elfman, P. Kristiansson, C. Nilsson and B. Åkerström.
   Nuclear Instruments and Methods in Physics Research B **267** (2009) 1199.

4. ***STIM evaluation in GeoPIXE II to complement quantitative dynamical analysis***

   J. Pallon, C.G. Ryan, N. Arteaga Marrero, M. Elfman, P. Kristiansson, E.J.C. Nilsson and C. Nilsson.
   Nuclear Instruments and Methods in Physics Research B **267** (2009) 2080.
   Proceedings of the 11^{th} International Conference on Nuclear Microprobe Technology and Applications.

5. ***First results from the LNM particle detector system***

   P. Golubev, P. Kristiansson, N. Arteaga-Marrero, M. Elfman, K. Malmqvist, E.J.C. Nilsson, C. Nilsson, J. Pallon and M. Wegdén.
   Nuclear Instruments and Methods in Physics Research B **267** (2009) 2065.
   Proceedings of the 11^{th} International Conference on Nuclear Microprobe Technology and Applications.

6. ***Characterization of a pre-cell hit detector to be used in single-cell irradiation experiments at the Lund Nuclear Microprobe***

   E.J.C. Nilsson, J. Pallon, G. Thungström, N. Arteaga Marrero, M. Elfman, P. Kristiansson, C. Nilsson and M. Wegdén.
   Nuclear Instruments and Methods in Physics Research B **266** (2008) 4808.

7. ***Symbiotic fungi that are essential for plant nutrient uptake investigated with NMP***

   J. Pallon, H. Wallander, E. Hammer, N. Arteaga Marrero, V. Auzelyte, M. Elfman, P. Kristiansson, C. Nilsson, P.A. Olsson and M. Wegdén.
   Nuclear Instruments and Methods in Physics Research B **260** (2007) 149.
   Proceedings of the 10^{th} International Conference on Nuclear Microprobe Technology and Applications.

8. ***Exposure parameters for MeV proton beam writing on SU-8***

   V. Auzelyte, M. Elfman, P. Kristiansson, C. Nilsson, J. Pallon, N. Arteaga-Marrero and M. Wegdén.
   Microelectronic Engineering **83** (2006) 2015.

9. ***Development of a microtomography system at the Lund sub-micron beamline***

   M. Wegdén, M. Elfman, P. Kristiansson, N. Arteaga-Marrero, V. Auzelyte, K. G. Malmqvist, C. Nilsson and J. Pallon.
   Nuclear Instruments and Methods in Physics Research B **249** (2006) 756.
   Proceedings of the 17^{th} International Conference on Ion Beam Analysis.

10. ***On-line measurement of proton beam current in the pA range***

    V. Auzelyte, F. Andersson, M. Elfman, P. Kristiansson, J. Pallon, M. Wegdén, C. Nilsson and N. Arteaga-Marrero.
    Nuclear Instruments and Methods in Physics Research B **249** (2006) 760.
    Proceedings of the 17^{th} International Conference on Ion Beam Analysis.

11. ***Evaluation of a pre-cell hit detector for the future single ion hit facility in Lund***

    Ch. Nilsson, J. Pallon, G. Thungström, N. Arteaga, V. Auzelyte, M. Elfman, P. Kristiansson, C. Nilsson and M. Wegdén.
    Nuclear Instruments and Methods in Physics Research B **249** (2006) 924.
    Proceedings of the 17^{th} International Conference on Ion Beam Analysis.

Conference abstracts

1. ***Status of the Single Ion Hit Facility at the Lund Nuclear Microprobe***

   N. Arteaga-Marrero, M.G. Olsson, M. Elfman, P. Kristiansson, C. Nilsson, E.J.C. Nilsson and J. Pallon.
   Proceedings of the 11^{th} International Conference on Nuclear Microprobe Technology and Applications.
   Debrecen (Hungary), 2008. *Oral presentation.*

2. ***Oxidative effects related to proton irradiation of a Hepatoma cell line***

   N. Arteaga-Marrero, M.G. Olsson, J. Pallon, M. Elfman, P. Kristiansson, Ch. Nilsson, C. Nilsson and M. Wegdén.
   Proceedings of the 13^{th} International Congress of Radiation Research.
   San Francisco (EEUU), 2007. *Poster presentation.*

3. ***Development of the Lund irradiation facility at the new submicrometer beamline***

   N. Arteaga-Marrero, J. Pallon, V. Auzelyte, M. Elfman, P. Kristiansson, K. Malmqvist, C. Nilsson and M. Wegdén.
   Radiation Research **166**(4)(2006) 655
   Proceedings of the 7^{th} International Workshop: Microbeam Probes of Cellular Radiation Response. New York (EEUU), 2006. *Oral and poster presentation.*

4. ***Single proton irradiation of living cells at the new Lund sub-micron beamline***

   N. Arteaga-Marrero, J. Pallon, J. Christensson, V. Auzelyte, M. Elfman,P. Kristiansson, K. Malmqvist, C. Nilsson and M. Wegdén.
   Proceedings of the 14^{th} International Symposium on Microdosimetry.
   Venice (Italy), 2005. *Poster presentation.*

5. ***First tests on single-hit cell detection at the new Lund sub-micron beamline***

   N. Arteaga-Marrero, J. Christensson, J. Pallon, V. Auzelyte, M. Elfman, P. Kristiansson, K. Malmqvist, C. Nilsson and M. Wegdén.
   Proceedings of the 17^{th} International Conference on Ion Beam Analysis.
   Seville (Spain), 2005. *Poster presentation.*

Abbreviations

A1M	α_1-microglobulin
BMC	*Bio-Medical Centre*
CAMAC	Computer Automated Measurement And Control
CENBG	*Centre d'Etudes Nucleaires de Bordeaux-Gradignan*
CM UJ	*Jagiellonian University, Medical College*
DAC	Digital-to-Analogue Converter
DSB	Double Strand Break
EBL	Electron Beam Lithography
FFT	Fast Fourier Transform
FI/FO	Fan-in-/-Fan-out
GBL	Gamma-ButyroLactone
GCI	*Gray Cancer Institute*
GJIC	Gap Junctions-mediated Intercellular Communication
GSI	*Gesellschaft für Schwerionenforschung*
HepG2	Human Hepatoma cell line
HRR	Homologous Recombination Repair
HRS	Hypersensitivity
ICRP	International Commission on Radiation Protection
IFJ PAN	*Institute of Nuclear Physics, Polish Academy of Sciences*
INFN	*Istituto Nazionale di Fisica Nucleare*
IRR	Increased radioresistance
LET	Linear Energy Transfer
LNP	Lund Nuclear Probe
LTH	*The Engineering Faculty of Lund University (Lunds Tekniska Högskola)*
MEMS	Micro-Electro-Mechanical System
MIBK	Methyl Iso-Butyl Ketone
NHEJ	Non-Homologous End Joining
NO	Nitric oxide
OER	Oxygen Enhancement Ratio
PDMS	Polydimethylsiloxane
PFT-α	Pifithrin-α
PGMEA	Propylene Glycol Methyl Ether Acetate
PI	Propidium Iodine
PIXE	Particle-Induced X-ray Emission
PMMA	Polymethyl Methacrylate
PMT	Photomultiplier tube
RBE	Relative Biologic Effectiveness

RF	Radio Frequency
RIBE	radiation-induced bystander effect
ROS	Reactive Oxygen Species
SIHF	Single-Ion Hit Facility
SSB	Single Strand Break
STIM	Scanning Transmission Ion Microscopy
SRIM	Stopping and Range of Ions in Matter
TA	Targeting Accuracy
TTL	Transistor-Transistor Logic
UVL	UltraViolet Lithography
W_R	Radiation Weighting factor
W_T	Tissue Weighting factor

Contents

1

Introduction

1.1 Cancer therapy

The objective of radiation therapy is to concentrate the radiation damage in the carcinogenic tissue producing as little damage as possible to surrounding healthy tissue, as well as to minimize the exposure of the patient to radiation.

Initially, the requirement for deep penetration was fulfilled by low-Linear Energy Transfer (LET) radiation (photons), and the risk of damaging healthy tissue was accepted. However, the search for a better form of ionization was aided by the early recognition that X-rays could produce local tumour control in some patients, although not in others [1].

Charged particles (protons, α particles and heavy ions) were introduced because of their superiority regarding physical dose distribution, as they do not suffer from scattering or attenuation problems [2]. High-LET radiation presents a characteristic inverse depth dose profile which minimizes the dose to surrounding normal tissue. Therefore, the high dose region is precisely confined to the tumour volume. The dose deposited by a beam of monoenergetic charged particles increases slowly with depth, but reaches a sharp maximum near the end of the particles' range, called the Bragg peak. The depth at which the Bragg peak occurs depends on the energy of the incoming particles.

Charged particle beams have sharp edges with little lateral scattering. Heavy ions have less lateral scattering than protons, leading to sharper beam edges. However, heavy ions do not share the advantage of protons that the dose stops sharply at the end of the range of the primary particle, i.e., the dose falls to zero after the Bragg peak. Furthermore, the Relative Biologic Effectiveness (RBE) is larger for heavier ions [3], but the correct value of the RBE is difficult to estimate since the data are derived from *in vitro* or animal experiments.

High-LET radiation has a very short range in matter. For instance, the range in tissue of proton beams with energies of 150 to 200 MeV is 16 to 26 cm. Therefore, its application may be limited to superficial tumours. Recently, protons have been used to treat ocular and also some specialised tumours close to the spinal cord [1].

The ability to produce sufficiently penetrating beams for the treatment of any cancer has led to current interest in the development of hospital-based proton facilities. The use of protons for broad-beam radiotherapy is being tested, but no

advantages have yet been demonstrated in controlled clinical trials [1].

1.2 Low-dose radiation risk

Conventionally, hereditary biological effects require direct damage to the DNA helix. Therefore, in order to estimate low-dose radiation risks a "Linear No-Threshold" (LNT) model is assumed since no radiation risk data are available. The model consists of a linear extrapolation, from the known risks at higher doses, to zero-effect at zero-dose [4].

The use of microprobes for cell irradiation started in 1953 [5] and, with the time, has led to the development of Single-Ion Hit Facilities (SIHFs) where it is possible to perform biological studies at low doses. The main advantage of using a SIHF relies on the fact that a precise number of ions can be delivered to individual living cells, thus the lower limit of the applied dose is a single ion. Additionally, the spatial dose distribution is confined to the ion beam size, providing the possibility to target subcellular compartments.

The use of these precise tools has revealed the existence of new effects, called non-targeted effects, characterized by a deviation of many cell lines from the standard linear quadratic responses at low doses [6]. Therefore, the genotoxic risk may be significantly underestimated [7, 8] and the validity of the LNT model seriously questioned.

The non-targeted effect may play an important role regarding radiation damage at very low doses since the therapeutic benefits of cancer therapy may increase. It will be possibly to modify the response to radiation, of either the tumour or the healthy surrounding tissue, if the factor that triggers these effects and their mechanism of function are fully understood. Nowadays, the modulation of the Radiation-Induced Bystander Effect (RIBE) is possible since treatment with certain signalling proteins is known to enhance or diminish it. For instance, RIBE can be reduced by α_1-microglobulin (A1M) [9] or pifithrin-α (PFT-α) and increased by wortmannin [10].

However, the following key questions remain: Are the non-targeted effects important *in vivo*? How should the *in vitro* observations be extrapolated to *in vivo* systems?

1.3 Outline of this thesis

The work described in this thesis has led to the development of a Single-Ion Hit Facility at the Lund Nuclear Microprobe (LNM-SIHF). The Facility is intended for the study of the effects of low-dose radiation on living cells. The understanding of the real effects of low-dose radiation will be used for radiation protection purposes. In addition, new data will be obtained for the establishment of proton beam therapy as an alternative to radiation therapy.

The thesis is based on the work presented in Papers I to V. This work can be divided into a larger technical part, which is described in Papers I to IV, and a biological part, described in Paper V. The technical part includes the development of the system, which consists of a combination of projects describing the work carried out to provide the tools necessary to perform cell irradiation. The biological part presents the preliminary biological results achieved at the LNM-SIHF. This thesis summary is divided into ten main chapters, which provide the theoretical background and additional information necessary to understand the fabrication and function of the tools developed.

Paper I contains an early description of the facility. A detailed description of the system can be also found in Chapter 6.

Paper II describes the fabrication and utilization of a Petri-type dish suitable for cell culture and also for cell irradiation. This first tool developed for the LNM-SIHF provides cell positioning and position recognition. A more detailed description of the irradiation dish designed can be found in Chapter 8, Section 8.1.

Paper III is dedicated to the artificial cell sample and the Ni dot arrays. These custom-made tools were developed for the evaluation of the system regarding targeting accuracy and software function. Additional information about the tools can be found in Chapter 8, Sections 8.2 and 8.3.

Paper IV describes the in-house software implemented at the LNM-SIHF and also presents its applications. In addition, Paper I contains a preliminary description of the software. Details of the routines developed to locate the cells can be found in Chapter 7.

Paper V presents the preliminary results of the method employed, at the LNM-SIHF, for cell damage determination by a the study of the oxidative effects on bystander cells using a human hepatoma cell line. A detailed description of the study can be found in Chapter 9.

2

The interaction of ions with matter and their physical effects

2.1 Mechanisms of interaction between radiation and the absorbing material

2.1.1 Indirectly ionizing radiation

Photons (X-rays and γ-rays) are indirectly ionizing radiation, as are fast neutrons. Photons do not cause chemical and biological damage in the absorber but they give up their energy leading to the production of fast moving secondary electrons that are able to cause such damage. Fast neutrons produce protons, α particles, and heavier nuclear fragments instead.

Direct inelastic collisions with atomic electrons are not possible, since photons and neutrons are not charged, and their main interactions in matter are:

1. The photoelectric Effect: An atomic electron absorbs a photon and the electron is subsequently ejected from the atom. This effect is always exhibited by bound electrons with the nucleus absorbing the recoil momentum.

2. Compton Scattering: The incoming photon interacts with a "free" electron, after energy transfer, a less energetic photon is deflected from the original path and the "free" electron is converted into a fast electron. Both particles may take part in further interactions. At high energy (typically 0.5 MeV), Compton and photoelectric absorption processes occur, but the Compton process dominates.

3. Pair Production: This involves the transformation of a photon into an electron-positron pair. Thus, the photon must have at least an energy of $2mc^2$ or 1.022 MeV.

These reactions explain the two main features of this kind of radiation: the photon beam is very penetrating (more than α particles) and is not degraded in energy, but attenuated in intensity.

Neutrons

The principal means of interaction between neutrons and living tissue is through the strong force with nuclei. The main nuclear processes involved depend on the neutron energy:

- *Fast neutrons* (energies between a few tens of MeV and a few hundred keV): Elastic scattering from hydrogen is the dominant interaction process since hydrogen is the most abundant atom in tissue and its collision cross section is large. This interaction produces a relatively high-LET proton. Also, interaction with heavier nuclei, like oxygen, may occur and a high-LET α particle is produced as a spallation product. Inelastic scattering occurs for energies of about 1 MeV or more.

- *Epithermal neutrons* (energies between approximately 100 keV and 0.1 eV): The nuclear processes involved are radiative neutron capture and other nuclear reactions where fast recoil protons, α particles, and heavier nuclear fragments are emitted.

- *Thermal or slow neutrons* ($\sim$ 0.025 eV): Absorption can lead to fission. Also, α particles and γ-rays can be emitted.

2.1.2 Directly ionizing radiation

Charged particles (protons, α particles and heavy ions) passing through matter experience energy loss and deflection from their incident direction. These effects are due mainly to inelastic collisions with the atomic electrons of the material and elastic scattering from nuclei.

Inelastic collisions are statistical in nature and are directly responsible for the energy loss of heavy particles in matter. These collisions can produce only excitation (soft collisions) or ionization (hard collisions). The energy transferred in hard collisions generates high-energy recoil electrons, also called δ-rays, which can cause substantial secondary ionization. Therefore, the inelastic energy transfer triggers the emission of various kinds of secondary radiation: photons, X-rays, γ-rays and visible light, scattered and recoiled particles, nuclear reaction products and Auger electrons.

When using high-energy ions, secondary electrons can extend for many micrometres or even millimetres. Thus, the track can be considered as a core with a penumbra region. The core is defined by the maximum extension of the excitations caused by the ion, and is normally less than 10 nm [13]. The penumbra region is defined by the maximum extension of the secondary electrons. The spread of beam damage outside the core region is called the proximity effect.

The energy transferred by elastic scattering from nuclei is normally small, due to the mass difference. However, repeated elastic Coulomb scattering from nuclei results in a small angular deflection of the particle.

Other reactions that can occur are the emission of Cherenkov radiation, nuclear reactions and bremsstrahlung.

2.1.3 Stopping power

The average energy loss per unit path length, called the linear stopping power dE/dx, is the sum of two components: electronic and nuclear.

Electronic stopping power arises from electromagnetic interaction, between the incoming ion and the target electrons, resulting in electronic excitation and ionization. The electronic stopping increases with the ion energy until it reaches a maximum near the Bohr velocity (see Figure 2.1).

Nuclear stopping arises from collisions with the target nuclei, and causes atomic vibrations (phonons) and atomic displacements if the energy transferred exceeds the atom displacement threshold [15]. Atomic displacements can create a cascade of electronic collisions. The nuclear stopping varies with the ion velocity as well as the charge of the colliding atoms. It becomes important when an ion slow down to approximately the Bohr velocity, near the end of its track, since it can penetrate electron clouds. Nuclear stopping by light atoms is negligible because the Rutherford cross section and momentum transfer are small [15].

The stopping power is expressed by the quantum mechanical Bethe-Bloch formula (Eq. 2.1).

$$-\frac{dE}{dx} = 2\pi N_a r_e^2 m_e c^2 \rho \frac{Z}{A}\frac{z^2}{\beta^2}\left[ln\frac{2m_e\gamma^2 v^2 W_{max}}{I^2} - 2\beta^2 - \delta - 2\frac{C}{Z}\right] \qquad (2.1)$$

r_e: Classical electron radius
m_e: Electron mass
ρ: Density of absorbed material
N_a: Avogadros´s number
z: Charge of incident particle (e units)
β = v/c of incident particle
I: Mean excitation potential
$\gamma = 1/\sqrt{1-\beta^2}$
Z: Atomic number of absorbing material
δ: Density correction
A: Atomic weight of absorbing material
C: Shell correction
W_{max}: Maximum energy transfer in a single collision

For non-relativistic charged particles ($v \ll$ c), dE/dx is inversely proportional to the particle energy ($1/v^2$). In this case, the particle spends a greater time in the vicinity of a given electron and, therefore, the energy transfer is large. For different charged particles with the same velocity, dE/dx is proportional to the charge (z^2), thus the particles with the highest charge will have the greatest energy loss. Regarding the absorbing material, high atomic number and high density materials result in the greatest linear stopping power [12].

The Bethe-Bloch formula begins to fail at low particle energies when charge exchange between the particle and the absorbing material becomes important. The incoming particle (positively charged) will tend to pick up electrons from the absorbing material, reducing its charge, and consequently, its energy loss. At the end of its track the particle has accumulated z electrons and becomes a neutral atom [12].

Two corrections are normally added to this expression: the density effect correction δ and the shell C correction. The density effect is due to the electric field of the particle, which tends to polarize the atoms along its path. This polarization shields electrons far from the particle's path and therefore, collision with these electrons contributes less to the predicted total energy loss. This effect becomes more important as the particle energy increases.

The shell correction becomes significant when the velocity of the incoming particle is comparable to or smaller than the orbital velocity of the bound electrons and therefore, the assumption that the electron is stationary with respect to the incident particle is no longer valid.

Linear Energy Transfer (LET)

In nuclear physics, if Bremsstrahlung can be neglected, LET is defined as the linear stopping power dE/dx [keV/μm]. Therefore, the LET is the average energy deposited per unit path length. Figure 2.1 shows simulations from Stopping and Range of Ions in Matter (SRIM) 2008 [16], thus the dependence of the LET with respect to the energy of the incoming particles can be observed.

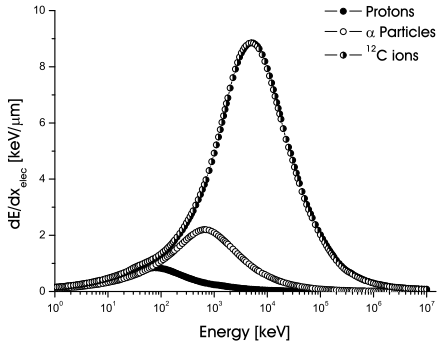

Figure 2.1: Simulations from SRIM 2008 where protons, α particles and ^{12}C ions traverse a water layer.

The Bragg curve

The Bragg curve shows the variation in dE/dx as a function of the penetration depth of the particle in matter. Figure 2.2 (a) shows the difference between heavy particles (^{12}C), α particles and protons. As can be seen, the particles are more ionizing towards the end of their path. This characteristic is very important in medical applications where a high dose of radiation is required in embedded tumours, causing minimum destruction to the overlying tissue.

The density of ionization depends on the energy deposited along the ion track, or the LET value [15]. It is greater for neutrons and heavy ions than for X- or γ-rays, and this accounts for the dramatic differences in the observed biological effects. As the density of ionization increases, the probability of a direct interaction between the particle and the target molecule increases. In addition, the density of ionization for a given type of particle or radiation decreases as the energy increases, as can be observed in Figure 2.2 (b).

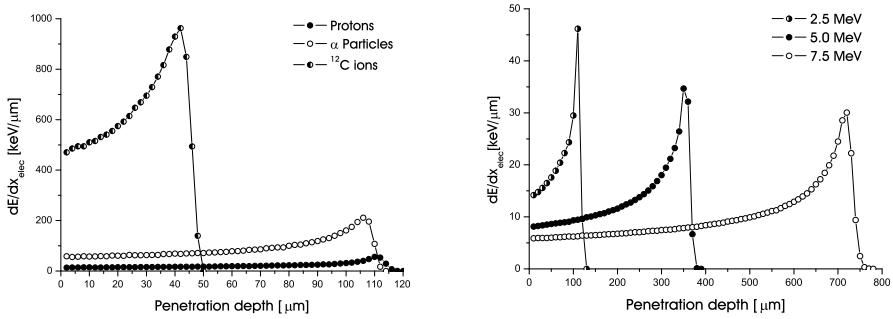

(a) (b)

Figure 2.2: Simulations from SRIM 2008 where a water layer is traversed by (a) protons, α particles and ^{12}C ions with an energy of 2.5 MeV/nucleon, i.e., the particles have the same velocity, and (b) protons of different energies.

2.1.4 Range

The range is defined as the distance that a charged particle can travel within a certain material before losing all its energy. The range depends on the incident material, the incoming particle and its energy.

To a first approximation, the range straggling follows a Gaussian distribution due to the statistical nature of the energy loss. The mean value of this distribution is known as the mean range.

High-LET radiation has a short range in matter as most of the energy is rapidly dissipated in collisions. Typical high LET values are above 100 keV/μm and the corresponding ranges are between 0.1 and 1.0 mm. Heavy ions, α particles and protons are considered to be forms of high-LET radiation.

Low LET values are defined, by the International Commission on Radiation Protection (ICRP), as below 10 keV/μm [2], and the corresponding ranges are of the order of centimetres. Electrons and photons are considered low-LET radiation.

3

Lithography

Lithography is the process of transferring patterns on a mask to a thin layer of radiation-sensitive material. Normally, the radiation-sensitive material covers the surface of a semiconductor wafer or an optical glass. The pattern is transferred by an etching process that selectively removes unmasked portions of the radiation-sensitive layer [17].

3.1 Photoresist

A photoresist is a radiation-sensitive compound normally classified according to its radiation response. Figure 3.1 shows the differences between a positive and a negative photoresist.

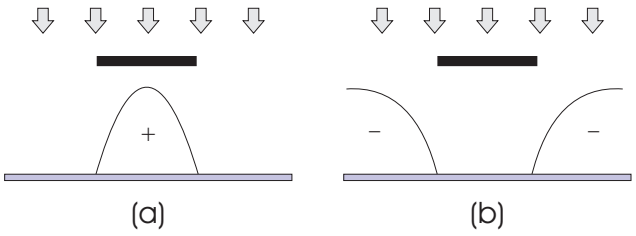

Figure 3.1: Cross section of the resist image after development. (a) Positive photoresist, (b) negative photoresist.

3.1.1 Positive photoresists

Positive photoresists are made of three components: a photosensitive compound, a base resin and an organic solvent. The chemical structure of the exposed regions of the photosensitive compound is changed and becomes soluble in the developing solution. The exposed areas are easily removed, creating a replica of the pattern on the mask in the resist.

PMMA A6 950

PMMA (polymethyl methacrylate) A6 950 is a positive photoresist. PMMA was designed to provide high contrast and high resolution for direct-write e-beam, deep UV (220 - 250 nm) and X-ray lithographic processes. In addition, PMMA is often used as a protective layer for wafer thinning applications, as a bonding adhesive and as a sacrificial layer [18].

3.1.2 Negative photoresists

Negative photoresists are polymers combined with a photosensitive compound. Exposure causes cross linking of the polymer molecules making the polymer insoluble in the developing solution. The unexposed regions are removed, creating a pattern in the resist which is the reverse of the one on the mask. The major drawback of negative photoresists is that during the development process, the mass of the resist may increase due to absorption of the developer solvent, limiting the resolution of the resist.

SU-8

SU-8 is a negative epoxy-based photoresist. The term epoxy refers to the bridge structure formed by an oxygen atom bound to two other atoms. SU-8 has the highest epoxy functionality commercially available, providing a high-sensitivity material with excellent adhesion. SU-8 has several advantages including its low molecular weight providing high contrast and excellent solubility in a large variety of organics solvents, e.g. propylene glycol methyl ether acetate (PGMEA), gamma-butyrolactone (GBL), and methyl iso-butyl ketone (MIBK) [19]. SU-8 also has a very high optical transmission, above 360 nm, it is thermally and chemically stable due to the highly cross-linked matrix and, in addition, is a biocompatible material. Very high aspect ratio structures can be made, with thicknesses up to 200 μm with a single spin coating. SU-8 is suitable for micromachining and other micro-electro-mechanical (MEM) applications [18].

3.2 UV lithography

The pattern can be transferred using lithographic exposure which, in the case of optical lithography, normally involves the use of ultraviolet light. There are two optical exposure methods: shadow and projection printing. A schematic of these methods can be seen in Figure 3.2.

Shadow printing

The mask and the resist-coated wafer are in contact or in close proximity. This technique provides a resolution of ~ 1 μm. However, the major drawback is that

dust particles can cause permanent damage to the mask and defects in the wafer after exposure [17].

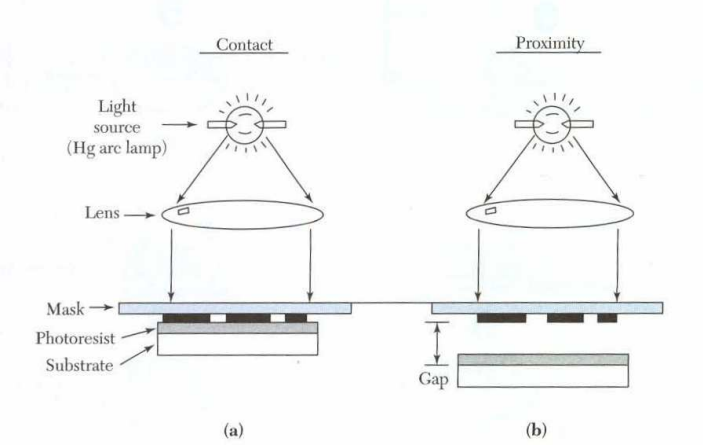

Figure 3.2: Schematic of optical shadow printing techniques [17]: (a) contact printing, (b) proximity printing.

Projection printing

The mask and the resist-coated wafer are separated by a few microns (10 to 50). This protects the mask from damage but produces optical diffraction in the edge features of the mask. Consequently, the resolution is reduced to the range of 2 - 5 μm and the minimum line-width or critical dimension (CD) is given by the expression:

$$CD \cong \sqrt{\lambda \cdot g}$$

where λ is the wavelength of the UV light and g is the separation between the mask and the wafer, including the resist thickness [17]. The minimum line-width can be improved by decreasing the wavelength or the gap. Nevertheless, dust particles whose diameter is larger than g can still damage the mask. Thus, a more advanced system is used where the mask image is projected onto the resist-coated wafer by means of electrostatic lenses.

3.3 Electron beam lithography

Electron Beam Lithography (EBL) is the most mature direct writing technique available, i.e., direct patterning without the use of a mask. However, due to its high cost and low throughput, the primary use of EBL is photomask production [20].

In optical lithography, the resolution is limited by light diffraction. However, in EBL, the minimum separation between the pattern features is limited by the proximity effect, since electron scattering (forward and backward) at the resist-substrate interface produces damage in the neighbouring areas. Therefore, high-energy light ions are preferable for local material modification, since the minimum damaging dose is deposited within a shorter distance of the ion track [15].

The work described in this thesis includes the application of UV lithography and EBL techniques. The epoxy-based photopolymer SU-8, patterned by UV lithography was used to produce custom-made irradiation dishes and other including an artificial cell sample and a calibration sample. Also, two Ni dot arrays were created mainly by EBL.

Details concerning sample fabrication and their applications can be found in *Paper II* and *Paper III*.

4

Radiation parameters

An elaborate set of definitions for standardizing the energy absorption by different materials exposed to ionizing radiation has been produced by the ICRP, based on the assumption of linearity between dose and risk.

4.1 Absorbed dose

Dose is defined as the energy absorbed [J] per unit mass [kg]. The SI unit for dose is the Gray [Gy]. The dose unit used in the past, was the radiation absorbed dose [rad], defined as an energy absorption of 100 erg/g. Consequently, 1 Gy is equivalent to 100 rad.

4.1.1 Low dose threshold

The low dose threshold of relevance to radiation risk analysis has been set by the ICRP at 0.2 Gy [21, 22]. However, several threshold values can be found in the literature, where low dose and very low dose are differentiated [23].

4.2 Relative biologic effectiveness

Since equal doses of different types of radiation do not produce the same biologic effects, the RBE was introduced. This is defined as the ratio of the dose of a certain kind of radiation to that of a dose of X-rays that produces the same biological effect. RBE is determined by the following factors:

- Radiation quality (LET): Type of radiation and energy.
- Radiation dose and dose per fraction: The shape of the dose-response relationship varies with the radiation LET. Generally, RBE increases as the dose is decreased thus, the RBE for a fractionated regimen of a specific kind of radiation is greater than for single doses.

- Dose rate: The dose-response curve, for sparsely ionizing radiation, varies critically with the dose rate. In contrast, the biological response to densely ionizing radiation depends little on the rate at which the radiation is delivered.

- Biological system or endpoint: RBE varies greatly according to the tissue for a given total dose or dose per fraction. In general, RBE values are high for tissues that accumulate and repair a great deal of sublethal damage, and low for those that do not.

4.2.1 RBE as a function of linear energy transfer

The most biologically effective LET is that at which the average separation of ionizing events coincides with the diameter of the DNA double helix (2 nm) [1]. Figure 4.1 shows the variation of RBE with the LET, showing a maximum for an LET value of 100 keV/μm. Therefore, the passage of a single charged particle has a high probability of causing a double-strand break. Kinds of radiation with this optimal LET include neutrons of a few hundred keV, low-energy protons and α particles.

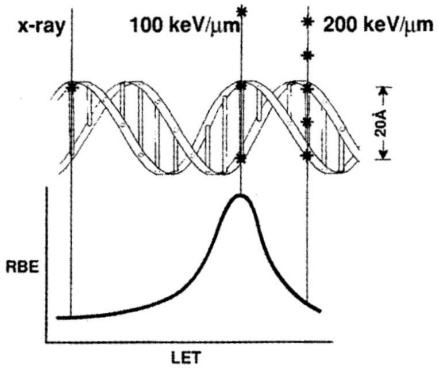

Figure 4.1: Variation of the RBE with the LET [1].

The probability of producing a double strand break (DSB), in a single track, is low for sparsely ionizing radiation. Therefore, lower biological effectiveness is observed (see Figure 4.1). At the other extreme, for more densely ionizing radiation (LET $\sim$ 200 keV/μm), DSBs are readily produced. However, the ionizing events are too close together and the energy is "wasted". Since RBE is the ratio of two doses producing the same biologic effect, the more densely ionizing radiation has a lower RBE than the optimal LET radiation, i.e., the radiation is more effective per track, but less effective per unit dose.

4.3 Radiation weighting factor

It is difficult to measure the RBE, therefore, the dimensionless parameter radiation weighting factor W_R was introduced to place the biological effects resulting from exposure to different types of radiation on a common scale. The W_R is calculated for a given type of radiation according to the energy deposited per unit path length. Radiation weighting factors are defined by the ICRP, and typical values are shown in Table 4.1.

Table 4.1: Radiation weighting factors [1, 14]

Radiation type and energy range	***Radiation Weighting Factor W_R***
Photons (X-rays, γ-rays) Electrons	1
Low energy protons	2
Energetic protons ($>$ 2 MeV)	5
α particles Fission fragments Heavy nuclei	20
Neutrons	A continuous curve is recommended with a maximum of 20 for the most effective ones ($>$ 100 keV to 2 MeV)

4.4 Equivalent dose

The equivalent dose is a normalized measure of the biological effect caused by radiation to a tissue or organ. It is obtained as follows:

$$Equivalent\ dose = Absorbed\ dose \times Radiation\ weighting\ factor$$

If the absorbed dose is measured in gray [Gy], the equivalent dose is given in sievert [Sv]. If the absorbed dose is expressed in rads, the equivalent dose is roentgen equivalent man [rem].

The equivalent dose for a combination of different kinds of radiation, is the sum of the individual doses of the various types of radiation, each multiplied by the appropriate radiation weighting factor.

4.5 Effective dose

The effective dose is the sum of all the weighted equivalent doses in all the tissues or organs irradiated. Some organs are particularly sensitive to radiation, and sometimes the equivalent doses differ substantially due to the variation in sensitivity to radiation-induced stochastic effects (cancer and hereditary effects). The

tissue weighting factor (W_T) represents the relative contribution of each tissue or organ to the total damage resulting from uniform irradiation of the whole body. Consequently,

$$Effective\ dose = \sum absorbed\ dose \times W_R \times W_T$$

Effective dose is in principle, as well as in practice, a non-measurable quantity.

4.6 The oxygen effect

Highly oxygenated tissues exhibit an unexpectedly high sensitivity to radiation. The destruction of a certain fraction of cells in tissue with a lack of oxygen requires a larger dose (D_2) than the dose (D_1) needed in healthy, oxygenated tissue. The ratio $D_2 : D_1$ for a particular kind of radiation is called the Oxygen Enhancement Ratio (OER). Consequently, a smaller OER is desirable since smaller doses are required to produce the same effect.

This property can be explained by the fact that if the material is rich in oxygen, the free radical $R\cdot$, produced by the ionizing radiation, can start a chain reaction:

$$R\cdot + O_2 \rightarrow RO_2\cdot \tag{4.1}$$

$$RO_2\cdot + RH \rightarrow RO_2H + R\cdot \tag{4.2}$$

An alternative series of chemical reactions can be initiated by the high electron affinity of O_2

$$O_2 + e^- \rightarrow O_2^- \tag{4.3}$$

This radiation damage cannot be healed since the electron cannot be recaptured by the original ions produced by the interaction.

Neutrons have a lower OER since they do not interact through Coulomb effects and therefore, they are less sensitive to the presence of higher-Z atoms. Additionally, there is little or no repair of sublethal damage and less variation in sensitivity through the cell cycle [1].

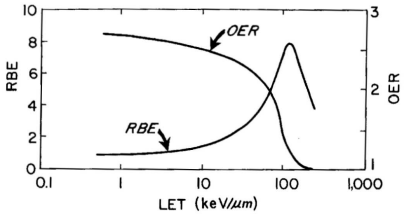

Figure 4.2: Variation of the OER and the RBE as a function of the LET [1].

Figure 4.2 shows the relation between OER and LET. As can be seen, the optimal RBE and the rapid fall of OER occur at about the same LET value, i.e., 100 keV/μm. Low-LET radiation exhibits a large OER and it decreases to unity at an LET of about 200 keV/μm.

5

The interaction of ions with matter and their biological effects

5.1 Mechanisms of interaction between radiation and the absorbing material

The ionizing ability of nuclear radiation is used in radiotherapy to destroy tissue, such as cancerous tumours, in the body. The destruction process occurs as follow:

1. The incident radiation ionizes atoms in molecules of the irradiated material (on a time scale of 10^{-16} s or less).

2. The ionized molecules give rise to free radicals or other excited molecules (10^{-15} s to 10^{-3} s).

3. Free radicals can be incorporated into complex biological structures at molecular level and modify their biological function. The biological change can take place within hours or years.

5.2 Direct action

The radiation interacts directly with the critical targets in the cells without the intermediate step of producing free radicals (R·). This interaction mechanism is dominant for radiations with high LET.

$$RH \rightarrow RH^{+} + e^{-} \tag{5.1}$$

$$RH^{+} \rightarrow R \cdot + H^{+} \tag{5.2}$$

Thus, charged particles, having sufficient kinetic energy, can disrupt the atomic structure of the absorber producing chemical and biological damage.

5.3 Indirect action

Ionizing radiation has the highest probability of interacting with water molecules since the human body is about 80% water. The water molecule can be ionized as follows:

$$H_2O \rightarrow H_2O^+ + e^- \tag{5.3}$$

In addition, the free electron can be captured by another neutral molecules:

$$H_2O + e^- \rightarrow H_2O^- \tag{5.4}$$

The unstable ions H_2O^+ and H_2O^- can dissociate into

$$H_2O^+ \rightarrow H^+ + OH\cdot \tag{5.5}$$

$$H_2O^- \rightarrow H\cdot + OH^- \tag{5.6}$$

where $OH\cdot$ and $H\cdot$ denoted free radicals. These extremely reactive free radicals can generate several inorganic compounds in an aqueous environment (H_2, H_2O_2 and H_2O) as well as new free radicals. Furthermore, the free radicals can diffuse a short distance and reach a critical target in the cell, i.e., a complex hydrogen-containing biological molecule, for instance, a chromosome. Thus, the production of a free radical may alter the function of the system.

5.4 DNA radiation damage

DNA is a large molecule with a double helix structure. In order to form the double helix two strands are held together by hydrogen bonds between bases. The "backbone" of each strand consists of alternating deoxyribose (sugar) and phosphate groups. Attached to the "backbone" are four bases that specify the genetic code. There are two different base groups: pyrimidines: including thymine and cytosine, which are single-ring groups, and purines: including adenine and guanine, which are double-ring groups. The bases on opposite strands must be complementary thus, adenine pairs with thymine and guanine pairs with cytosine.

DNA irradiation can produce:

- *Single strand breaks (SSBs)*: Cell killing is not possible since the damage can be repaired. SSBs are repaired using the opposite strand as a template. Therefore, if both strands are broken and the breaks are well separated, the DNA can also be repaired because the breaks are handled separately. However, mutation may result from SSBs due to misrepair (incorrect repair).

- *DSBs*: The interaction of two DSBs may result in cell death, carcinogenesis or mutation. Thus, DSBs are considered the most important lesion produced

in chromosomes by radiation. DSBs are produced when both strands are broken and the breaks are opposite or separated by only a few base pairs. They are induced linearly with dose, indicating that they are formed by single tracks of ionizing radiation. DSB repair is possible by Homologous Recombination Repair (HRR), which requires an undamaged DNA strand, and Non-Homologous End Joining (NHEJ) which mediates end-to-end joining.

- *Locally multiply damaged sites*: The energy from ionizing radiation is not deposited uniformly, but located along the tracks of the charged particles. The ion pairs produced combine and form groups whose dimensions are comparable to the diameter of the DNA double helix. Consequently, complex lesions may be produced, including DSB and base damage.

5.5 Mechanism of cell killing

The definition of cell death depends on the kind of cells in question. Death is defined as the loss of a specific function for differentiated cells that do not proliferate (nerve or muscle). However, for proliferating cells, death, also referred as reproductive death, is defined as the loss of reproductive capacity. Cell death may be due to mechanisms such as mitotic death or apoptosis.

In order to eradicate a tumour, it is necessary to kill the cells, i.e., to stop their division avoiding further growth and spread of the malignancy. In general, a dose of 100 Gy is necessary to destroy cell function in non-proliferating systems. In contrast, the mean lethal dose for loss of proliferative capacity is usually less than 2 Gy [1].

5.5.1 Mitotic death

Cells die while attempting to divide because of damaged to their chromosomes due to ionizing radiation. This is the most common form of cell death, and may occur in the first or subsequent division following irradiation.

In most tumour cells, mitotic cell death is at least as important as apoptosis and, in some cases, the only mode of cell death.

The survival curve

A close relationship has been reported between cell killing and the induction of specific chromosomal aberrations [24]. For instance, exchange-type aberrations require two chromosome breaks, and the damaged cells lose their reproductive capacity [1].

Figure 5.1 shows two typical survival curves, which describe the relationship between the radiation dose and the proportion of cells that survive. In the case of low-LET radiation (the solid curve), at low doses, the two breaks may result from the passage of a single particle. Then, the probability of an interaction between the

two breaks leading to a lethal exchange-type aberration is proportional to the dose. Consequently, the survival curve is linear. At higher doses, the two chromosome breaks may result from two separate particles and the probability of interaction between the two breaks is then proportional to the square of the dose. Thus, if the quadratic term dominates, a linear-quadratic relationship appears in the survival curve.

In the case of high LET radiation (the dotted curve), the damage may result from the passage of a single particle. Therefore, the survival curve is linear, independently of the dose.

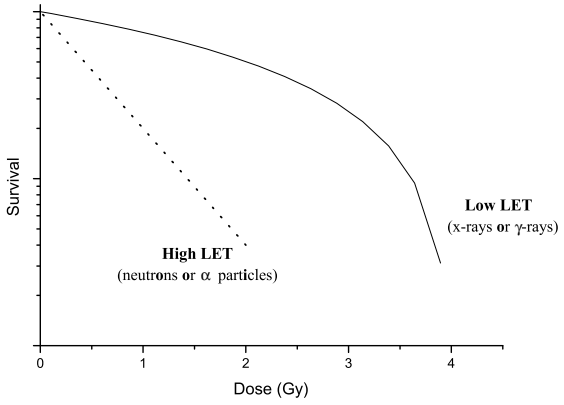

Figure 5.1: Relationship between chromosome aberration and cell survival.

5.5.2 Apoptosis

Apoptosis, or programmed cell death, is highly dependent on the type of cell, as is radiation-induced cell death. The morphological hallmark of apoptosis is the condensation of the nuclear chromatin in either crescents around the periphery of the nucleus or a group of spherical fragments.

Apoptosis is characterized by a sequence of morphological events that start in the cell by a cease in communication with its neighbours. The dying cell rounds up and detaches from its neighbours. The cell shrinks due to cytoplasmatic condensation and eventually separates into a number of membrane-bound fragments of different sizes called apoptotic bodies.

5.6 Non-targeted responses

Non-targeted effects are considered to be those inducing biological effects in cells that are not directly traversed by a charged particle, but are in close proximity to directly irradiated cells. This kind of effect, which is significant at low doses, has been reported during recent decades due to the increased use of single-particle microbeams.

The relevance of these effects is due to the fact that the fundamental dogma that the DNA helix is the ultimate target to produce cell damage has become obsolete. The target for radiation damage is larger than the cell nucleus and indeed larger than the cell itself.

Non-targeted, cellular responses include adaptive response, bystander effect, gene expression, genomic instability, inverse dose-rate effect, low-dose hypersensitivity [7] and the recently added death-inducing effect [25].

The causes of these effects are still poorly understood, and several attempts are being made worldwide to define the mechanisms behind them at the molecular level. The sensitive target within the cell that triggers the non-targeted response in neighbouring cells is unknown. However, recent studies have shown that low- and high-LET ionizing radiation can affect unirradiated cells via secreted soluble extracellular factors and direct cell-to-cell communication [26]. Furthermore, the mitochondria has been reported to play an important role in the bystander effect [4].

5.6.1 Adaptive responses

The adaptive response is observed when cells exposed to a low priming dose are subsequently challenged by a higher dose and show a lesser response. This effect has been observed for several endpoints including survival, mutation, transformation and chromosomal damage [27, 28].

The mechanism behind the adaptive response is unclear, but it has been suggested that it involves the induction of signalling pathways, including a novel chromosome break/repair mechanism [27], or down-regulation of heat-shock-related proteins [29]. Adaptation after the priming low dose takes a few hours, between 4 and 6 h [28] depending on the cells, to become totally effective, and it disappears if a few cell cycles, approximately 3 [28], elapse between the two doses.

In summary, the adaptive response to low doses requires a minimal activation dose and depends on the genetic constitution of the person or animal exposed, and the dose-rate employed. Furthermore, the adaptive response can also occur *in vivo* [30].

5.6.2 The bystander effect

The bystander effect arises when unirradiated cells are damaged through signalling pathways initiated by nearby irradiated cells [31]. Two types of bystander effect can be considered, depending on the signal pathway: those induced by gap

junction-mediated intercellular communication (GJIC), and those induced by secreted soluble factors such as reactive oxygen species (ROS). Whether GJIC is an adjunct or a essential mechanism producing the bystander effect is still a matter of controversy [32].

The bystander effect has some important characteristics.

1. The bystander effect is very dependent on the type of cell; not all types of cell show the bystander response [2].

2. The bystander effect seems to be a binary effect, i.e. the damage observed is independent of the number of particles traversing the cells [2, 32].

3. The bystander effect is triggered to maximum effect once a threshold dose is exceeded (between 0.05 Gy and 0.2 Gy) [7].

4. The bystander response seems to have no correlation with distance. Nevertheless, the distribution of damage shows a tendency to clustering among damaged cells [22] suggesting a limiting diffusion distance [32].

5. The bystander effect is independent of the LET of the radiation induced by high- as well as low-LET radiation [2]. However, the LET of the radiation may have different activation mechanisms, although similar endpoints [32]. Furthermore, bystander responses have also been seen following treatment with photodynamic therapy, ultraviolet light, heat and chemotherapy [33].

6. The evidence suggests that, for cells exposed to at least low-LET radiation, the signal and response are modulated separately [32].

7. The DNA damage in bystander cells seems to persist for a prolonged time, in contrast to that produced by direct irradiation, which is repaired completely within several hours depending on the dose [34].

8. There are limited reports of radiation-induced bystander responses *in vivo* being premature differentiation the major response [6].

Several bystander effects have been reported following:

- *Cytoplasmic irradiation*: The mutagenicity depends upon the generation of radiation-induced soluble signalling factors such as ROS [35] and nitric oxide (NO) [36]. Also, rapid calcium flux is an early event in the radiation-induced bystander effect [34].

- *Irradiation with low fluences of α particles*: GJIC appears to be involved in the activation of the bystander effect [31].

- *Irradiation with a charged-particle microbeam*: Most microbeam studies have reported bystander effects using α particles but it has also been shown using protons, soft X-rays and heavy ions. The bystander response appeared to

be independent of the target within the cell, i.e., the cytoplasm and the nucleus can trigger the response [7]. In this case, bystander effects have been demonstrated for chromosomal aberrations, cell killing, mutation, oncogenic transformation, and alteration of gene expression [37].

- *Transfer of medium from irradiated cells*: The transfer of medium from irradiated cells to a healthy cell culture can also trigger the bystander response [35]. Medium transfer experiments have shown, for instance, the reduction of cloning efficiency and the induction of genomic instability in non-irradiated cells [32]. Additionally, the temporal aspect of the bystander effect has been studied, using induced mutations as the endpoint, revealing that up to 1 h is required to generate the bystander signal and, after a stability period, the bystander signal is diminished in 12 to 24 h [29].

5.6.3 Death-inducing effect

This phenomenon is similar to the bystander effect observed in medium transfer experiments. However, the death-inducing effect is characterized by the reduced survival of non-irradiated cells that have been incubated in medium from cells showing radiation-induced chromosomal instability. This effect is seen many generations after the initial radiation exposure. For instance, RKO36 cells have been reported to produce death-inducing effect in human-hamster hybrid GM10115 cells [25].

5.6.4 Gene expression

Gene expression refers to the up- or down-regulation of several stress-responsive genes, at doses below levels causing significant DNA damage. There is no indication of a threshold for gene induction, and low doses were found to be more toxic than higher ones [38].

5.6.5 Genomic instability

Genomic instability is defined as genome-wide changes in the surviving progeny of irradiated cells. Instability is observed in cells at various times after irradiation, and there are multiple pathways for initiating and perpetuating induced instability [39]. There is emerging evidence that extra-nuclear and extra-cellular events initiate radiation-induced chromosomal instability. For instance, a persistent increase in ROS has been observed in cell cultures showing radiation-induced genomic instability [31, 39].

Multiple endpoints are associated with radiation-induced instability. The primary aberrations observed are chromosomal changes such as gaps or breaks. However, the more significant changes are gross chromosomal rearrangements [31]. The endpoints associated with radiation-induced genomic instability and bystander effect are the same: chromosomal rearrangement, micronuclei, increased mutation,

increased transformation, and cell killing. Thus, both effects seem to be linked, and may be the manifestation of the same non-targeted process, in other words, the bystander signal may be able to induce genomic instability [6, 32].

5.6.6 Inverse dose-rate effect

The term inverse dose-rate effect is used to refer to the response shown at very low dose rates ($\sim$ 0.1 - 1 cGy/min [40]) where increased levels of mutation or transformation are observed [6]. The mutagenic effect of ionizing radiation is usually reduced for a given dose as the dose rate is reduced, and this effect is defined as a direct dose-rate effect [40]. This response results from the repair of sublethal damage and occurs in tumour and normal tissues, *in vivo* as well as *in vitro* [1].

5.6.7 Low-dose hypersensitivity

The term low-dose hypersensitivity refers to a two-phase phenomenon [6]:

1. hypersensitivity (HRS), where the cells exhibit increased sensitivity at very low doses (less than 10 cGy [8]), and

2. increased radioresistance (IRR) where the cells exhibit a radioresistant phase at higher doses (up to approximately 1 Gy [8]).

The activation and operational mechanisms of the process are still unknown. However, two hypothesis have been proposed: 1) the injury produced by these low doses is either below the threshold required to activate, fast or efficient DNA repair [38] or 2) changes in the DNA structure or organization are not produced inhibiting repair [8]. In addition, induced radioresistance and the adaptive responses to small conditioning doses may be due to an increased repair capacity, but on different time scales [8].

The bystander effect and low-dose hypersensitivity are similar in that, in any cell line, only one or the other occurs [32]. Furthermore, there is no clear published evidence of the HRS/IRR phenomenon *in vivo* but cellular repopulation seems to obscure the effect, to some extent [8].

6

Development of the Lund Nuclear Microprobe Single-Ion Hit Facility

Biological applications of ion beams have become an important research field since the development of single-ion hit facilities for cell irradiation. The main advantage of these facilities is their capability to precisely deliver a predetermined number of particles to a single living cell, the ultimate limit for the delivered radiation at low doses being a single ion. Furthermore, the damaged induced can be analysed on a cell-by-cell basis.

Other advantages of microbeam irradiation can be summarized as follows:

- The irradiation is highly localized spatially, allowing specific subcellular compartments within the cell or a particular cell in a cell culture to be targeted. Thus, more biological information can be obtained regarding cell-to-cell communication, the functionality of components within the cell, the sensitivity of subcellular targets and intracellular communication [41].

- Certain cells within a population can remain unirradiated allowing the study of "bystander" effects.

- Temporal separation of irradiation is possible allowing investigations of the dynamics of cellular repair since individual cells can also be monitored in time.

Several effects, only observed at low doses, have been reported, and these might be important if it can be shown that they also play a role at higher doses.

6.1 Types of single-ion hit facilities

Several approaches can be employed to create a SIHF.

- Facilities originating from microbeam facilities initially developed to study radiation damage to living cells. These normally have a collimated beam and a vertical arrangement.

- Facilities originating from the modification of an existing analytical microprobe. These could be existing probes with highly collimated and focused ion beams initially designed for ion beam analysis. These facilities normally have a horizontal arrangement.

- Stand-alone microbeam facilities where a radioactive ion source is used instead of a particle accelerator. This novel approach, employed at Columbia University [42], can deliver one α particle per second in a 10μm diameter spot, using a polonium source and a compound magnetic lens.

Focused microbeams have a higher targeting accuracy (TA) and throughput than collimated microbeams since the beam is deflected towards the targeted cells without moving the sample stage. The ion LET is better defined for a focused microbeam and the ion scattering is reduced. Therefore, the achievable beam spot is smaller [2, 43, 44].

A horizontal system configuration requires a vertically positioned Petri dish containing the cell culture. However, the vertical system arrangement provides a more cell-friendly environment. The displacement of the cells due to gravity effects can be minimized using monolayer cell cultures which are attached to the surface on which they were cultivated. In addition, the vertical arrangement requires the removal of the cell culture medium prior to irradiation. A layer of cell culture medium remains, the thickness of which is approximately the same as the diameter of the cells. Nevertheless, the cells are stressed because their vital nutrients have been removed during irradiation.

6.2 The CELLION Network

A Marie Curie Research Training Network, CELLION, was established in 2004 to study cellular response to targeted single ions using nanotechnology. Several European research institutes and universities joined this network. The project included two lines of research, technical and biological, to provide the tools and technical advances necessary for the study of the effects of radiation on living cells. The aim of the research on instrumentation was to construct a SIHF for cell irradiation. The aim of the biological research was to study the relationship between cell damage and repair, particularly at low doses, where the dynamics of radiation is still poorly understood and new effects has been discovered.

Tables 6.1 and 6.2 present the main SIHFs worldwide and their main applications.

Table 6.1: Description of SIHFs worldwide I

SIHF	***BEAMLINE ORIENTATION***	***EXIT WINDOW***	***DETECTOR TYPE***	***DETECTOR LOCATION***
CENBG France (Bordeaux) [a]	Horizontal	150 nm Si_3N_4	Pre-cell	Protons 7.5 μm BC400 scintillator + PTM Alphas Proportional counter (10 mbar, isobutane)
GCI UK (Oxford)	Vertical	3 μm Mylar	Pre-cell	18 μm BC400 scintilator + PMT
GSI Germany (Darmstadt)	Horizontal	200 nm Si_3N_4 + 20 nm Au + 50 $\mu g/cm^2$ CsI	Pre-cell	Channeltron
IFJ PAN Poland (Cracow)	Horizontal	200 nm Si_3N_4	Post-cell	Silicon particle detector and/or channeltron
JAERI Japan (Takasaki)	Vertical	5 μm aperture on a 100 μm thick tantalum disk	Post-cell	BC400 scintillator + PMT
LIPSION Germany (Leipzig)	Horizontal	100nm Si_3N_4	Post-cell	Windowless p-i-n diode
LTH, Lund University Sweden (Lund)	Horizontal	200 nm Si_3N_4	Post-cell	Silicon PIN photodiode
PTB Germany (Braunschweig)	Vetical	5 μm Mylar	Pre-cell	BC400 scintillator + PMT
RARAF USA (New York)	Vertical	100 nm SiN	Post-cell	Ion counter (P10) (90% argon + 10% methane)
SNAKE Germany (Munich)	Horizontal	7.5 μm Kapton	Post-cell	1mm BC400 scintillator + PMT
SPICE Japan (Chiba)	Vertical	1 μm Si_3N_4	Post-cell	Scintillator

[a] Nanobeam line in progress, expected beam resolution in STIM mode below 100 nm [45]

Table 6.2: Description of SIHFs worldwide II

SIHF	***TARGETING ACCURACY***	***THROUGHPUT (CELLS/HOUR)***	***BIOLOGICAL STUDIES***
CENBG	Alphas $\pm$ 2μm 95%	2000	Clonogenic survival [46]
GCI	Protons $\pm$ 5 μm 96% Alphas $\pm$ 2 μm 99%	36000	Cell signaling, low-dose hypersensitivity, genomic instability and visualization of DNA repair [44, 47]
GSI	C ions $\leq$ 0.5 μm 99.5%	—	DNA damage [43], radiation induced cell cycle arrest [48], tumuor cell migration after heavy ion irradiation [49]
IFJ PAN	Protons $\pm$ 40 μm 90%	—	Double strand break formation [50, 51]
JAERI	—	—	Effects of heavy ions in cell growth [52, 53]
LIPSION	Protons $\leq$ 0.5 μm 99.8% [b]	—	Cell survival [54]
LTH, Lund University	Protons $\leq$ 5μm 97%	5000	Bystander cell death and stress response [56]
PTB	Protons and alphas $\leq$ 2 μm	50000	Survival fraction by colony forming ability test and gene expression [57–59]
RARAF	Protons $\leq$ 3.7 μm 92% [c]	11000	Bystander effect, genomic instability and adaptive response [41, 47]
SNAKE	55 MeV C ions $\leq$ 2 μm 100 MeV ^{16}O ions $\leq$ 1 μm	—	Live protein dynamics studies [61–63]
SPICE	–	400-500	Induction of DNA stand breaks [64, 65]

[b] Nanobeam line being reconstructed, hit accuracy values have to be updated [55]
[c] Microbeam II endstation being built, hit accuracy values have to be updated [60]

6.3 Development of a single-ion hit facility

For successful cell irradiation, an accurate, controlled, fast system is required. Biological experiments using microbeams also require a stress-free environment for the cells, efficient cell recognition, high experimental speed and degree of automation, and the availability of flexible modes of irradiation [58].

The creation of a SIHF requires the following elements:

1. An ion source of appropriate energy to define the type of particle and LET.
2. An ion location limitation device in order to obtain a small beam diameter.
3. Biological sample positioning which includes target location recognition.
4. An ion detection system that allows the number of ions delivered to be controlled.
5. An exit window for beam extraction into air.
6. A suitable culture surface for the cells, which is compatible with the irradiation system.
7. A biological evaluation procedure, i.e., a method of assessing cell damage.

6.3.1 The Lund Nuclear Microprobe

The LNM uses a 3-MeV single-ended NEC Pelletron Electrostatic accelerator. The radio frequency (RF) ion source allows the delivery of protons, α particles and deuterons (^2H). After the accelerator, the beam is directed towards the macro and nano beamlines using switching magnets.

The macro beamline is located at +30° and provides a beam size in the millimetre range. This beamline is used mostly for Particle-Induced X-ray Emission (PIXE) elemental analysis on aerosol filter samples.

The nano beamline is located at -15° and was designed to achieve a sub-micron beam size. However the size of the beam today is in the micrometer range. This beamline is commonly used for ion beam analysis, including PIXE, tomography and biological applications.

6.3.2 The nano beamline

The SIHF at the LNM has been constructed at the *nano* beamline, the configuration of which is shown in Figure 6.1.

The beam is focused in a two-stage system with a quadrupole doublet at each stage, i.e., four magnetic quadrupole lenses placed in a split Russian configuration. The first stage focuses the beam into the intermediate chamber and the virtual image created here is used as a virtual object for the second stage [66].

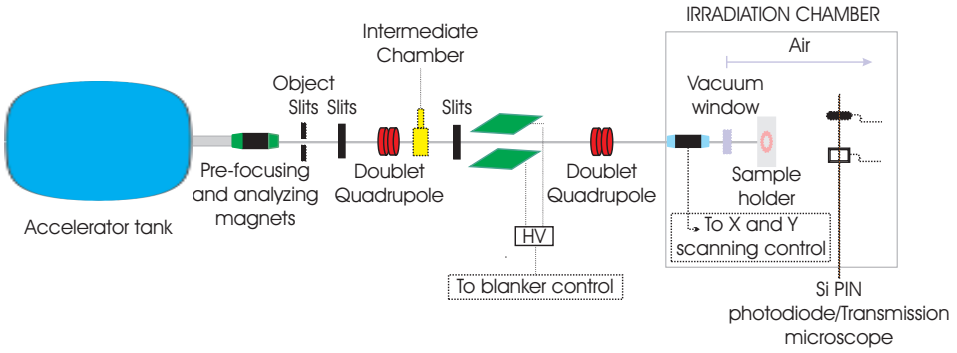

Figure 6.1: Scheme of the nano beamline (not to scale).

Two components of the beamline are vital for single-ion hit detection: the collimating slits and the fast beam-deflection system. Three sets of collimating slits along the beamline are used to shape the beam and to reduce the beam current, thus providing the ion location limitation system. The deflecting system consists of two parallel metal plates connected to a high voltage, which are used to deflect the beam on demand, thus controlling the number of ions delivered [67].

6.3.3 The irradiation chamber

The irradiation chamber at the nano beamline was designed to accommodate different detector systems. Usually, an 8-element, large solid-angle HPGe detector for PIXE analysis and/or the Scanning Transmission Ion Microscopy (STIM) system are operative. The STIM system, used for imaging and mass normalization, can be combined with PIXE and Rutherford backscattering [68]. Additionally, a double-sided silicon strip detector can be installed allowing measurement of angular distributions [69].

The chamber is also equipped with two microscopes for monitoring purposes: transmission and backside. The transmission microscope objectives are mounted on a translation stage, and image magnification is achieved by computer-controlled movement [70]. Furthermore, cell images can be obtained on-line as the transmission microscope is connected to a CCD camera.

The samples to be analysed are mounted in a sample holder also on a translation stage. The sample holder can accommodate five samples. However, for biological applications, three cell cultures can be accommodated.

6.3.4 Detection system

Two detection systems can be defined, depending on the detector location.

Pre-cell

The irradiated ions are detected before hitting the cells. For instance, some facilities use a channeltron as the pre-cell detector [43].

At the LNM, an alternative detector has been tested as the pre-cell detector: an ultra-thin silicon transmission detector. The detector has a thickness of 9 μm and an active area of 4 mm^2. In addition, this detector can be used as a vacuum window [71]. The performance of the detector was recently tested, showing a promising efficiency of 99% for a proton energy of 2 MeV [72].

Post-cell

The ions are detected after passing through the cell culture. The LNM-SIHF employs the on-axis STIM detector as a post-cell detection system. This windowless PIN photodiode (Hamamatsu S1223-01N 7139 (4 mm^2)) [73] measures the energy loss of the beam particles after travelling through the sample and, in combination with the beam-deflection system, controls the applied dose. The detector is mounted on the same translation stage as the microscope objectives.

6.3.5 Beam extraction into air

A 200 nm thin Si_3N_4 membrane (1.5 x 1.5 mm^2), purchased from Silson Company [74], was chosen for beam extraction at the LNM-SIHF. The beam has to be extracted into air since living cells need oxygen as well as a wet environment. Beam extraction results in degradation of the beam quality. Therefore, the material used for the vacuum window must minimize beam scattering and also have high resistance to radiation damage.

A vacuum guard has been installed as a safety measure in case of membrane breakage. The same Si_3N_4 membrane can be used for several experiments. However, the vacuum is visibly degraded when the membrane is damaged or/and needs to be replaced. Seven vacuum sensors are connected along the beamline which isolate the non-evacuated regions if the quality of the vacuum should be decreased.

In order to bring the exit window as close as possible to the sample, an extended pipe is used. The vacuum window is glued onto an end cup, attached to the extended pipe, as can be seen in Figure 6.2.

The thickness of the system must be minimized since the proton energy loss is measured at the end of the path. The beam path after passing the exit window is shown in Figure 6.2. The thickness of the first air gap is the major source of scattering, as can be seen in Figure 6.3, which shows the beam spread as a function of gap thickness.

The procedure used to minimize the separation between the vacuum window and the sample starts with visual approximation. In order to reduce this critical air gap, a lateral camera is employed to place the vacuum window and the sample close to each other. The vacuum window is then focused using a movable transmission

objective which is calibrated. In this way, the objective can be positioned providing the desired separation between the vacuum window and the sample. Finally, the sample is moved towards the vacuum window until the focal plane is reached. Normally, a separation of 500 μm is employed.

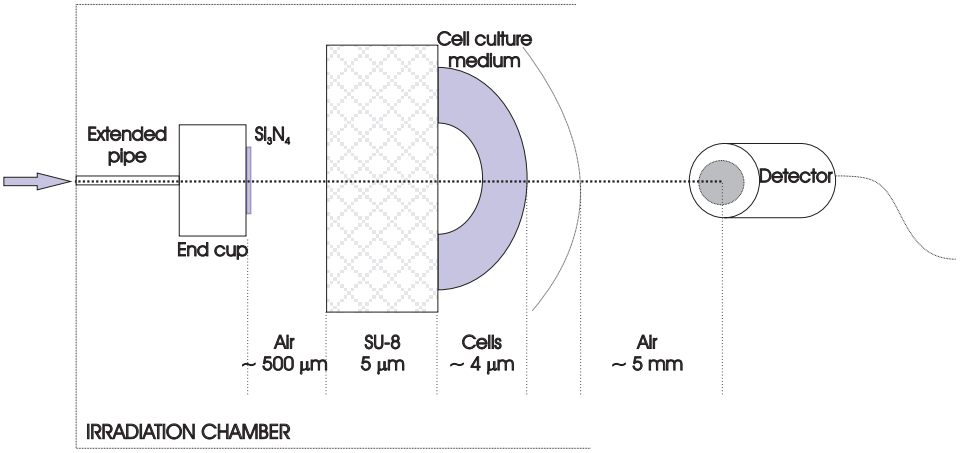

Figure 6.2: Scheme showing the beam path through the irradiation chamber (not to scale). The arrow shows the beam direction.

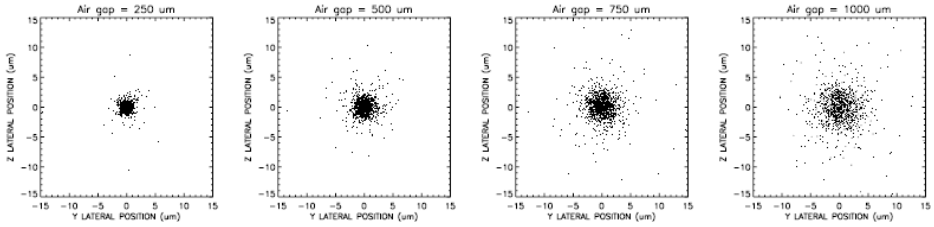

Figure 6.3: SRIM (2008) simulations showing the beam spread as a function of the first air gap thickness.

6.3.6 Single-ion hit system

The LNM data acquisition and beam control system are fully controlled by a CAMAC (Computer-Automated Measurement And Control) crate. The software is

based on the Kmax environment for the development and operation of data acquisition and instrument control. A detailed description of the system can be found elsewhere [75].

The beam position is controlled by a DAC (Digital-to-Analogue Converter) card in the CAMAC crate, which can also be clocked externally at any frequency by means of a TTL (Transistor-Transistor Logic) signal [76]. The analogue DAC output voltage drives a scanning amplifier, which sends a current through the beam scanning coils situated at the irradiation chamber. The actual scanning range is limited by the scanning magnet current to an area of approximately 4 x 4 mm^2 which is determined by the selected gain in the scanning amplifier.

Any predefined pattern of pixels (maximum size 4096 x 4096) can be uploaded into the system and subsequently used to irradiate the sample. The pattern consists of black and white pixels, the black ones representing the regions to be irradiated, and it is scanned line by line in a raster mode (see Figure 6.4 (a)). The TTL signal driving the scanning amplifier controls the dwell time of the beam in a pixel, i.e., the beam remains at a certain pair of irradiation coordinates for the time elapse at which the TTL signal is low. The falling edge of the TTL signal triggers the movement of the beam to the next pair of irradiation coordinates. The beam is usually deflected off the sample between pairs of coordinates to avoid mid-pixel exposure, and a "settling" delay time is also added for current stabilization. The beam deflection time is less than 200 ns [67] and the beam dwell time per pixel is usually 1 to 10 ms. Therefore, the beam blanking time is very short in comparison to the dwell time. The system is illustrated in Figure 6.4 (b).

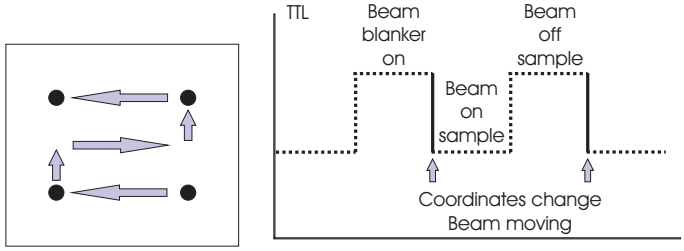

Figure 6.4: (a) The uploaded patterns are used to irradiate the sample in a raster mode. The black dots represent the regions to be irradiated. (b) Beam position and beam blanker function scheme.

Figure 6.5 shows the electronics scheme for single-ion irradiation. The irradiation pattern is uploaded into the Kmax software and the beam is positioned at the first pair of irradiation coordinates. The beam remains in this position until the desired number of protons is delivered, and subsequently the beam is deflected off the sample while moving to the next pair of coordinates. This process is repeated

until the sample has been irradiated according to the predefined pattern, and the beam is then permanently deflected off the sample.

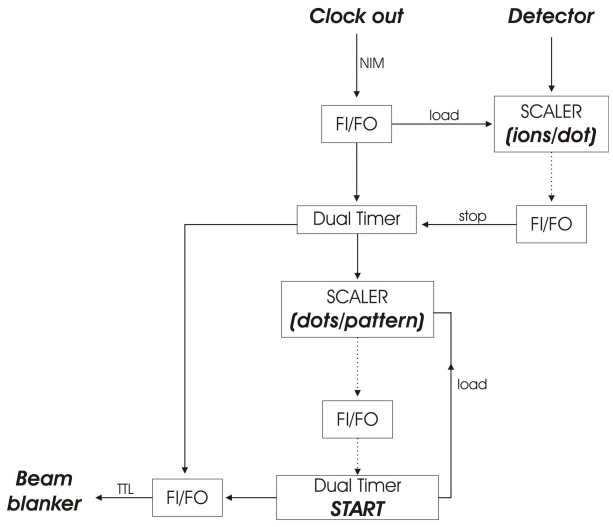

Figure 6.5: The electronics scheme for single-ion irradiation.

The STIM detector cannot be used when irradiating thick samples. Thus, the pre-sample charge measurement system [77] is employed which, in normal operation, measures the average beam current during beam-off periods. The output clock signal from the DAC is used to trigger the beam blanker. The deposited charge is thus controlled by varying the amplitude of this signal. A schematic layout of the electronics can be seen in Figure 6.6.

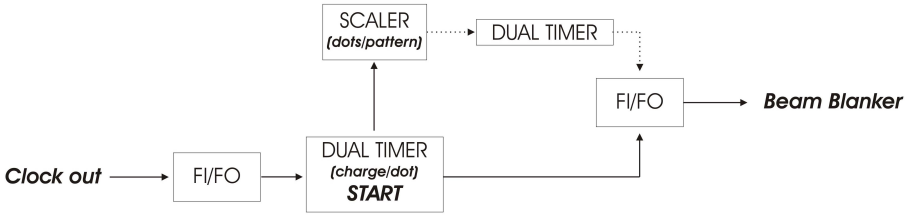

Figure 6.6: Scheme showing the electronics for thick-sample irradiation.

6.3.7 Cell recognition

Target selection for irradiation is performed using in-house cell recognition software *SeACell*. The software is described in more detail in *Paper IV* and Chapter 7.

The application for single-ion irradiation uses the system's capability to irradiate any uploaded pattern. An on-line image of the living cells is acquired prior to irradiation and analysed by the *SeACell* software. The coordinates provided by the software are then used to create an irradiation pattern, which is subsequently uploaded into the system.

6.3.8 System targeting accuracy

The TA of the system has to be precisely determined since the irradiation of subcellular compartments is desired. The main factors that influence the accuracy of the system are beam geometry and aiming accuracy [44, 46]. Beam geometry includes effects that arise from the initial size and shape of the beam, the effect of scattering sources and the geometrical arrangement of various elements. Aiming accuracy addresses factors such as the accuracy with which the targets can be identified (the cell recognition software), the accuracy of the sample and beam position (the scanning system), and the ability to align the target.

At the LNM-SIHF, the aiming accuracy depends mainly on the scanning system and the *SeACell* software. The coordinates provided by the software are sent to the scanning system and some uncertainty may occur in the translation. An additional uncertainty arises from the difference between the scanning system coordinates and the position at which the particles are finally delivered, i.e., the beam localization accuracy. Thus, excluding the spatial resolution of the beam, the TA is considered to be the difference between the image coordinates at which the particles are intended to be delivered and the actual coordinates where the particles are deposited. Commonly reported values of TA are in the micrometre range (see Table 6.2).

The first attempt to determine the TA of the system was reported in *Paper I*. The method employed was to obtain a STIM image of a copper grid and, using the software developed, irradiate the wires. The difference in energy loss of the protons between the grid bars and the air gap was studied, taking into account the energy loss spectrum. The results were not as expected since an additional peak was observed, associated with the protons scattered at the edges of the wires. The randomly distributed irradiated regions were not centred or equidistant to the wires since they were selected using a preliminary version of the cell recognition software SeACell.

The method described above was refined by the fabrication of two Ni dot arrays with differently sized dots: 5 μm and 2 μm, separated by 50 μm and 10 μm, respectively. This study is presented in *Paper III*. The data analysis, in the vacuum case, shows a spatial TA not exceeding 5 μm and 97% targeting efficiency. However, the 2 μm array could not be used to estimate the system accuracy since the beam diameter exceeded the dot size. In air, neither of the fabricated arrays could be

successfully employed.

In summary, the sizes chosen for the Ni dot array were too small in comparison to the beam size. Beam focusing problems result in a micrometre beam spot instead of the predicted nanometre diameter [66]. Additionally, the fabrication of larger Ni dot arrays is extremely time consuming, and there is a serious risk that the metal layer will become detached from the supporting layer due to the side evaporation effect produced by the metal deposition system [56]. Therefore, CR-39 track etch film was used to study the TA of the system.

CR-39 is a polymer of allyl diglycol carbonate ($C_{12}H_{18}O_7$) widely used as etched track type particle detectors for protons since it is highly sensitive to low-LET particles [78]. CR-39 is commonly employed for TA measurements where ions are used to irradiate a sample according to a regular pattern. The track of each particle can be observed after etching the film. The solutions most commonly used to etch CR-39 are 6.25N NaOH solution at 70°C [79] and 6N KOH at 70°C [80]. However, at the LNM, the CR-39 irradiated samples are etched in 12N KOH at 80°C for approximately 10 min as recommended by the provider [46].

Figure 6.7 shows the pattern of irradiation formed by single-pixel dots at different separations using 2.5 MeV protons and an average beam current of approximately 1 nA. In both patterns a downward shift of the last dot column can be observed, and failures in reproducing the pattern are visible as missing dots (see Figure 6.7(b)). These effects are due to failures in the beam-scanning system when large areas are scanned. In air, single-pixel dots separated by approximately 20 μm are only resolved in the Y direction due to beam focusing problems in the X direction during these experiments.

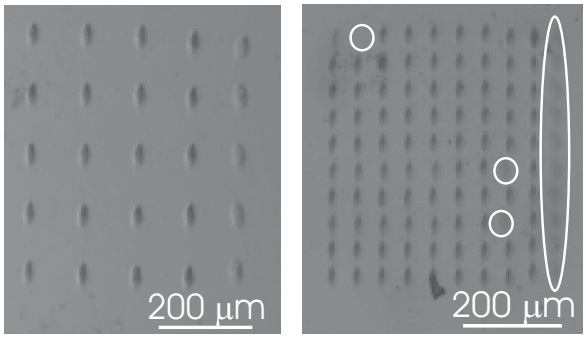

(a) (b)

Figure 6.7: CR-39 track etch film irradiated by a 512 x 512 pixel pattern formed by single-pixel dots separated by approximately (a) 90 μm and (b) 50 μm. The circles indicate missing or shifted dots in the pattern.

The minimum field of view of the camera at the irradiation chamber is 480 x 480 pixels, which corresponds to the size of the on-line input image of the living

cells in the SeACell software. Therefore, the scanning size area required is within the interval where the mentioned problems arise. Consequently, apart from the systematic fluctuations in beam focusing, which can be solved, and the reduction of the irradiation area, the accuracy of the scanning system must be improved in order to obtain reliable targeting irradiation accuracy at the LNM-SIHF.

Regarding the system's ability to irradiate subcellular targets, the SeACell feature of localizing subcellular targets must be complemented with precise system TA in air. The size of the human hepatoma cell line (HepG2), commonly used for biological experiments at the LNM-SIHF, is approximately 11 μm. Thus, the accuracy of the current system does not allow subcellular irradiation. Either the accuracy of the system must be improved, by reliable scanning system and better beam focusing, or bigger cell lines must be employed.

6.4 Additional parameters important in cell irradiation

6.4.1 Irradiation mode: targeted and non-targeted irradiation

Targeted irradiation implies aiming at and irradiating all the cells in the cell culture. The target within the cell can be varied, the cytoplasm, the nucleus or other subcellular compartments, depending on the technical resources available at the facility and the final biological endpoint being studied.

Non-targeted irradiation occurs when all the cells in a particular sample have not been directly irradiated or have not been uniformly exposed to radiation. A simple, standard approach to achieve non-targeted irradiation involves distributing the incoming particles to form a pattern across the cell culture. The irradiation of specific cells or cell compartments of certain cells also leads to non-targeted irradiation regarding the entire culture.

There is some controversy concerning the differences between targeted and non-targeted irradiation. A pattern may be considered targeted irradiation on a microscopic scale but not on a macroscopic scale, thus it is a matter of scale. At the LNM-SIHF all the cells within the culture are never irradiated. Therefore, non-targeted irradiation is assumed, and refers to a pattern of irradiation of the cell culture unless otherwise stated. Figure 6.8 shows the differences between targeted and non-targeted irradiation.

Targeted irradiation requires more advanced technical resources than non-targeted irradiation since all the cells must be localized before irradiation. However, some low-dose radiation effects can only be observed following non-targeted irradiation, for instance, the bystander effect.

Technically, subcellular targeting is the most demanding since this requires high accuracy during the procedure. Also, a beam size smaller than the cell size is

required. The cell size depends on the cell line used, and is normally 10 to 20 μm.

Most facilities worldwide have a beam size in air in the micrometre range. However, some facilities have achieved sub-micron beam sizes, for instance, the LIPSION facility has reported a beam size of 350 nm in the low-current mode [81].

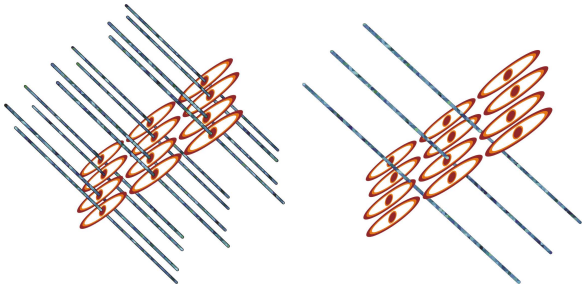

(a) (b)

Figure 6.8: Illustration of the difference between targeted and non-targeted irradiation. (a) Targeted irradiation: all cells in the culture are targeted, aiming at the cell nucleus. (b) Non-targeted irradiation: the cell culture is irradiated by a pattern consisting of three spots in a row. The position of the cell culture at the time of irradiation determines the number of cells hit.

6.4.2 Throughput

The non-targeted cell irradiation experiments carried out at the LNM-SIHF to date have consisted of irradiating several dots within the cell culture. These dots are irradiated in a very short time in comparison with the time required for sample positioning, i.e., repositioning the three culture dishes that can be accommodated in the sample holder. Thus, assuming that an average of 6 cells are irradiated per minute, the throughput is approximately 400 cells/h. However, this is an underestimation of the system's capabilities.

A more accurate estimate can be made by considering the time required to irradiate a pattern in CR-39, which depends on the number of dots per pattern and the dose applied per dot. An irradiation pattern such as the one shown in Figure 6.7(b), assuming an average charge deposition within 10 ms, is completed in less than one minute. Therefore, since 100 cells can be irradiated per minute, a direct average throughput of approximately 6000 cells/h can be achieved. However, it should be noted that during the irradiation procedure the culture medium is removed, and the viability of the cells will be compromised after 5 minutes. Therefore, cell culture dishes must be replaced every 5 minutes, and a more realistic throughput is thus approximately 5000 cells/h.

The efficiency of the system has been improved in some facilities by optimizing the irradiation procedure. Instead of using the common raster-like/line-scan mode

for the scanning system, extra computing time is used to calculate the fastest path to irradiate the cells, improving the throughput by up to 60% depending on the cell number and loop size [82].

6.5 Exposure routine

The protocol for cell irradiation at the LNM-SIHF can be summarized as follows.

1. The transmission microscope objective is placed behind the sample.
2. The origin of the reference system, for all single-cell coordinates, is established according to the beam position. (A special sample was created for this purpose. Further details can be found in Section 8.4.)
3. The cell culture medium is removed from the culture dishes. The dishes are then loaded into the sample holder.
4. The sample holder is positioned on the translation stage in the irradiation chamber.
5. The cells to be targeted within the objective's field of vision are localized using the SeACell software. Thus, the number of cells and their coordinates are determined, as well as the targeting mode: uniform, subcellular, site-specific (nucleus or cytoplasm) or patterned targeting.
6. The transmission microscope objective is replace by the detector.
7. The targeted coordinates are sent to the scanning system. The single-ion hit electronics described previously allows the scanning system to position the beam at the selected coordinates with the condition that the beam is only active at the positions where a cell has been found. The rest of the time, the beam is off the sample.
8. The number of protons to be delivered to each targeted cell is selected.
9. The selected cells are irradiated.
10. The sample holder containing the culture dishes is removed from the irradiation chamber and fresh culture medium is added to the irradiated cells.

7

Development of routines to locate the cell position

SIHF systems must be fully automated throughout the irradiation process due to technical issues related to the use of living cells. Target identification is the first step. Commonly, nuclear and/or cytoplasmic stains are used to image cells. However, these can change the nature of the subcellular compartment being analysed. For example, DNA-labelling dyes can have radio protective effects due to the scavenging of hydroxyl radicals and possibly other unknown mechanisms [83].

Cell recognition algorithms are commercially available. However, they are not compatible with microprobe control software, thus in-house code has to be developed. For instance, the recognition software used at GSI in Germany and CENBG in France, was written as a plug-in for the commercial image processing program Image Pro Plus (Media Cybernetics Inc., Silver Spring, MD, USA) [43, 46].

At the LNM-SIHF, the SeACell software was developed in-house for on-line cell recognition and localization. No stain is used for imaging purposes at the LNM-SIHF, and non-stained cells can be identified in a short time, with high efficiency. The program has been developed using common image processing routines in IDL 6.2 language [84]. Therefore, SeACell can be run on any computer equipped with an IDL Virtual Machine.

7.1 Automatic cell recognition algorithms

Several algorithms have been implemented for automatic cell recognition providing the coordinates of the centre of each located cell. This automatic cell recognition procedure is based on a set of linked procedures which consists of the application of morphological filters to the input image.

The software efficiency is obtained by calculating the percentage of cells located by the program versus the total number of cells in a set of input images. This value is highly dependent on the input image.

7.1.1 Preliminary cell recognition

This algorithm performs rough cell recognition, and is based on two basic things.

- Threshold and scaling filter: A threshold value is selected using an intensity histogram of the image. This threshold value is used as the lower (or upper) limit to discard some image pixels and rescale the remaining ones creating a greyscale image.
- Erode/Dilate operator: Image details that do not match the "structuring element" are eliminated. The structuring element is designed to simulate the shape of cells and therefore, a disc is usually chosen.

This preliminary algorithm has a few drawbacks: a single cell can be identified and localized twice, noise can be considered as a target, and overlapping objects can be regarded as single objects. Therefore, further image processing is needed.

7.1.2 The cell validation algorithm

The automatic procedure for cell recognition is completed by a cell validation routine, which can be applied multiple times if required. The target is defined by the intersection of two erosion operators based on hit and miss structuring elements. The hit structuring element is chosen to match the size and shape of the cell. The miss structuring element is used to check the separation between cells and the number of hits per cell.

The function of this algorithm is explained more extensively in *Paper VI*.

7.1.3 Cell selection by area distribution

Additionally, cell selection can be performed by area distribution before or after the cell validation algorithm. This procedure is completed in two steps.

- Localized cells that depart from a certain distribution are excluded. Usually, the probability distribution function of the detected areas follows a log-normal distribution.
- Detected regions are selected or discarded attending to their R value, which is defined as the ratio between the area and the perimeter of each region.

The function of this algorithm is explained more extensively in *Paper I*.

7.2 Manual cell recognition

The automatic cell recognition procedure described above provides the coordinates of all the cells appearing in the input image. However, studies on the bystander effect require non-targeted cell irradiation in which not all the cells are irradiated.

Therefore, manual cell recognition was implemented. No algorithm is used but the user selects the targeted cell and the region where the cell is to be irradiated. However, manual target selection may be time-consuming and an expert may be required for complicated images.

The automatic cell validation algorithm is exploited for bystander studies using the so-called "dynamic cell targeting". This software feature offers a clear advantage to the manual cell recognition since cells with the desired characteristics can automatically be identified by modifying the size parameter of the hit and miss structuring element.

7.3 Other application: Evaluation of irradiation damage

An easy-to-use application of the software includes cell damage evaluation after α source irradiation. Bystander effects in human hepatoma cells following α irradiation have been studied at the Bio-Medical Centre (BMC) at Lund University [9]. In order to investigate the cells after irradiation two stains are used: Hoechst 33342 and propidium iodine (PI). Hoechst stain is used to determine the number of living cells in the cell colony, and the nucleus-staining dye PI is used to count the number of dead cells. The proportion of dead cells is calculated as the ratio between the cells stained with PI and the cells stained with Hoechst, and is given by the SeACell software.

Thus, the developed SeACell software can be used as a cell counter, allowing users to obtain statistical data for specific biological experiments.

7.4 The SeACell user interface

Figure 7.1 shows a screen shot of the SeACell software, which will be described below.

7.4.1 Choice of algorithm

The software interface contains two buttons to allow the user to choose between automatic and manual cell recognition.

A third button is used to transfer the coordinates of the cells to the CAMAC control system of the LNM-SIHF.

Cell selection by area distribution has not been integrated into the software since it is not commonly used.

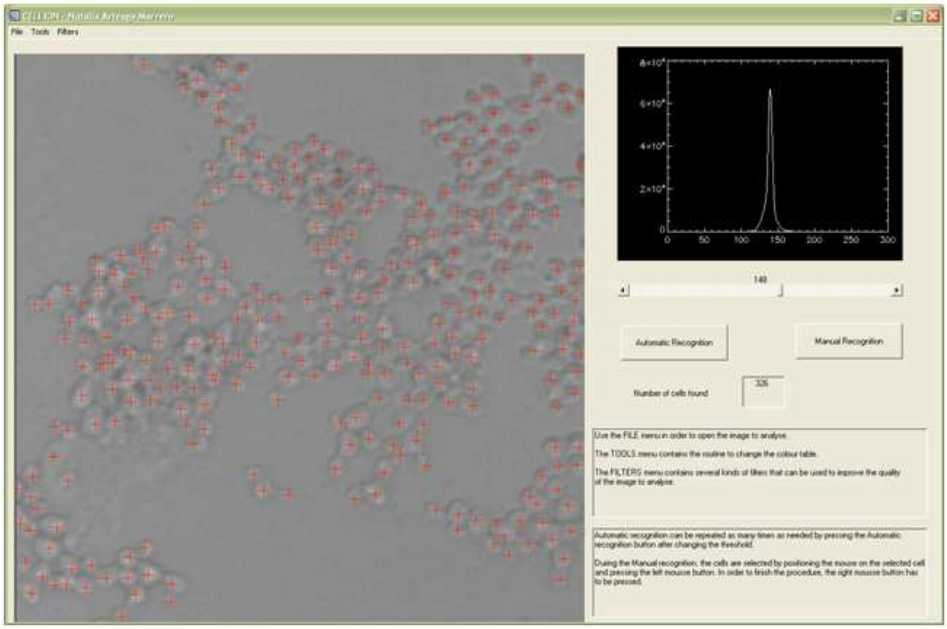

Figure 7.1: Screen shot of the SeACell software, where an image of the artificial cell sample has been analysed. The red crosses indicate the localized cells. The upper right image shows the intensity histogram of the input image.

7.4.2 Data output

The input images are visualized in a large image together with the results of the cell recognition procedure. The intensity histogram of the input image is shown in a smaller image (see Figure 7.1) in which the number of pixels, at each intensity value found in the input image, is plotted versus pixel intensity values.

The number of cells located is given in a window. Since the software can also be used as a cell counter, the total area (in pixels) and the perimeter occupied by the cells is also given.

7.4.3 Drop-down menus

Three drop-down menus have been implemented.

File

This drop-down menu offers basic features:

- Open - A dialogue box appears for uploading the image to be analysed. The preferred image format is jpeg.
- Save - Modifications for image improvement applied to the input image by the user can be saved.
- Exit - This option is used to terminate the program.

Tools

A colour display table is activated with this menu. Changing the input image colour may be as effective as applying an image filter since some image features may be enhanced.

Filters

Low frequencies represent gradual variations in an image and they determine the overall shape or pattern in the image. High frequencies correspond to abrupt variations and provide image details. However, they are often contaminated by spurious effects due to noise.

Image filters enhance image features that improve the quality of the input image and therefore, the efficiency of the program. An image filter is defined by a kernel (a small array) which is applied to each pixel and its neighbours in an image. The process used to apply filters to an image is known as convolution, and may be applied in either the spatial or the frequency domain. The entire image is modified by multiplying the elements of the kernel by the corresponding pixel values when the kernel is centred over a pixel. The average of the resulting array elements replaces the original pixel value.

Fast Fourier Transforms (FFTs) transform an image between the spatial and frequency domains. In the frequency domain, the convolution is called windowing and it is performed by multiplying the FFT of the image by the FFT of the kernel. The result is then transformed back into the spatial domain.

There is no single recipe for image improvement, and the order in which the filters are applied to the input image may influence the final result. The filters are classified by their main application [84].

- ***Edge detection***: An edge is detected when a steep gradient occurs between adjacent pixel values. This gradient is measured calculating the first derivatives (or slopes) of an image. Four filters have been implemented which compute derivatives in any selected direction:
  - Direct: This filter computes the first derivatives of an image. An example of the filter function can be seen in Figure 7.2.
  - Laplace: This filter calculates the second derivatives of an image, i.e. the rate at which the first derivatives change. This helps to determine if a change in adjacent pixel values is an edge or a continuous progression.

- Robert: This filter computes a first-order partial derivative of an image [85].
- Sobel: This filter calculates the first derivatives of an image with slightly superior noise-suppression characteristics [85].

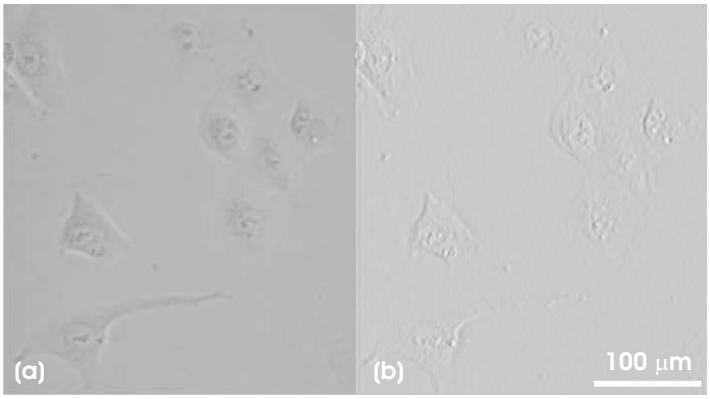

Figure 7.2: (a) Image of cells from a human lung adenocarcinoma epithelial cell line (A549). (b) Cell edges have been enhanced by applying a direct filter. The image contrast has been modified to make the features of the filter clearer.

- ***Sharpening***: An image is sharpened when the contrast between bright and dark regions is enhanced. The sharpening process consists of the application of a high-pass filter, which tends to retain the high-frequency information while reducing the low-frequency information in an image. Two sharpening filters can be used.
  - High-pass: This filter is implemented using a kernel designed to increase the brightness of the centre pixel relative to neighbouring ones.
  - Sharp: The kernel of this filter is similar to the high-pass one but the central value has more weight.

- ***Smoothing***: Smoothing filters are often used to reduce noise or to produce a less pixelated image. An image is smoothed by the application of a low-pass filter, which decreases the disparity between pixel values by averaging nearby pixels. Three different filters are including in this drop-down sub-menu:
  - Low-pass: This filter retains the low-frequency information in an image while reducing the high-frequency information.
  - Smooth: This filter replaces each point with the average value of the neighbouring n pixels.
  - Median: This filter replaces each point with the median of neighbouring n pixels. It is very effective in removing isolated high or low noise values since

it does not blur edges larger than the neighbourhood. An example of the filter function can be seen in Figure 7.3.

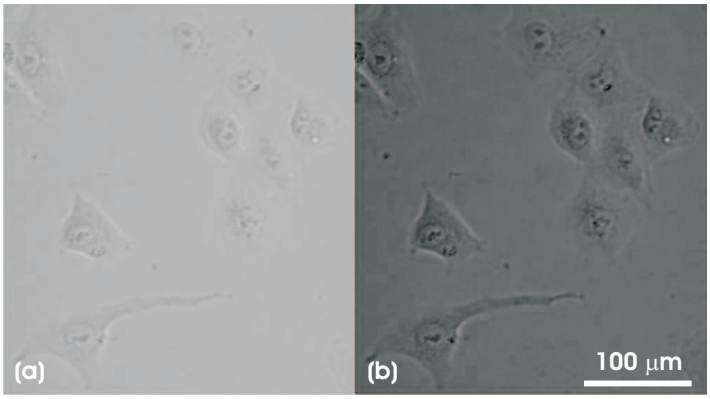

Figure 7.3: (a) Image of cells from a human lung adenocarcinoma epithelial cell line (A549). (b) The image has been smoothed with a median filter. The image contrast has been modified to make the features of the filter clearer.

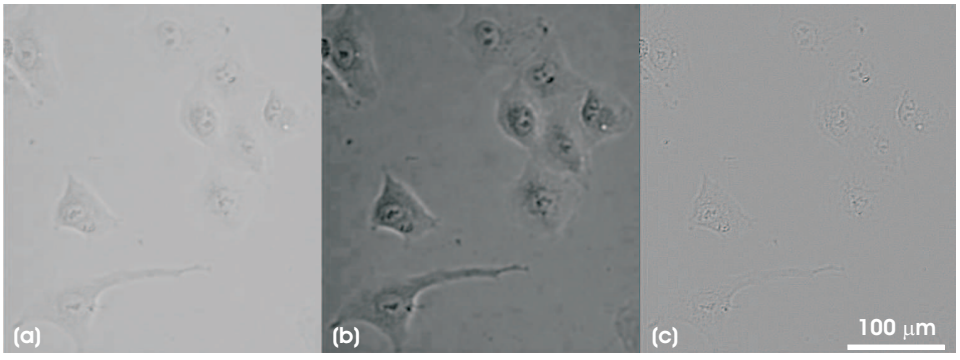

Figure 7.4: (a) Image of cells from a human lung adenocarcinoma epithelial cell line (A549). (b) The background noise has been removed by applying a Lee filter. (c) Cell structures can be enhanced by combining the original and filtered images. The image contrast has been modified to make the features of the filter clearer.

- ***Remove noise***: - FFT: The image is transformed into the frequency domain and thresholded to remove the noise.
  - Hanning: This filter removes background noise and retains the low-frequency information in the image.

- Lee: This adaptive filter removes background noise. An example of the filter function can be seen in Figure 7.4.

7.4.4 User guide

In order to facilitate the use of the SeACell software, a simplified user guide is constantly visible when the program is running. The instructions are given below.

Use the FILE menu to open the image to be analysed. Jpeg images are preferred.
The TOOLS menu allows the colour display to be changed.
The FILTERS menu contains various image filters that can improve the quality of the input image.

A modified input image must be saved and re-opened before Automatic or Manual cell recognition can be applied.

Automatic cell recognition can be repeated as many times as required with different threshold values by clicking the appropriate button.

For Manual cell recognition, the target is selected by positioning the mouse over the centre of the cell and pressing the left mouse button. To complete the procedure, press the right mouse button.

The button "Coordinates to KMaX" is clicked to upload the targeted coordinates into the LNM-SIHF software system.

8

Custom tools for the LNM-SIHF

8.1 "Petri-type" dishes for irradiation

Specially developed Petri-type dishes allow the position of cell growth to be controlled to a certain degree. The cells can be confined by fabricating very small structures on the floor of the dish. In order to evaluate the damage to a single cell, the position of each cell must be determined before and after irradiation, i.e., the location of each cell should be maintained facilitating repeated access to them.

The irradiation dishes developed in this work have the advantage of being suitable for both cell incubation and holding the cells during irradiation. The cells are thus grown and irradiated on the same surface, which is an important technical advantage.

8.1.1 Custom-designed dishes for targeted irradiation

Several techniques were evaluated to fabricate the dishes. The first promising option was the use of soft lithography techniques in combination with polydimethylsiloxane (PDMS) as fabrication material. PDMS is deformable, homogeneous and durable elastomer consisting of repeating units of OSi(CH3)2-. After oxygen plasma treatment its surface becomes hydrophilic and is therefore cell friendly.

Special masks were fabricated to confine one cell in the PDMS structure by replica moulding. The result can be seen in Figure 8.1. However, the post-cell detection system at the LNM-SIHF restricts the thickness of the irradiation dishes, and as the fabrication technique used did not permit the thickness of the PDMS to be changed, this method was abandoned.

An alternative approach was used employing UV lithography in combination with the epoxy-based photopolymer SU-8 [18] as fabrication material, to obtain irradiation dishes with the desired thickness. The cell-friendly SU-8 dishes consist of a supporting layer with a thickness of approximately 5 μm, with 5 μm walls forming the structure. The entire structure occupies an area of 2 by 2 mm^2 and contains 400 squares of 80 x 80 μm, separated from the neighbouring ones by 20 μm wide walls. Each square can be identified by a row letter and column number printed outside the grid.

In order to supply the cell with the necessary culture medium, the SU-8 irradiation dish is glued onto a polystyrene cup forming an effective area of approximately $\pi/4$ cm^2.

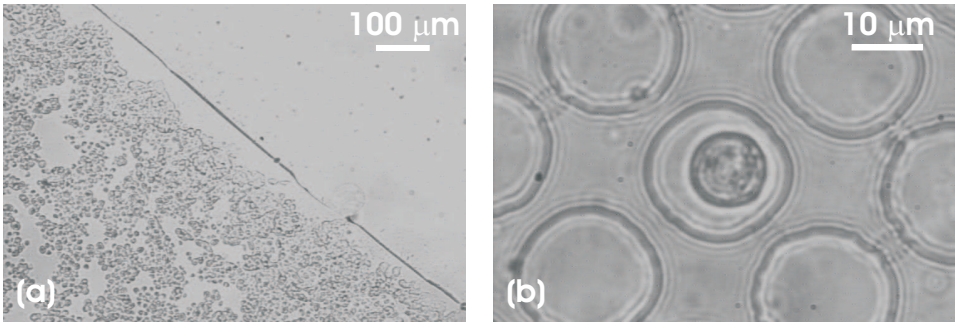

Figure 8.1: Tests were performed to check the viability of PDMS as fabrication material for an irradiation dish using the Chinese hamster V79 cell line. (a) The cell viability depends on the surface; only the hydrophilic part is suitable for cell growth. (b) PDMS irradiation dish where one cell can be grown in isolation. The effective culture area was 25 mm^2 and consists of circles 20 μm in diameter, 50 μm in depth, separated by 10 μm.

Details concerning the fabrication and performance of the SU-8 irradiation dish are given in *Paper II*.

8.1.2 Custom-designed dishes for non-targeted irradiation

High throughput is required for non-targeted irradiation experiments. The fabrication of the SU-8 irradiation dishes, designed for targeted irradiation, was time consuming. Moreover, they offered no advantages, and simpler approaches providing a larger effective culture area were therefore investigated.

Thin SU-8 film

A thin (5 μm) SU-8 film was used as the growing surface, without any pattern or barriers. The fabrication procedure was quite fast as only one UV exposure was required per irradiation "dish". The dish was manufactured by spin-coating a 5 μm SU-8 (2005) film on an optical glass. Then, the sample was soft baked and flood exposed with UV light. After exposure, the resist was post-baked. In order to lift the irradiation film off the glass, the sample was introduced into a NH_3:H_2O (1:1) + 3% H_2O_2 solution. Finally, the thin film was glued onto a polystyrene cap providing a cell culture area of approximately $\pi/4$ cm^2. Figure 8.2(a) shows the custom-made SU-8 irradiation dish.

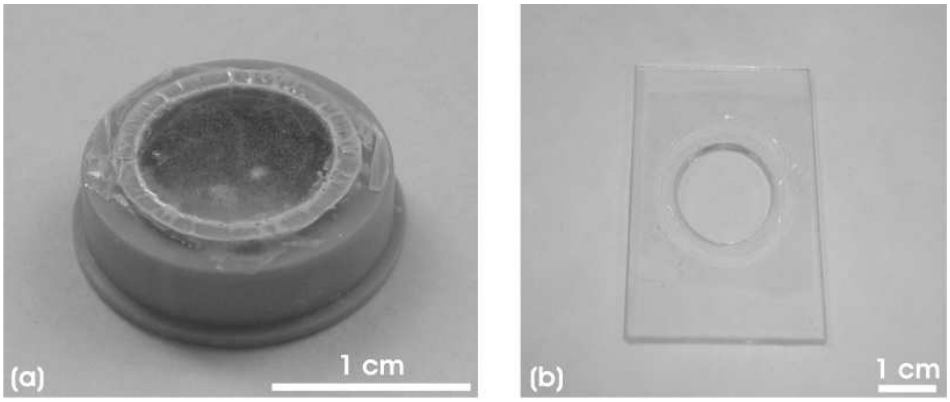

Figure 8.2: Custom-made "dishes" for non-targeted irradiation, mounted in their respective supports: (a) SU-8 and (b) Polypropylene.

Polypropylene

An 8 μm thick polypropylene layer, purchased from Goodfellow (England) [86], was used to culture the cells. This layer is attached by heat treatment to a polypropylene holder, 0.2 mm in thickness with a 7 mm radius hole. The effective culture area is thus $\pi/2$ cm^2. Figure 8.2(b) shows the polypropylene irradiation dish.

8.2 Artificial cell sample

Working with living cells is challenging since they need a controlled environment at a specific temperature and CO_2 concentration to maintain their viability. Removal of the cell culture medium prior to irradiation deprives the cells of their vital nutrients. They then start to die and detach from the surface in which they are growing. Consequently, the time available for the adjustment of the equipment and execution of the experiments is limited.

In order to solve this problem, a semi-realistic scenario was developed by the fabrication of an artificial cell sample in which the shape and size of the cells were maintained. The sample was manufactured by embedding living cells in the SU-8 photoresist and exposing them to UV radiation.

This artificial cell sample has been used for the following applications.

- To test the in-house cell recognition software, SeACell, *in vivo*. The implemented algorithm allows the parameterization of the cell shape and size when growing in the irradiation dishes (SU-8 or polypropylene).

- To test the illumination system, at the irradiation chamber, taking advantage

of the optical transparency of the resist.

- ❑ To calibrate the position of the selectable objectives (20X and 50X) used for sample inspection.

Paper III describes sample fabrication and its features in detail. The function of the SeACell software using the artificial cell sample is described in *Paper VI*.

8.3 Ni dot array

A custom-made sample was created to test the TA of the system. It was manufactured by UV lithography and EBL techniques using the photopolymers SU-8 and PMMA as fabrication materials. The two arrays have 5 μm and 2 μm diameter dots separated by 50 μm and 10 μm, respectively. For location purposes a cross formed by 70 μm x 20 μm lines, visible without a magnification lens, was also printed in the photopolymer.

These Ni dot arrays can also be used to estimate the beam size. However, they do not provide any information when the beam size is larger than the sample structures.

Paper III describes the sample fabrication and gives an account of the measured TA of the system.

8.4 Reference cross

A calibration sample was manufactured to establish the coordinates of the irradiation point in all the microscopes where the cells are inspected. The sample consists of a cross printed in the photopolymer SU-8 by UV lithography. The lines were 100 μm thick.

9

Biological applications at the LNM-SIHF

Collaboration has been established between BMC and the Engineering Faculty (LTH) at Lund University. The purpose of this is to investigate the importance of reactive oxygen species (ROS) in bystander cells following proton irradiation.

ROS are normally produced as a by-product of metabolism and are also considered to act as signal molecules in intracellular communication [87]. The production of ROS, which include superoxide anions (O_2^-), hydrogen peroxide (H_2O_2) and hydroxil radical (OH·), can be initiated in human cells by α particle irradiation [88]. An uncontrolled increase in the amount of ROS, either in the culture medium or intracellularly, will damage DNA in bystander cells [26]. In addition, high concentrations of ROS can also induce cell cycle arrest, senescence and cell death [89,90].

The cell protective effects of A1M against this process has been studied as there is evidence indicating that A1M is involved in the defence against oxidation caused by ROS [91].

9.1 The human hepatoma cell line

The cell line used for this research is the human hepatoma cell line (HepG2). This cell line was established in 1975 from the tumour tissue of a 15-year-old Argentinean boy with hepatocellular carcinoma. HepG2 cells are adherent, epithelial-like cells, growing as monolayer and in small aggregates. The population doubling time is approximately 50 to 60 hours [92].

Human hepatoma cells have been employed in several research studies. The SMMC-7721 cell line has been used to study the genotoxic effects of heavy-ion irradiation using single-cell electrophoresis [93]. Alterations in the cell cycle of the HepG2 cell line has been studied after ^{60}Co γ-irradiation, showing that cell growth is inhibited in a dose-dependent manner [94]. Moreover, photo-irradiation, using a 130 mW, 808 nm GaAlAs continuous-wave laser, has also been reported to have an inhibitory effect on cell proliferation [95].

9.2 The oxidation-sensitive probe H_2DCFDA

In order to investigate the oxidative status of the bystander cells, the oxidation-sensitive probe 2´,7´-dichlorodihydrofluorescein diacetate (H_2DCFDA) was used. After being added to the culture medium, this probe passes freely across the cell membrane and is cleaved intracellularly by esterases. Therefore, it is unable to cross back over the cell membrane, according to the manufacturer (Invitrogen [96]). Oxidative products formed and released by cells exposed to radiation have the ability to oxidise the intracellularly loaded probe. Consequently, the probe sends out fluorescent light that can be detected by fluorescence microscopy.

The use of the cell dye H_2DCFDA does not affect or facilitate the visualization of the cells prior to irradiation. Thus, a non-stained imaging system is still assumed at the LNM-SIHF.

9.3 Dose calculation

The absorbed dose can be obtained in terms of the fluence by applying the following formula:

$$Dose[Gy] = \frac{1.6 \cdot 10^{-9} \cdot LET[keV/\mu m] \cdot Fluence[particles/cm^2]}{\rho[g/cm^3]} \tag{9.1}$$

The LET of the incoming particle can be obtained, for example, using the program SRIM [16] with water as a target.

The fluence is related to the targeted area. The HepG2 cell line has a measured average cell area of 140 μm^2 [56]. Assuming an effective irradiation energy of 2.5 MeV at the cell monolayer, protons in water have an LET value of approximately 13.92 keV/μm. Therefore,

$$Dose\ per\ particle = 0.016\ Gy$$

Consequently, the maximum dose that can be delivered to a cell in the low-dose range, i.e., less than 0.2 Gy [21], is equivalent to approximately 12 protons.

This calculation does not include the finite width of an ion's track due to the lateral extension resulting from secondary electrons. This contribution can not be neglected for high-charge and high-energy particles since the geometrical cross-sectional area of the track exceeds the cross-sectional area of the cell. Consequently, the additional interactions can damage neighbouring cells or contribute to the bystander effect on cytoplasm.

The concept of radial dose is introduced to estimate the number of particle-track traversals per cell taking into account the contribution of the secondary electrons.

The effective area of a particle track, A_{track}, is defined by the average radial distribution in ionization and an appropriate cut-off value of the radial dose, D_{cut} [13]:

$$A_{track} = \pi \cdot (r_{track} + r_{cell})^2$$

where r_{track} is the radius of the track at the cut-off and r_{cell} the cell radius. The use of average quantities ignores stochastic variations, but the radial dose also neglects the increased biological effectiveness observed with low-energy electron fields. However, a reasonable estimate of the number of traversals is obtained.

The proximity effect is negligible for MeV protons and keV heavy ions since the energy is deposited within a radius of a nanometre [20]. Thus, the energy dissipated by secondary recoils can be neglected. Therefore, in the context of this thesis, where 2.5 MeV protons are used, Equation 9.1 provides a suitable dose estimate.

9.4 Preliminary results

HepG2 cells were cultured in thin film SU-8 irradiation dishes until they reached a confluent state. One hour prior to irradiation, the cells were loaded with the probe H_2DCFDA (3 μM concentration), incubated at 37°C for 30 minutes, washed and resuspended in fresh medium.

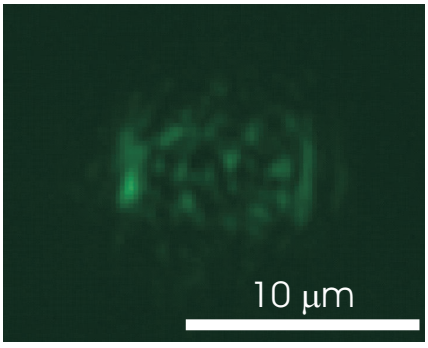

Figure 9.1: Oxidation levels approximately 24 hours after irradiation with single proton ($\sim$ 0.02 Gy).

Non-targeted irradiation was carried out in the absence of medium for the technical reasons discussed above. The cell cultures were exposed to 2.5 MeV focused protons in a single spot using a range of low doses, from 0.02 to 0.5 Gy. Two irradiation dishes were irradiated at each dose and a third one was used as a control sample. The control sample was exposed to the same protocol but no

protons were deposited in this sample. After irradiation, the cells were re-suspended in fresh culture medium. The induction of oxidation of the redox-sensitive probe H_2DCFDA was analysed using a fluorescence microscope. Figure 9.1 shows the damage caused to a single cell by single-proton irradiation.

The cell irradiation experiments carried out at the LNM-SIHF are explained extensively in *Paper V*.

9.5 Project status and future outlook

Further experiments are required to understand which processes lead to cell dead after irradiation. Data from several replicate experiments did not show cell damage concentrated in one spot, but a high background was observed in all the samples including the control one as can be seen in Figure 9.2. This fact indicates the existence of some mechanism, independent of the irradiation procedure, which produces extra oxidation. For instance, the cells were transported from the BMC to the LNM-SIHF, suffering temperature changes during the way which may cause stress.

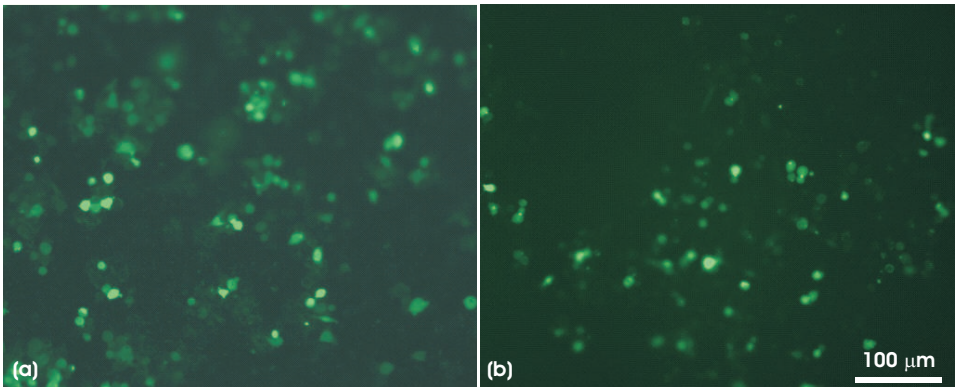

Figure 9.2: Oxidation levels approximately 3 hours after irradiation. (a) Control sample. (b) Irradiated sample: 0.1 Gy in a single spot.

The strategy chosen was based on the assumption that the cells should be as stress-free as possible to avoid undesiderable confounding factors that could influence the results. Thus, the project was focused on studying the bystander cell response to radiation in detail. Therefore, an α source was employed to simplify the irradiation procedure, avoiding the trip between facilities. Additionally, commercially available culture dishes were employed for the experiments. Finally, in order to check the amount of living and dead cells, new probes were purchased: Hoechst 33342 and PI.

These simplified experiments have shown an increase in cell death of both irradiated and bystander cells. Moreover, an increase in apoptosis, protein carbonyl groups and expression of the stress response genes heme oxygenase-1, p21 and p53 was observed. Additionally, A1M reduced the amount of dead cells and inhibited apoptosis, the formation of carbonyl groups and upregulation of heme oxygenase-1, p21 and p53 [9].

The next step is to verify these results by performing proton irradiation at the LNM-SIHF.

10

Popular scientific summary

A Single-Ion Hit Facility (SIHF) consists of a custom-build facility based in particle accelerators which offers irradiation controlling the number of delivered particles with a precise targeting localization. The irradiation spot can be confined down to the nanometre scale allowing the irradiation of subcellular compartments with a single particle. Therefore, these facilities have become a very powerful tool for biological applications specifically to study low-dose radiation effects on living cells.

A SIHF has been created at the Lund Nuclear Microprobe (LNM-SIHF) and, in order to make it operational, several tools were fabricated. These tools included the necessary software for cell recognition, custom-designed Petri-type dishes suitable for cell culture and irradiation, and other tools which allow the evaluation of the system. Additionally, the importance of reactive oxygen species (ROS) in bystander cells after non-targeted proton irradiation was investigated on the human hepatoma cell line (HepG2).

In-house implemented software, SeACell, provides on-line cell recognition and localization in a short time and high efficiency without the use of cell-staining dyes. The program was developed using IDL 6.2 language, and includes automated and manual targeting selection through a user-friendly interface. In addition, table colour display and filter drop-down menus were added to improve the quality of the input image if required.

Custom-designed irradiation dishes permit controlling the cells growth position by confining them through limiting structures on the floor of the dish and therefore, facilitating repeated access to the cell position. The epoxy-based photopolymer SU-8 was patterned by UV lithography technique producing irradiation dishes, with a supporting layer of approximately 5 μm thick, where 5 μm height walls were used to form the limiting structure. The entire structure contains 400 squares that can be located by a row letter and column number printed outside the grid.

Other tools were manufactured by UV large exposure and the SU-8 photoresist: an artificial cell sample, which offered a semi-realistic scenario to test the system's capability, and a calibration sample used to establish the coordinates of the irradiation point in all the microscopes in which the cells were inspected. Also, two Ni dot arrays were fabricated using electron beam lithography to test the targeting accuracy of the system.

Acknowledgments

I would like to express my most sincere gratitude to my supervisor, Dr. Jan Pallon, who gave me the opportunity to carry out this work.

My deepest gratitude goes to my assistant supervisor, Professor Per Kristiansson, for his help, especially at weekends and after office hours.

Obviously, this thesis would not have been possible without the contributions of co-authors and collaborators. Special thanks to the rest of the Microprobe Group at the Nuclear Physics Department: Dr. Vaida Auzelyte, Dr. Marie Wegdén, Dr. Mikael Elfman, Dr. Charlotta Nilsson, Christer Nilsson and PhD student Maciek Borysiuk. My sincere gratitude also goes to collaborators at the Division of Infection Medicine at the BMC: Dr. Magnus Olsson, Professor Bo Åkertström and PhD student Sigurbjörg Rutardóttir.

I would like to apologise to Christer Nilsson for all the things I have broken in my attempt to learn, *förlåt!!* I hope you are aware that the list is in reality shorter than it seems, but the buck always stops with the person lowest in the hierarchy.

On a personal level, I really appreciate the help of our secretary, Britt-Marie Kallerhed, for handling the complicated Swedish bureaucracy regarding work and, even more complicated, getting a doctor's appointment. Thank you from the bottom of my heart!

I would also like to thank the past and present PhD students who have made daily life more pleasant during the past years.

My life in Sweden would not have been the same without my friends. I have become a extremely rich person regarding the mixture of cultures and the large amount of stories I have collected to entertain my children and hopefully grandchildren. Luckily for me, you are too many to be named. Thanks to all of you for an enjoyable experience.

I would like to especially thank my "best friends forever": Vaida, Cintia and Valeria for teaching me the simple things that makes one enjoy life in many different ways. You are, and always will be, part of my life.

Olga and Josep, thanks for always being there, for listening to my "complains" and for all the valuable time we spent together.

Last but not least, I want to express my gratitude to the most precious gifts I have received from Sweden: Audrius and Norberto. You have been the source of my inspiration, unconditional support and encouragement - my reason for living. Unfortunately, you have paid the highest price in the accomplishment of this PhD. No words can express how much I appreciate your sacrifices, due to my absences.

Me gustaría agradecer a mis padres, Tomás y Pilar, mis hermanas, Nuria y Nayra, y mis "hermanos", Fran y Juan, por siempre estar ahí. Su apoyo constante me ha ayudado a seguir adelante y, aunque nada podrá compensar mi larga ausencia, quiero que sepan que aprecio sinceramente su sacrificio.

A mis primas, Mana y Susi, quiero darles las gracias por sus continuas palabras de ánimo y por bombardearme con sus emails para mantenerme al tanto de la vida en el paraíso.

Finalmente, me gustaría agradecer a mi querido Eduardo su amistad y a sus padres por compartir su pérdida conmigo. Eduardo fue el culpable de que quisiera ser doctora y una de las razones que me han empujado todos estos años a continuar a pesar de los obstáculos. Siempre estas y estarás presente. Te echo de menos!

Bibliography

[1] Eric J. Hall and Amato J. Giaccia. *Radiobiology for the Radiologist*. Lippincott Williams & Wilkins, 2006.

[2] D. J. Brenner and E. J. Hall. Microbeams: A potent mix of Physics and Biology. Summary of the 5^{th} International Workshop on Microbeam Probes of Cellular Radiation Response. *Radiation Protection Dosimetry 99, 283*, 2002.

[3] G. Taucher-Scholz and W.K. Weyrather. Physical and molecular basis of the biological effects of charged particle radiation. *European Journal of Cancer Supplements 5 (4), 23*, 2007.

[4] M. Folkard, K.M. Prise, G. Grime, K Kirkby, and B. Vojnovic. The use of microbeams to investigate radiation damage in living cells. *Applied Radiation and Isotopes 67, 436*, 2009.

[5] R.E. Zirkle and W. Bloom. Irradiation of Parts of Individual Cells. *Science 117, 487*, 1953.

[6] K.M. Prise, O.V. Belyakov, H.C. Newman, S. Patel, G. Schettino, M. Folkard, and B.D. Michael. Non-targeted effects of radiation: Bystander responses in cell and tissue model. *Radiation Protection Dosimetry 99, 223*, 2002.

[7] M. Folkard, K. Prise, G. Schettino, C. Shao, S. Gilchrist, and B. Vojnovic. New Insights into the cellular response to radiation using microbeams. *Nuclear Instruments and Methods in Physics Research B 231, 189*, 2005.

[8] M.C. Joiner, B. Marples, P. Lambin, S.C. Short, and I. Turesson. Low-Dose Hypersensitivity: Current status and possible mechanisms. *International Journal of Radiation Oncology Biology Physics 49, 379*, 2001.

[9] M.G. Olsson, E.J.C. Nilsson, J. Paczesny, S. Rutardottir, J. Pallon, and B. Åkeström. Bystander cell death and stress response is inhibited by the radical scavenger α_1-microglobulin in irradiated cell cultures. *Submitted to Radiation Research*, 2010.

[10] C. Shao, J. Zhang, and K.M. Prise. Differential modulation of a radiation-induced bystander effect in glioblastoma cells by pifithrin-α and wortmannin. *Nuclear Instruments and Methods in Physics Research B 268, 627*, 2010.

[11] Kenneth S. Krane. *Introductory Nuclear Physics*. John Wiley & Sons, 1988.

[12] Glenn F. Knoll. *Radiation Detection and Measurement.* John Wiley & Sons, 1979.

[13] F.A.Cuccinota, H. Nikjoo, and D.T. Goodhead. The Effects of Delta Rays on the Number of Particle-Track Traversals per Cell in Laboratory and Space Exposures. *Radiation Research 150, 115*, 1998.

[14] William R. Leo. *Techniques for Nuclear and Particle Physics Experiments.* Springer-Verlag, 1994.

[15] E. H. Lee. Ion-beam modification of polymeric materials - fundamental principles and applications. *Nuclear Instruments and Methods in Physics Research B 151, 29*, 1999.

[16] Information available at www.srim.org.

[17] S.M. Sze. *Semiconductor devices. Physics and Technology.* John Wiley & Sons, 2002.

[18] Information available at www.microchem.com.

[19] J.M. Shaw, J.D. Gelorme, N.C. LaBianca, W.E. Conley, and S.J. Holmes. Negative photoresist for optical lithography. *IBM Journal of Research and Development, 41.*

[20] Vaida Auzelyte. *Direct writing with an MeV proton beam. Development and applications.* Doctoral Thesis, 2006.

[21] K.M. Prise, M. Folkard, and B.D. Michael. A review of the Bystander Effect and its implications for low-dose exposure. *Radiation Protection Dosimetry 104, 347*, 2003.

[22] G. Schettino, M. Folkard, K.M. Prise, B. Vojnovic, K.D. Held, and B. D. Michael. Low-Dose Studies of Bystander Cell Killing with Targeted Soft X Rays. *Radiation Research 160, 505*, 2003.

[23] C. Seymour and C. Mothersill. *Radiation Risk Estimates in Normal and Emergency Situations. Low dose radiation effects in the environment: Is fear or the science irrational?* Springer, 2006.

[24] K.M. Prise, G. Schettino, M. Folkard, and K.D. Held. New insights on cell death from radiation exposure. *The Lancet Oncology 6, 520*, 2005.

[25] L. Huang, P.M. Kim, J.A. Nickoloff, and W.F. Morgan. Targeted and Nontargeted Effects of Low-Dose Ionizing Radiation on Delayed Genomic Instability in Human Cells. *Cancer Research 67 (3), 1099*, 2007.

[26] R. Iyer and B.E. Lehnert. Factors underlying the Cell Growth-related Bystander Responses to α Particles. *Cancer Research 60, 1290*, 2000.

[27] G. Olivieri, J. Bodycote, and S. Wolff. Adaptive response of Human Lymphocytes to Low Concentrations of Radioactive Thymidine. *Science 223, 594*, 1984.

[28] J.D.Shadley, V. Afzal, and S. Wolff. Characterization of the Adaptive Response to Ionizing Radiation Induced by Low Doses of X rays to Human Lymphocytes. *Radiation Research 111, 511*, 1987.

[29] Y. Zhang, J. Zhou, J. Baldwin, K.D. Held, K.M. Prise, R.W. Redmond, and H.L. Liber. Ionizing radiation-induced bystander mutagenesis and adaptation: Quantitative and temporal aspects. *Mutation Research/Fundamental and Molecular Mechanisms of Mutagenesis 671, 20*, 2009.

[30] S. Wolff. The Adaptive Response in Radiobiology: Evolving Insights and Implications. *Environmental Health Perspectives 106, 277*, 1998.

[31] W.F Morgan. Non-targeted and Delayed Effects of Exposure to Ionizing Radiation: I. Radiation-Induced Genomic Instability and Bystander Effects *in Vitro*. *Radiation Research 159, 567*, 2003.

[32] C. Mothersill and C. Seymour. Radiation-Induced Bystander Effects: Past History and Future Directions. *Radiation Research 155, 759*, 2001.

[33] N. Rubio, A. Rajadurai, K.D. Held, K.M. Prise, H.L. Liber, and R.W. Redmond. Real-time imaging of novel spatial and temporal response to photodynamic stress. *Free Radical Biology and Medicine 47, 283*, 2009.

[34] S. Burdak-Rothkamm and K.M. Prise. New molecular targets in radiotherapy: DNA damage signaling and repair in targeted and non-targeted. *European Journal of Pharmacology 625, 151*, 2009.

[35] B.E. Lehnert and E.H. Goodwin. Extracellular Factor(s) following Exposure to α particles can cause Sister Chromatid Exchanges in Normal Human Cells. *Cancer Research 57, 2164*, 1997.

[36] C. Shao, M. Folkard, B.D. Michael, and K.M. Prise. Targeted cytoplasmic irradiation induces bystander responses. *Proceedings of the National Academy of Sciences USA 101, 13495*, 2004.

[37] K.M. Prise, S. Burdak-Rothkamm, M. Folkard, G. Kashino, C. Shao, and L. Tartier. New insights on radiation-induced bystander signalling and its relationship to DNA repair. *International Congress Series 1299, 121*, 2007.

[38] S.A. Amundson, K.T. Do, and A.J. Fornace Jr. Induction of Stress Genes by Low Doses of Gamma Rays. *Radiation Research 152, 225*, 1999.

[39] E.G. Wright. Inherited and inducible chromosomal instability: A fragile bridge between genome integrity mechanisms and tumourigenesis. *The Journal of Pathology 187, 19*, 1999.

[40] M.M. Vilenchik and A.G. Knudson. Inverse radiation dose-rate effects on somatic and germ-line mutations and DNA damage rates. *Proceedings of the National Academy of Sciences USA 97, 5381*, 2000.

[41] G. Randers-Pehrson, C. R. Geard, G. Johnson, C. D. Elliston, and D. J. Brenner. The Columbia University Single-Ion Microbeam. *Radiation Research 156, 210*, 2001.

[42] G. Garty, G. J. Ross, A. W. Bigelow, G. Randers-Pehrson, and D. J. Brenner. Testing the stand-alone microbeam at Columbia University. *Radiation Protection Dosimetry 122, 292*, 2006.

[43] M. Heiss, B. Fischer, B. Jakob, C. Fournier, G. Becker, and G. Taucher-Scholz. Targeted Irradiation of Mammalian Cells using a Heavy-Ion Microprobe. *Radiation Research 165, 231*, 2006.

[44] M. Folkard, B. Vojnovic, S. Gilchrist, K.M. Prise, and B.D. Michael. The design and application of ion microbeams for irradiating living cells and tissues. *Nuclear Instruments and Methods in Physics Research B 210, 302*, 2003.

[45] Ph. Barberet, S. Incerti, F. Andersson, F. Delalee, L. Serani, and Ph. Moretto. Technical description of the CENBG nanobeam line. *Nuclear Instruments and Methods in Physics Research B 267, 2003*, 2009.

[46] Ph. Barberet, A. Balana, S. Incerti, C. Michelet-Habchi, Ph. Moretto, and Th. Pouthier. Development of a focused charged particle microbeam for the irradiation of individual cells. *Review of Scientific Instruments, 76, 015101*, 2005.

[47] A.W. Bigelow, D.J. Brenner, G. Garty, and G. Randers-Pehrson. Single-Particle/Single-Cell Ion Microbeams as Probes of Biological Mechanisms. *IEEE Transactions on Plasma Science, 36, 4*, 2008.

[48] C. Fournier and G. Taucher-Scholz. Radiation induced cell cycle arrest:an overview of specific effects following high-LET exposure. *Radiotherapy and Oncology 73(2), S119*, 2004.

[49] K. Goetze, M. Scholz, G. Taucher-Scholz, and W. Mueller-Klieser. The impact of conventional and heavy ion irradiation on tumor cell migration in vitro. *International Journal of Radiation Biology 83(11-12), 889*, 2007.

[50] R. Ugenskiene, J. Lekki, V. Polak, K.M. Prise, M. Folkard, O. Veselov, Z. Stachura, W.M. Kwiatek, M. Zazula, and J. Stachura. Double strand break formation as a response to X-ray and targeted proton-irradiation. *Nuclear Instruments and Methods in Physics Research B 260, 159*, 2007.

[51] V. Polak, O. Veselov, J. Lekki, Z. Stachura, M. Zazula, R. Ugenskiene, M. Polak, and J. Styczen. Irradiating single cells using Cracow microprobe facility. *Nuclear Instruments and Methods in Physics Research B 249, 743*, 2006.

[52] Y. Kobayashi, T. Funayama, S.Wada, M. Taguchi, and H. Watanabe. Irradiation of single mammalian cells with a precise number of energetic heavy ions - Applications of microbeams for studying cellular radiation response. *Nuclear Instruments and Methods in Physics Research B 210, 308*, 2003.

[53] T. Funayama, S.Wada, Y. Kobayashi, and H. Watanabe. Irradiation of Mammalian Cultured Cells with a Collimated Heavy-Ion Microbeam. *Radiation Research 163, 241*, 2005.

[54] T. Reinert, A. Fiedler, J. Skopek, J. Tanner, J. Vogt, and T. Butz. Single ion bombardment of living cells at LIPSION. *Nuclear Instruments and Methods in Physics Research B 219-220, 77*, 2004.

[55] M. Rothermel, T. Butz, and T. Reinert. Rearranging a nanoprobe: Line foci, grid shadow patterns and performance tests. *Nuclear Instruments and Methods in Physics Research B 267, 2017*, 2009.

[56] N. Arteaga-Marrero, G. Astromskas, M.G. Olsson, M. Elfman, P. Kristiansson, E.J.C. Nilsson, C. Nilsson, and J. Pallon. Applications of SU-8 in the development of a Single Ion Hit Facility. *Nuclear Instruments and Methods in Physics Research B 267, 2117*, 2009.

[57] K.-D. Greif, H.J.Brede, D. Frankenberg, and U. Giesen. The PTB single ion microbeam for irradiation of living cells. *Nuclear Instruments and Methods in Physics Research B 217, 505*, 2004.

[58] K.Greif, W. Beverung, F. Langner, D. Frankenberg, A. Gellhaus, and F. Banaz-Yasar. The PTB microbeam: A versatile instrument for radiobiological research. *Radiation Protection Dosimetry 122, 313*, 2006.

[59] C.E.Hellweg, L. Spitta, A. Arenz, S. C. Bogner, R. Ruscher, C. Baumstark-Khan, K.-D. Greif, and U. Giesen. Transcriptional response of human cells to microbeam irradiation with 2.1 MeV α-particle. *Advances in Space Research 39, 1056*, 2007.

[60] A.W. Bigelow, G. J. Ross, G. Randers-Pehrson, and D.J. Brenner. The Columbia University microbeam II endstation for cell imaging and irradiation. *Nuclear Instruments and Methods in Physics Research B 231, 202*, 2005.

[61] G. Dollinger, V. Hable, A. Hauptner, R. Krücken, P. Reichart, A.A. Friedl, G. Drexler, T. Cremer, and S. Dietzel. Microirradiation of cells with energetic heavy ions. *Nuclear Instruments and Methods in Physics Research B 231, 195*, 2005.

[62] A. Hauptner, S. Dietzel, G.A. Drexler, P. Reichart, R. Krücken, T. Cremer, A.A. Friedl, and G. Dollinger. Microirradiation of cells with energetic heavy ions. *Radiation Environmental Biophysics 42(4), 237*, 2004.

[63] V. Hable, C. Greubel, A. Bergmaier, P. Reichart, A. Hauptner, R. Krücken, H. Strickfaden, S. Dietzel, T. Cremer, G.A.Drexler, A.A.Friedl, and G. Dollinger. The live cell irradiation and observation setup at SNAKE. *Nuclear Instruments and Methods in Physics Research B 267, 2090*, 2009.

[64] H. Imaseki, T. Ishikawa, H. Iso, T. Konishi, N. Suya, T. Hamano, X. Wang, N. Yasuda, and M. Yukawa. Progress report of the single particle irradiation system to cell (SPICE). *Nuclear Instruments and Methods in Physics Research B 260, 81*, 2007.

[65] T. Konishi, T. Ishikawa, H. Iso, N. Yasuda, M. Oikawa, Y. Higuchi, T. Kato, K. Hafer, K. Kodama, T. Hamano, N. Suya, and H. Imaseki. Biological studies using mammalian cell lines and the current status of the microbeam irradiation system, SPICE. *Nuclear Instruments and Methods in Physics Research B 267, 2171*, 2009.

[66] A. Shariff, C. Nilsson, V. Auzelyte, M. Elfman, P. Kristiansson, K. Malmqvist, J. Pallon, and M. Wegdén. The Lund Nuclear Microprobe sub-micron set-up. Part I: Ion optics calculation. *Nuclear Instruments and Methods in Physics Research B 231, 7*, 2005.

[67] V. Auzelyte, M. Elfman, P. Kristiansson, K. Malmqvist, L. Wallman, C. Nilsson, J. Pallon, A. Shariff, and M. Wegdén. The beam blanking system for microlithography at Lund Nuclear Microprobe. *Nuclear Instruments and Methods in Physics Research B 219-220, 485*, 2004.

[68] J. Pallon, V. Auzelyte, M. Elfman, M. Garmer, P. Kristiansson, K. Malmqvist, C. Nilsson, A. Shariff, and M. Wegdén. An Off-axis STIM procedure for precise mass determination and imaging. *Nuclear Instruments and Methods in Physics Research B 219-220, 988*, 2004.

[69] P. Golubev, P. Kristiansson, N. Arteaga-Marrero, M. Elfman, K. Malmqvist, E.J.C. Nilsson, C. Nilsson, J. Pallon, and M. Wegdén. First results from the Lund NMP particle detector system. *Nuclear Instruments and Methods in Physics Research B 267, 2065*, 2009.

[70] M. Elfman, J. Pallon, V. Auzelyte, P. Kristiansson, K. Malmqvist, C. Nilsson, A. Shariff, and M. Wegdén. The Lund Nuclear Microprobe sub-micron set-up. Part III: Sample stage, optical imaging and detector configuration in the experimental chamber. *Nuclear Instruments and Methods in Physics Research B 231, 14*, 2005.

[71] Ch. Nilsson, J. Pallon, G. Thungström, N. Arteaga, V. Auzelyte, M. Elfman, P. Kristiansson, C. Nilsson, and M. Wegdén. Evaluation of a pre-cell hit detector for the future single ion hit facility in Lund. *Nuclear Instruments and Methods in Physics Research B 249, 924*, 2006.

[72] E.J.C. Nilsson, J. Pallon, G. Thungström, N. Arteaga Marrero, M. Elfman, P. Kristiansson, C. Nilsson, and M. Wegdén. Characterization of a pre-cell hit detector to be used in single-cell irradiation experiments at the Lund Nuclear Microprobe. *Nuclear Instruments and Methods in Physics Research B 266, 4808*, 2008.

[73] M. Elfman, P. Kristiansson, K. Malmqvist, and J. Pallon. The layout and performance of the Lund nuclear microprobe trigger and data acquisition system. *Nuclear Instruments and Methods in Physics Research B 158, 141*, 1999.

[74] Information available at www.silson.com.

[75] Mikael Elfman. *Development of a Data Acquisition System at a Nuclear Microprobe with Applications in the Geo- and Biosciences*. Doctoral Thesis, 2001.

[76] M. Elfman, P. Kristiansson, K. Malmqvist, J. Pallon, A.Sjöland, R. Utui, and C. Yang. New CAMAC based data acquisition and beam control system for Lund nuclear microprobe. *Nuclear Instruments and Methods in Physics Research B 130, 123*, 1997.

[77] P. Kristiansson, M. Borysiuk, N. Arteaga-Marrero, M. Elfman, E.J.C. Nilsson, C. Nilsson, and J. Pallon. A pre-sample charge measurement system for quantitative NMP-analysis. *Nuclear Instruments and Methods in Physics Research B - In Press*, 2010.

[78] I. Ratja, E. Baradács, A.A. Bettiol, I. Csige, K. Tökési, L. Budai, and Á.Z. Kiss. Optimization of particle fluence in micromachining of CR-39. *Nuclear Instruments and Methods in Physics Research B 231, 384*, 2005.

[79] D. Xiaojiao, L. Xiaofei andT. Zhixin, H. Yongsheng, G. Shilun, Y. Dawei, and W. Naiyan. Calibration of CR-39 with monoenergetic protons. *Nuclear Instruments and Methods in Physics Research A 609, 190*, 2009.

[80] M. Luszik-Bhadra, F. dÉrrico, L. Lusini, and B. Wiegel. Microdosmetric investigations in a proton therapy beam with sequentially etched CR-39 track detectors. *Radiation Protection Dosimetry 66, 353*, 1996.

[81] Ch. Nilsson, S. Petriconi, T. Reinert, and T. Butz. The new target chamber at LIPSION: The new translation stage and goniometer and the new irradiation platform for single cell experiments. *Nuclear Instruments and Methods in Physics Research B 260, 71*, 2007.

[82] Hu Zhiwen, Yu Zengliang, Wu Lijun, Hu Suhua, and Xu An. An optimization control program for the ASIPP microbeam. *Nuclear Instruments and Methods in Physics Research A 507, 617*, 2003.

[83] R. Iyer and B.E. Lehnert. Effects of Ionized Radiation in Targeted and Non-targeted Cells. *Archives of Biochemistry and Biophysics 376, 14*, 2000.

[84] Information available at www.ittvis.com/idl.

[85] R.C. Gonzalez and R.E. Woods. *Digital Image Processing*. Prentice-Hall, Inc., 2002.

[86] Information available at http://www.goodfellow.com.

[87] I.A. Gamaley and I.V. Klyubin. Roles of Reactive Oxygen Species: Signaling and Regulation of Cellular Functions. *International Review of Cytology 188, 203*, 1999.

[88] P.K. Narayanan, E.H. Goodwin, and B.E. Lehnert. α Particles initiate biological production of superoxide anions and hydrogen peroxide in human cells. *Cancer Research 57, 3963*, 1997.

[89] J.B. Little, E.I. Azzam, S.M. de Toledo, and H. Nagasawa. Characteristics and mechanisms of the bystander response in monolayer cell cultures exposed to very low fluences of alpha particles. *Radiation Physics and Chemistry 72, 307*, 2005.

[90] J.B. Little, H. Nagasawa, S.M. de Toledo, and E. Azzam. Transmission of damage signals from irradiated to nonirradiated cells. *International Congress Series 1236, 229*, 2002.

[91] M.G. Olsson, M. Allhorn, T. Olofsson, and B. Åkeström. Up-regulation of α_1-microglobulin by hemoglobin and reactive oxygen species in hepatoma and blood cell lines. *Free Radical Biology & Medicine 42, 842*, 2007.

[92] Information available at http://www.dsmz.de/index.htm.

[93] L.M Qiu, W.J. Li, X.Y. Pang, Q.X. Gao, Y. Feng, L.B. Zhou, and G.H. Zhang. Observation of DNA damage of human hepatoma cells irradiated by heavy ions using comet assay. *World Journal of Gastroenterology 9(7), 1450*, 2003.

[94] X.X. Guan, L.B. Chen, G.X. Ding, W. De, and A.H. Zhang. Transfection of $p27^{kip1}$ enhance γ radiosensitivity induced by ^{60}Co gamma irradiation in hepatocellular carcinoma $HepG_2$ cell line. *World Journal of Gastroenterology 10(21), 3103*, 2004.

[95] Y.H. Liu, C.C. Ho, C.C.Cheng, Y.H. Hsu, and Y.S. Lai. Photoirradiation could influence the cytoskeleton organization and inhibit the survival of human hepatoma cells in vitro. *Lasers in Medical Sciences 21, 42*, 2006.

[96] Information available at http://www.invitrogen.com.

I

The New Cell Irradiation Facility at the Lund Nuclear Probe

Paper I

II

A SU-8 Dish for Cell Irradiation

Paper II

III

Applications of SU-8 in the Development of a Single-Ion Hit Facility

Paper III

IV

SeACell: Cell Recognition Software for a Single-Ion Hit Facility

Paper IV

V

Oxidative Effects Studies and Updated Technical Description of the Lund Nuclear Microprobe Single-Ion Hit Facility

Paper V

Available online at www.sciencedirect.com
ScienceDirect
Nuclear Instruments and Methods in Physics Research B 260 (2007) 91–96
NIM B
Beam Interactions with Materials & Atoms
www.elsevier.com/locate/nimb

The new Cell Irradiation Facility at the Lund Nuclear Probe

N. Arteaga-Marrero [a,*], J. Pallon [a], M.G. Olsson [b], V. Auzelyte [a], M. Elfman [a], P. Kristiansson [a], K. Malmqvist [a], C. Nilsson [a], M. Wegdén [a]

[a] Division of Nuclear Physics, Department of Physics, Lund Institute of Technology, Lund University, Professorsgatan 1, Box 118, SE-22100 Lund, Sweden
[b] Clinical and Experimental Infection Medicine (BMC), Sölvegatan 19, B14, SE-22184, Lund, Sweden

Available online 11 February 2007

Abstract

The CELLION project is directed towards the studies on cellular response to targeted single ions. This paper gives an account of the modifications made at the Lund sub-micron beam line in order to create a Single Ion Hit Facility for biological applications within the CELLION project.

The most relevant new feature is the specially developed software used to locate the cells. A program for cell recognition and localization that gives the coordinates of the centre of the cells has been designed. The recognition is made online. A picture taken by a microscope is used as input parameter for the recognition program. Using V79 Chinese hamster cells, the recognition procedure can be done in less than 0.5 s for a picture size of 800×600 pixels with approximately 96% efficiency.

This paper also reports target accuracy test results and the first non-targeted irradiation procedure performed at the Lund sub-micron beam line.

Keywords: CELLION; Single ions; Cell; Irradiation

1. Introduction

The CELLION project was designed to investigate the different aspects of cellular response to targeted single ions. The final aim of the project is to study low dose radiation effects, and further the relation between low dose radiation and radiotherapy. Several institutions in Europe are dedicated to this objective and a few of them are already operational like the Gray Cancer Institute in the UK [1,2] or GSI in Germany [3]. These facilities are leading the knowledge race and setting the research lines for the other institutions. For instance, the Gray Cancer Institute is already studying which part of the cells (cytoplasm, nucleus, membrane, etc) is triggering the response of the cell to the irradiation process, and thus should be considered as the actual target for the incoming protons [4].

The Lund Nuclear Probe has been subjected to some modifications to create a Single Ion Hit Facility. For the facilities still under development, the questions established by the leading institutions can direct in a more efficient way the modifications which should be done to achieve a full operational state. In addition, these institutions define the important parameters that should be checked for a correct performance of the facility: target accuracy, speed of the irradiation procedure, and so on [3,4].

The Lund Single Ion Hit Facility is currently operative. This paper describes the system operation and tests the key parameters to perform cell irradiation. In addition, there is an alternative to single ion irradiation: non-target irradiation, which has been achieved successfully at the Lund facility.

2. System description

The Lund Nuclear Probe is using a 3 MeV single-ended Pelletron electrostatic accelerator. The sub-micron beam

* Corresponding author. Tel.: +46 46 2227630; fax: +46 46 2224709.
E-mail address: natalia.arteaga@nuclear.lu.se (N. Arteaga-Marrero).
URL: http://www.pixe.lth.se/cellion/ (N. Arteaga-Marrero).

0168-583X/$ - see front matter © 2007 Elsevier B.V. All rights reserved.
doi:10.1016/j.nimb.2007.01.255

line uses a two stage beam focusing system with a doublet at each stage. In the first stage the beam is focused into an intermediate chamber. The virtual image created at the first stage is used as a virtual object for the second stage [5]. A fast beam deflecting system, which consists of two parallel metal plates connected to a high voltage generator, is used to switch off the beam on demand. This system has an activation speed of 200 ns [6].

The irradiation chamber at the sub-micron beam line has been adapted for biological experiments by extracting the beam to the atmospheric environment. Vacuum window key requirements are low beam induced background emission, radiation damage resistance, minimized straggling production and minimum thickness. In our system a 200 nm (1.5×1.5 mm) Si_3N_4 layer is used as vacuum window. This material is used at other facilities [3,7] but also a Mylar foil can fulfil the requirements [1,8]. The beam quality deteriorates outside the vacuum system due to scattering processes in air; thus, the distance which the beam travels through air has to be minimised. An extensible pipe brings the beam close to the sample in order to minimize the air gap (Fig. 1). Occasional damage of the vacuum system can occur by the breakage of the vacuum window. To avoid accelerator damage a vacuum guard has been installed. When the vacuum sensor detects a vacuum level higher than 10^{-3} mbar, all valves are closed immediately.

The magnetic scanning system [9], positioned inside the irradiation chamber, allows us to direct the ion beam towards the desired cell coordinates. A silicon surface barrier detector is used to detect the protons that have passed the cells, post cell detection.

A microscope connected to a CCD camera is located at the end of the experimental chamber. The detector as well as several objective lenses with different magnifications are mounted on a movable platform. In order to visualize the cells, the detector position is replaced by the selected objective.

A more detailed description of the beam line can be found in previous papers [9,10].

A vital requirement for single ion detection is to have a low beam current. Since single protons are needed, the current is limited by closing the object and aperture slits to the beam intensity of 1000 ions per second. The beam deflection system combined with the after target particle detector is used to prevent secondary hits, i.e. to limit the dose applied: once a cell has been irradiated, the beam is blanked while the magnetic steerers prepares for the position of the next cell.

3. Cell recognition software

Once the dish with the cells is positioned vertically on the sample holder and visualized, a picture is captured. The system operation begins by introducing this picture as an input parameter into the cell recognition program. The recognition is made online using the specific implemented software written in IDL language [11]. The goal is to obtain the central coordinates of the cells identified. Since non-stained cells have been used so far and the procedure is not completely optimized, our main purpose at the moment is to identify and locate the cells as single entities, i.e. we do not intend yet to distinguish between cytoplasm and nucleus. Usually, the cells are darker than the background; thus, applying a threshold we can select the darker regions which thereafter are labelled as probable cells. Among the cell candidates there can also be water drops, bubbles, dead cell fragments, etc. Thus, we need a selective procedure that can identify the real cells.

The probability distribution function (PDF) of the areas of each detected region was studied. Fig. 2 shows that, overall, the function follows a log-normal distribution. This kind of distribution is expected if a variable is the product of a large number of independent, identically-distributed variables [12]. The population doubling level of a

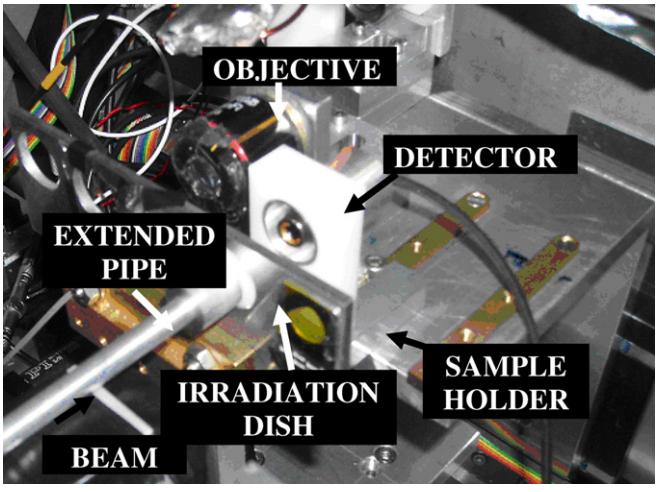

Fig. 1. Picture of the most important components at the irradiation chamber.

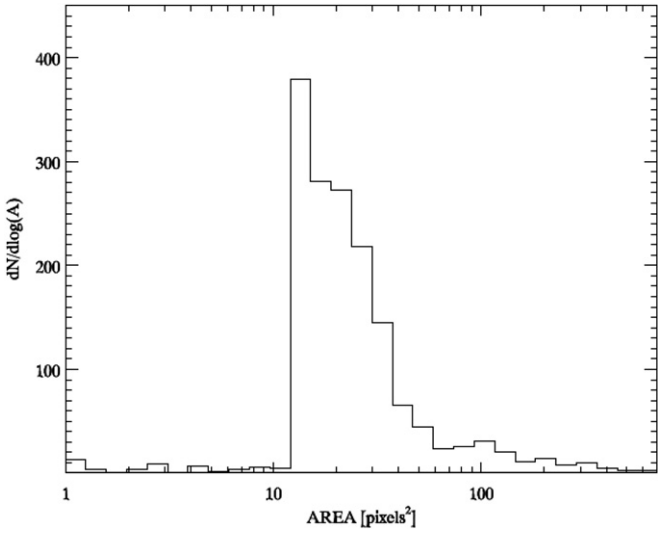

Fig. 2. Probability distribution function of the areas of the cell candidates.

cell culture is based on the assumption that the population increases exponentially. Each cell undergoes sequential symmetric divisions and at the end of N generations, each cell produces 2^N cells. Since the areas correspond to 2^N cells instead of N, the distribution that the areas follows is log-normal and not just Gaussian [13].

Notice that the areas below 10 depart substantially from the distribution that the values above 10 follow. This likely means that they do not correspond to real cells but rather to cell fragments or just noise in the detection procedure. Consequently, all the cell candidates which do not follow the log-normal distribution are excluded.

However, not all the remaining regions are real cells. Therefore, we need another criterion in order to pin down the actual cells. We can use the parameter R, which we defined as the ratio between the area and the perimeter of a cell candidate. Cells have a preferred ratio and this is different from the R that other particles prefer. For a drop of water (spherical shape) the R values are expected to follow the relation: $R \approx \frac{\text{perimeter}}{4\pi}$. In the cells case, since the cells shape is more irregular, a different relation is expected: $R < \frac{\text{perimeter}}{4\pi}$. Thus, attending to this R parameter, all the regions that differ from the mean by more than a certain fraction of standard deviation are also discarded. The remaining regions are considered real cells since they have approximately the same R value.

The appropriate value for the standard deviation was chosen following Fig. 3, where a study of the relation between the efficiency and the standard deviation values is shown. The best results were obtained for a value of 1σ.

Afterwards, the coordinates of the centres of the selected cells are transferred to the beam positioning system in a text file form. The text file contains a complete list of all image pixel coordinates (x, y). The controlling software reads the coordinates of the pixels that contain the centre of the cells to be irradiated, and thereafter sends its coordinates to CAMAC (Data Acquisition System) where they can be clocked with any frequency [14]. The scanning magnet controller receives position information and directs the beam.

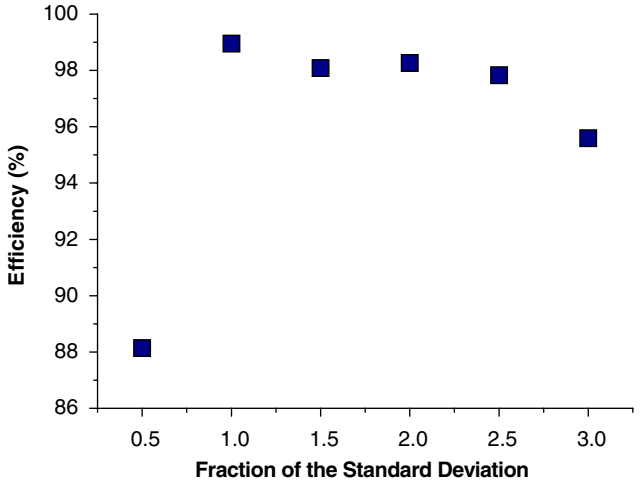

Fig. 3. Diagram showing the program efficiency in recognising real cells versus possible fractions of the standard deviation of the PDF of the R (area/perimeter) parameter.

The cells used for the analysis of the performance of the program were V79 Chinese hamster cells. In Fig. 4, the original image (800×600 pixels) and the results after processing can be seen. It should be mentioned that the picture was taken after trypsinization and the cells were not attached to the surface. That is the reason why they appear to have circular shape.

The recognition procedure for this picture is done in 0.2 s and the conversion to a text file in 0.3 s. The total procedure takes 0.5 s to be completed. The efficiency of the program is calculated counting the real number of cells in the picture and the number of real cells detected by the program. The ratio between these parameters defines the efficiency which in this case is $96\% \pm 4\%$. Some cell fragments are still considered as possible targets and some cells are missed as well. The program has been tested only with this image; thus, more input data is required in order to establish new parameters or criteria which can improve the performance of the program.

It is important to mention that the irradiation of the medium where the cells are kept can produce the activation of some free radicals. These may trigger some response from the cells. Since this effect has not been completely understood yet, it is crucial to target only the real cells and no other particles.

4. Target accuracy

In order to check the target accuracy of the system as well as the capability of the routine to locate the cells, scanning transmission ion microscopy (STIM) images were used. A copper grid was imaged in vacuum. These images were introduced into the cell recognition software to locate some points of the grid bars which we wanted to target (Fig. 5(a)). The white crosses show the places where the system is supposed to locate a proton. The beam is scanned over the sample and an energy loss spectrum is recorded (see Fig. 5(b)). This method was utilized previously at the GSI facility [15].

Two peaks where expected a priori. The peak associated with the protons that hit the grid bars is located at the lower energies. The second peak corresponds to the protons which pass through the grid holes without energy loss. Most of the protons fall inside the first peak but also some "miss" protons are detected. Besides, an additional peak is detected, which can be explained assuming that some protons hit the edges of the grid bars. In order to evaluate the hit accuracy we calculate the ratio between the number of protons which hit the bar and the total amount of protons detected. The hit rate was estimated to be close to 90%. However, the beam focusing was not optimized during the experiment and the beam size was 7 μm in the X direction and 7 μm in the Y direction. The beam size is modified when the protons are travelling through air even if the air gap between the vacuum window and the sample is

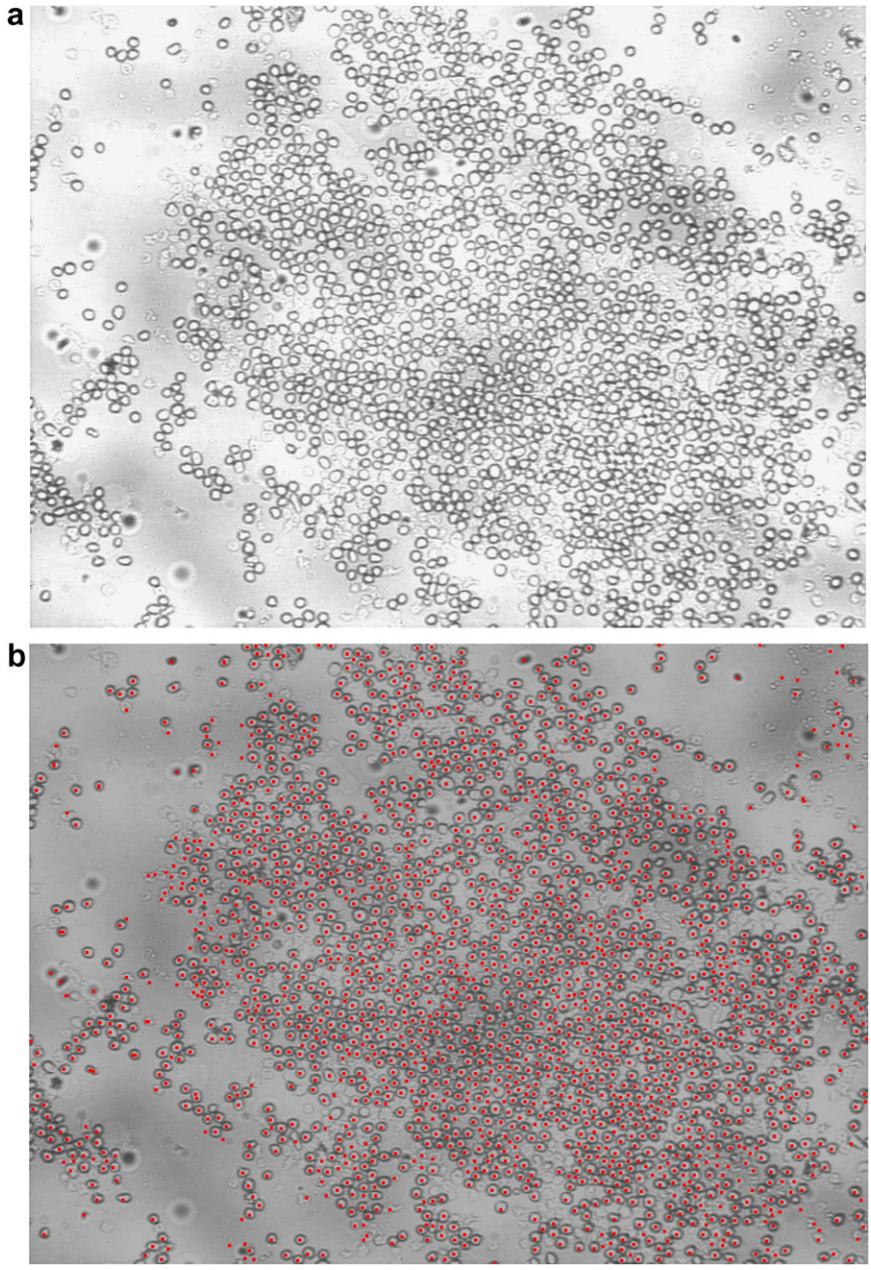

Fig. 4. Demonstration of the functioning of the cell recognition program. The original image (a) is displayed along with the processed one (b).

reduced. The accuracy of the system in vacuum must be improved, the test in air case remains to be done.

5. Irradiation

Technical and biological requirements are needed to develop an irradiation system for living cells. In order to evaluate the response of the cells to irradiation, it is very important to avoid procedures that can modify their natural state, i.e. the manipulation of the cells should be done without disturbing the function of the system. Otherwise factors unrelated to the irradiation process might influence the results. A wet environment as well as a good oxygen supply are important elements for the cell culture to stay healthy.

5.1. Technical issues

The cells used for the experiments are cultivated and analysed in a building situated at 5 min walk distance from the Lund Nuclear Probe. The survival of the cells was studied independently of the irradiation process. No increase in the cell mortality rate as a result of the transportation or the exposure to the facility environment was identified.

The Petri dish used to hold the cells has been fabricated using a very simple arrangement. A Si_3N_4 layer (200 nm thick) has been glued to the bottom of a polystyrene cup which fits into the sample holder. The culture medium is removed from the dish prior to the irradiation to ensure the detection of the protons after passing through the tar-

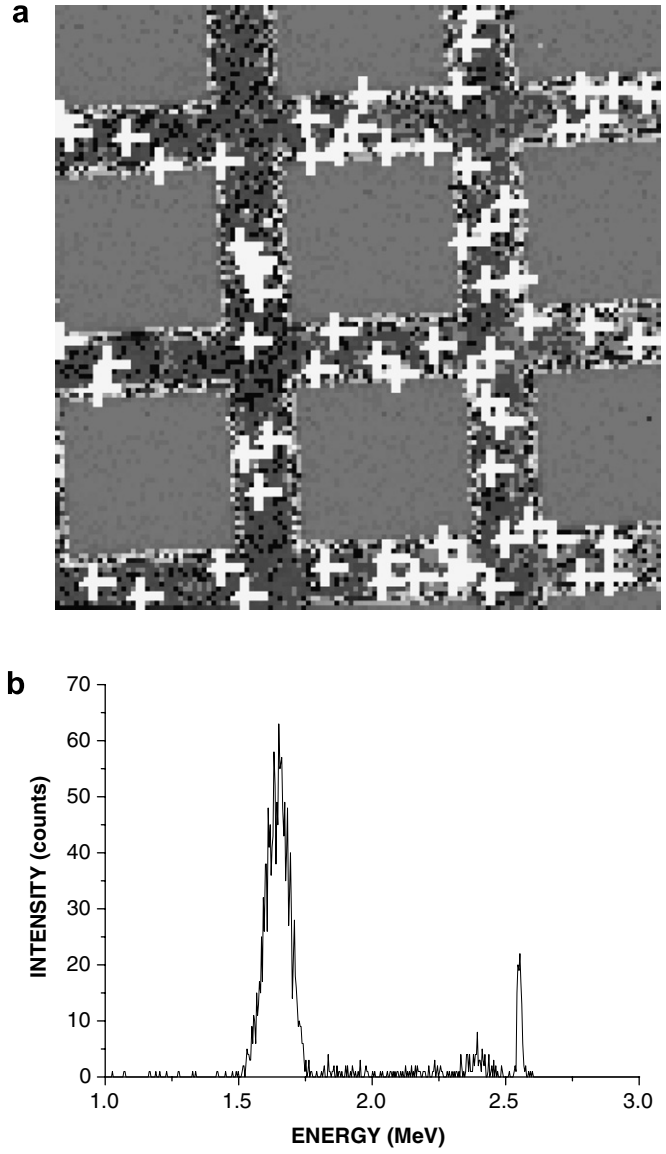

Fig. 5. Demonstration of the target accuracy of the system. (a) Selected regions to target in vacuum and (b) Energy loss spectrum recorded from the target accuracy experiment.

get. New medium is added after the irradiation; nevertheless, the irradiation procedure should be done as fast as possible because the cells need nutrients, oxygen and a wet environment.

The first cell irradiation carried out at the Lund Nuclear Probe has been non-targeted irradiation. Hepatoma cells (HepG2) were seeded and incubated one day before the irradiation. Previous to the irradiation procedure, the cells where observed at the microscope. They looked confluent and forming a homogenous layer above the surface. The pattern used is shown in Fig. 6. The pattern has 19 points and each dot in the pattern corresponds to two protons of 2.5 MeV except the points in the corners which receive an extra proton. The cell irradiation was recorded as an event file. These files contain information about the position and time of each signal coming to the acquisition system. The

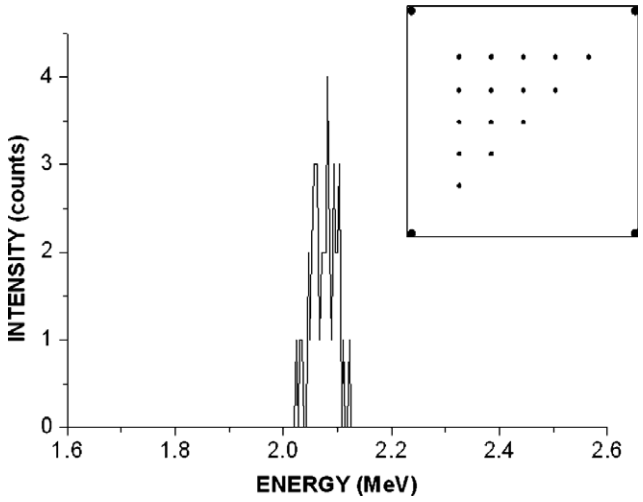

Fig. 6. Energy loss spectrum recorded and pattern stamped into the cell culture during the non-target irradiation procedure.

acquisition system also registered the energy loss spectrum during the event. It can be seen in the spectra (Fig. 6), that all the protons show the same energy loss. The peak contains exactly 42 counts, this means that the ions where shot and detected individually with 100% efficiency. The whole process was performed in approximately 3 min.

5.2. Biological issues

After the irradiation, the cells were stained with Trypan blue in order to determine the amount of dead cells. Only one proton was shot per pixel and after staining the cells there was no sign of the pattern shape. Subsequently, the cells were trypsinated and seeded in an ordinary Petri dish to follow their behaviour. No appreciable changes in cell growth were observed. Apparently, the dose applied was not enough to cause an observable damage to the cells.

6. Summary and future work

It has been shown that the Lund Nuclear Probe Facility has been adjusted for biological applications in air. The system is capable to control single ions. The cell recognition procedure is used with two purposes: to recognize possible cells and to upload the desired coordinates into the scanning system in order to target the cells. Regarding the cell recognition task, the implemented program capabilities can be improved but it is performing well. The targeting performance of the system in vacuum was tested using a copper grid and it was close to 90%. In addition, the system capabilities are not optimised yet but it has been possible to perform the first non-targeted cell irradiation successfully.

Important technical improvements are required in order to get a routinely operating cell irradiation system at the Lund sub-micron beam line. Fine tuning of the quadrupole magnets is needed to achieve a sub-micron beam size.

The scanning system must be improved in order to be able to irradiate large areas within the cell culture. New scanning coils have recently been installed and a new power supply is now being developed to increase the accuracy of the system.

Regarding biological aims, since the development of the facility has reached the appropriate state to start cell irradiation studies, two research lines should be kept: non-targeted irradiation and target irradiation. Non-target irradiation will be performed to study the variability of the culture redox state. Target irradiation is also planned but the spreading of the beam in air should be corrected in order to accomplish it.

Acknowledgements

We would like to thank Johan Christensson at the Department of Radiation Physics, The Finsen Centre (Copenhagen), who provided the cell picture that was used to test the cell recognition software and Eduardo J. Delgado-Donate at the IAC (Instituto de Astrofísica de Canarias) for his helpful suggestions on the data analysis. The support to the Lund Nuclear Microprobe facility by the Faculty of Engineering (LTH) is also acknowledged.

This work is supported by Marie Curie Research Training Network, MRTN-CT-2003-503923 and Crafoordska Stiftelsen N °20041003.

References

[1] M. Folkard, B. Vojnovic, K.M. Prise, A.G. Bowey, R.J. Locke, G. Schettino, B.D. Michael, Int. J. Radiat. Biol. 72 (1997) 375.
[2] M. Folkard, B. Vojnovic, K.J. Hollis, A.G. Bowey, S.J. Watts, G. Schettino, K.M. Prise, B.D. Michael, Int. J. Radiat. Biol. 72 (1997) 387.
[3] Markus Heiβ, Bernd E. Fischer, Burkhard Jakob, Claudia Fournier, Gudrun Becker, Gisela Taucher-Scholz, Radiat. Res. 165 (2006) 231.
[4] Melvyn Folkard, Kevin Prise, Giuseppe Schettino, Chulin Shao, Stuart Gilchrist, Boris Vojnovic, Nucl. Instr. and Meth. B 231 (2005) 189.
[5] A. Shariff, V. Auzelyte, M. Elfman, P. Kristiansson, K. Malmquist, C. Nilsson, J. Pallon, M. Wegdén, Nucl. Instr. and Meth. B 231 (2005) 1.
[6] Vaida Auzelyte, Mikael Elfman, Per Kristiansson, Klas Malmqvist, Lars Wallman, Christer Nilsson, Jan Pallon, Asad Shariff, Marie Wegdén, Nucl. Instr. and Meth. B 219–220 (2004) 485.
[7] T. Reinert, A. Fiedler, J. Skopek, J. Tanner, J. Vogt, T. Butz, Nucl. Instr. and Meth. B 219–220 (2004) 77.
[8] Klaus-D. Greif, Hein J. Brede, Dieter Frankenberg, Ulrich Giesen, Nucl. Instr. and Meth. B 217 (2004) 505.
[9] A. Shariff, C. Nilsson, V. Auzelyte, M. Elfman, P. Kristiansson, K. Malmquist, J. Pallon, M. Wegdén, Nucl. Instr. and Meth. B 231 (2005) 7.
[10] M. Elfman, J. Pallon, V. Auzelyte, P. Kristiansson, K. Malmquist, C. Nilsson, A. Shariff, M. Wegdén, Nucl. Instr. and Meth. B 231 (2005) 14.
[11] <http://www.ittvis.com/idl/index.asp>.
[12] <http://mathworld.wolfram.com/>.
[13] J.M. Davis, Basic Cell Culture, Oxford University Press, 2002.
[14] M. Elfman, P. Kristiansson, K. Malmqvist, J. Pallon, A. Sjoland, R. Utui, C. Yang, Nucl. Instr. and Meth. B 130 (1–4) (1997) 123.
[15] Guanghua Du, Bernd Fischer, Philippe Barberet, A fast online hit verification for the single ion hit system at GSI, in: Conference proceedings, 14th International Symposium on Microdosimetry, 2005.

Available online at www.sciencedirect.com
ScienceDirect
Nuclear Instruments and Methods in Physics Research B 263 (2007) 523–528
NIM B
Beam Interactions with Materials & Atoms
www.elsevier.com/locate/nimb

A SU-8 dish for cell irradiation

N. Arteaga-Marrero [a,*], V. Auzelyte [a,1], M.G. Olsson [b], J. Pallon [a]

[a] Division of Nuclear Physics, Department of Physics, Lund Institute of Technology, Lund University, Professorsgatan 1, Box 118, SE-221 00 Lund, Sweden
[b] Clinical and Experimental Infection Medicine (BMC), Sölvegatan 19, B14, SE-221 84 Lund, Sweden

Received 13 March 2007; received in revised form 5 June 2007
Available online 22 June 2007

Abstract

The objective of the CELLION project is radiation research at low doses. The main cell responses to low dose irradiation are bystander effects, genomic instability and adaptive responses. In order to study these effects it is convenient to make the cells addressable in space and time through locking the cell position. A new alternative dish has been developed for irradiation procedures at the Lund Nuclear Probe. The versatile dish can be used both to cultivate and to hold the cells during the irradiation procedure.

The irradiation dish is made of an epoxy-based photopolymer named SU-8 chosen by its flexibility, non-toxicity and biological compatibility to cell attachment. It has been fabricated using a UV lithographic technique. The irradiation dish forms a 2×2 mm^2 grid which contains 400 squares. Each square has 80 μm side and is separated from neighbouring ones by 20 μm wide walls. The location of each square is marked by a row letter and column number patterned outside the grid.

The Cell Irradiation Facility at the Lund Nuclear Probe utilizes protons to irradiate living cells. A post-cell detection set up is used to control the applied dose, detecting the number of protons after passing through the targeted cell. The transmission requirement is fulfilled by our new irradiation dish. So far, the dish has been used to perform non-targeted irradiation of Hepatoma cells. The cells attach and grow easily on the SU-8 surface. In addition, the irradiation procedure can be performed routinely and faster since the cells are incubated and irradiated in the same surface.

PACS: 87.50.−a; 87.80.Mj; 83.80.−k

Keywords: CELLION; Cell irradiation; Low dose effects; Microfabrication; SU-8

1. Introduction

Cellular response to very low doses has become a popular field of research and has set the trend for radiation exposure research over the past two decades. Responses such as the bystander effect, genomic instability and adaptive response are widely known but still poorly understood [1]. CELLION [2] is a European project directed towards the study of cellular responses to targeted single ions. Within these studies some responses are particularly relevant when the exposure is spread over time, i.e. the cells are irradiated, incubated for a variable time interval and irradiated again. Thus, it is important to control the area where the radiation is applied. That is, knowledge of the targeted cell and the region targeted within the cell are of vital importance in order to study low dose radiation responses. Cell position control is also a key parameter in the development of applications like cellular biosensors and tissue engineering [3].

In this paper, we describe the fabrication and operation of a new designed irradiation dish to be utilized at the Lund Nuclear Probe. The dish can be used to incubate and transport the cells to the irradiation facility, and also to hold the cells during the irradiation procedure. The cells

* Corresponding author. Tel.: +46 46 2227630; fax: +46 46 2224709.
E-mail address: natalia.arteaga@nuclear.lu.se (N. Arteaga-Marrero).
URL: http://www.pixe.lth.se/cellion/ (N. Arteaga-Marrero).
[1] Present address: Laboratory for Micro- and Nanotechnology, Paul Scherrer Institut, CH-5232 Villigen, Switzerland.

0168-583X/$ - see front matter © 2007 Elsevier B.V. All rights reserved.
doi:10.1016/j.nimb.2007.06.012

do not have to be changed to a different surface during the diverse steps of incubation, transportation and irradiation which minimizes the possibility of cell damage.

The dish was fabricated with the epoxy-based photopolymer SU-8. This negative photo resist has been widely used to fabricate high aspect ratio microstructures in addition to biological applications [4]. These applications include optical waveguides for on-line cell counting and sorting [5], bio-fluidic dermal patches to measure the concentration of bio-molecules [6], micro-channels for thermal flow-sensors [7] and the fabrication of SU-8 pallets to sort monolayer cultures for posterior cell assays [8].

2. Irradiation dish

At other facilities within the CELLION project, the cells are held in a vertical position for the irradiation procedure using modified commercial "Petri" dishes, the bottom of which are partially removed and substituted by a 200 nm Si_3N_4 film [9]. So far, at the Lund Nuclear Probe, 200 nm Si_3N_4 films were glued directly to a polystyrene sample holder avoiding the use of commercial plastic "Petri" dishes. The main advantage of the Si_3N_4 films is minimized straggling and maintained adequate beam focus. However, the necessity to utilize glue, which might be toxic to the cells, is a drawback. Additionally, the Si_3N_4 films are very fragile and expensive. They usually break during the preparation phase when gluing them to the selected surfaces. Another common problem is that after cell incubation, the Si_3N_4 films might present some culture medium leakage or break due to culture medium crystallization. The breakage of Si_3N_4 films is a common and frequent problem among the different facilities which use these thin films as "Petri" dishes. Hence improved irradiation dishes can increase the experimental throughput. As cell irradiation is intended to be done routinely, cheap and easier to handle alternatives must be developed.

The Lund Nuclear Probe uses a 3 MV single-ended electrostatic accelerator. The sub-micron beam line uses a two stage beam focusing system with a doublet at each stage [10,11]. Several experimental requirements should be fulfilled in order to expose living cells to single ions. The irradiation chamber has been adapted for biological experiments by extracting the beam into air. For that purpose a 200 nm Si_3N_4 film is used as a vacuum window, which holds a 10^{-6} mbar pressure.

The Cell Irradiation Facility at the Lund Nuclear Probe is a horizontal system; therefore, the irradiation dish which contains the cells must be vertically positioned. In addition, our set up has an after target particle detector (p–i–n diode) and consequently, the thickness of the irradiation dish has to be minimized to ensure the detection of the protons. A more detailed description of the Lund Cell Irradiation Facility can be found in a previous paper [12].

The selected cell type must grow in a monolayer culture. Basic cell requirements for the dish material are non-toxicity, transparency, a negatively charged and hydrophilic surface.

The above requirements demand:

(1) a design where cells will be confined in fixed positions to facilitate their location,
(2) a material whose thickness can be easily chosen,
(3) a material compatible with the living cells where they can attach and grow,
(4) a low atomic mass material to prevent a significant energy loss of the beam.

Additionally, since a large amount of cells should be irradiated routinely, the material should be cheap, have a long life time and be easy to handle. It should also be easily fabricated, in a fast and standardized fashion.

The SU-8 material fulfils those requirements, it is flexible, non-toxic and biologically compatible to cell attachment. It has good optical transmittance allowing visualization of the cells in our offline transmission microscope. SU-8 has low polymer shrinkage and can be easily patterned using conventional fabrication techniques that provide sufficient accuracy.

In our case, UV lithography has been chosen as the fabrication technique. A chromium mask is used to produce many dishes per exposure. The technique resolution is limited by wavelength and proximity effects (bad contact between mask and substrate). The resolution of the UV lithography system used to obtain the irradiation dishes is approximately 1 μm. However, it is further increased by the limitation produced by the fabricated mask, which is also 1 μm.

The UV mask was manufactured while taking into consideration the cell size and the irradiation procedure to be performed, in this case, non-targeted irradiation. In future a new mask will be designed in order to place one cell per square and to perform targeted irradiation.

The designed irradiation dish in which the cells can be seeded, grown and positioned during the irradiation procedure consists of a 2×2 mm^2 grid. The grid is divided in 400 squares by 20 μm wide walls. Each square has 80 μm side and its centre is marked by 10 μm wide cross, also patterned via mask, for irradiation purposes. The location of each square is externally labelled by a row letter and column number.

Two different thicknesses of SU-8 were used to fabricate the irradiation dishes: 2 μm flat base plus 2 μm tall walls on the top and 5 μm base plus 5 μm walls. The separation walls and the crosses have a similar height. Fig. 1 shows a top view of the dish with 5 μm base plus 5 μm walls, where the raised areas appear as darker regions compared with the bottom layer within the irradiation dish.

Non-targeted irradiation is planned to be accomplished in order to measure the system redox level after the irradiation procedure. The Hepatoma cells (HepG2) utilized are approximately 10 μm in size. Each square grid contains some cells. The dish allows individual doses per square

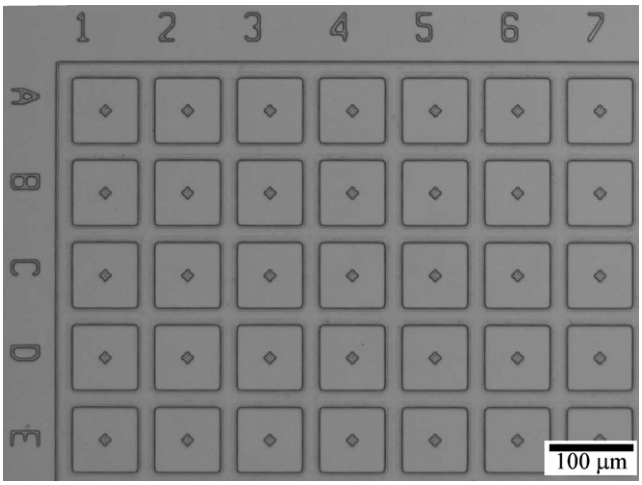

Fig. 1. The fabricated dish before being lifted off the substrate. The row letter and the column number are used in order to locate the different squares for irradiation purposes.

and several irradiations can be performed in the same dish. By not irradiating some regions, these can be used as control samples. It also allows for bystander effect studies: the walls that separate the squares are high enough to confine different regions, although the cells still can cross the walls facilitating interactions between different regions. However, the walls between squares cannot avoid contact among regions via culture medium after irradiation.

Another interesting characteristic of the SU-8, related to cell culture requirements is that the degradation temperature of SU-8 occurs at 380 °C [13]. This means that after baking at 95 °C, the irradiation dish survives the sterilization procedure (121 °C for 40 min) and consequently, can be re-used several times. So far, the irradiation dish life time is approximately four irradiation procedures, including sterilization.

In summary, cells can be easily grown and addressed in the dishes. Hence, the dish can be taken out of the irradiation system to incubate the cells and then be repositioned for later irradiations. The response of the cells to various irradiation procedures in different time intervals can thus be studied.

3. Fabrication

The cell irradiation dish was made in several steps. Two different substrates were tested in the microfabrication process, a silicon wafer and an optical glass.

In the silicon case, a four-inch Si wafer was sputtered with a Ti (10 nm)/Cu (200 nm) layers, cleaved, cleaned in acetone and isopropyl alcohol and baked for 30 min at 180 °C. The Ti/Cu coating is used as a release layer which allows the fabricated device to be easily lifted off the wafer. Titanium deposition is needed as an adhesion support for the copper [14]. Subsequently, the substrate is spin-coated with 2 μm or 5 μm of SU-8 (2005), soft baked and flood-exposed with UV-light. After this exposure, the resist was post-baked. This first SU-8 layer forms the base of the irradiation dish, which will support the grid patterned in the following UV lithography step.

A second layer 2 μm or 5 μm SU-8 was spin-coated again; soft baked, and patterned using UV lithography via a chromium mask with a dose of 100 mJ/cm^2. After exposure, the samples were post-baked again and developed. The baking and developing procedure were performed as recommended by the resist manufacturer [15].

In the following step, the two SU-8 layers structure was released from the substrate by etching the underlying Cu layer in NH_3:H_2O (1:1) + 3% H_2O_2 solution.

The fabrication process is similar when optical glass is used as a substrate except that no Ti/Cu release layer is needed. The irradiation dish is manufactured directly on the glass and no etching procedure is required. In order to release the structure from the substrate, the samples are immersed in a deionised water bath for approximately 10 min. This option is much simpler and requires less chemical agents than using Si as a substrate. However, we observed that cells were attached to the surface but they did not spread or grow when a glass substrate was used. The viability of the cell culture should be independent of the substrate used in the fabrication. Thus, the chemical agents used to lift the dish off the surface seem to affect the cell behaviour.

SU-8 is initially a hydrophobic polymer and the cells need a hydrophilic surface to attach and grow. Several methods have been reported to convert the SU-8 hydrophobic surface into hydrophilic one, for instance, oxygen plasma and wet chemical treatment with ethanolamine [16,17]. It has also been reported that the procedure to etch the Cu layer using cericammoniumnitrate (CAN) also modifies slightly the contact angle of the SU-8 surface but not as efficiently as ethanolamine [16]. To enhance cell attachment and cell growth, the surface of these kind of structures can be treated also physically by forming periodic nanogrooves [18]. Initially, it was assumed no extra surface treatments with the fabrication method which involves the use of silicon as fabrication substrate.

In order to lift the irradiation dishes off the glass substrate, NH_3:H_2O (1:1) + 3% H_2O_2 was used instead of just deionised water. It seems that this treatment also can be used to modify the SU-8 surface. It is not clear how efficiently the surface is changed into hydrophilic and this requires further investigations. Nevertheless, the produced effect is enough to promote cell growth which is the main aim of the fabricated dish.

The UV lithography mask was designed to produce nine irradiation dishes per one exposure. The sample is cut into smaller pieces separating the different irradiation dishes. Subsequently, each dish is attached to the bottom of a polystyrene cup, where a thin SU-8 layer was previously deposited. Finally, the cell dish is baked for 3 min at 100 °C, after which the dishes dry out at atmospheric temperature for approximately 30 min. Fig. 2 shows a fabricated irradiation dish.

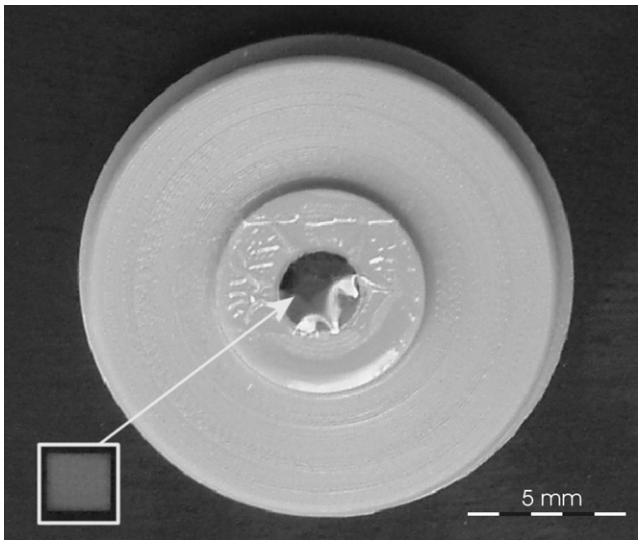

Fig. 2. SU-8 irradiation dish attached to a polystyrene cup (bottom view).

4. Testing

A few cells can be located in each square of the designed irradiation dish. Fig. 3 shows the cell distribution within the irradiation dishes. Fig. 3(a) shows the cells evenly distributed on the "treated" surface (lifted off using NH_3:H_2O (1:1) + 3% H_2O_2). The cells appear to grow normally, spread and attach to the surface. The cell pseudopods (temporary projections of eukaryotic cells used for locomotive function) cover the surface entirely and the nucleus can also be distinguished. Fig. 3(b) shows the cells in the "un-treated" dishes (lifted off using deionised water); the cells have attached but do not spread or grow. There are a lot of dead cells floating in the medium and no visible pseudopods. In addition, the cell nucleus became darker.

The 2 μm base plus 2 μm tall walls irradiation dish was tested but was found easily breakable. Instead, the 5 μm base plus 5 μm tall walls irradiation dish was easier to handle and still thin enough to let the protons pass through. Consequently, the results discussed in this paper correspond solely to the 5 μm base plus 5 μm tall walls irradiation dish.

The irradiation dishes were tested at the Lund Nuclear Probe using a focused proton beam of 2.5 MeV. After passage through the irradiation dishes, the energy of the protons was measured for three different settings labelled as "vacuum", "air" and "cells". The set up is shown in Fig. 4. The "vacuum" and "air" settings were performed in the respective environment but without any cell in the dish. The "cells" setting was performed in air and with cells in the dish. The dish position is chosen to minimize the air gap between the dish and the exit window. If the dish is positioned in the opposite direction, the walls of the irradiation dish can be bent against the exit window attempting to reduce the air gap. This can lead to an increased risk to either destroy the cells or to break the vacuum window. It remains to optimize the position of the dish to minimize the air gap in the experimental set up (*cf.* Fig. 4).

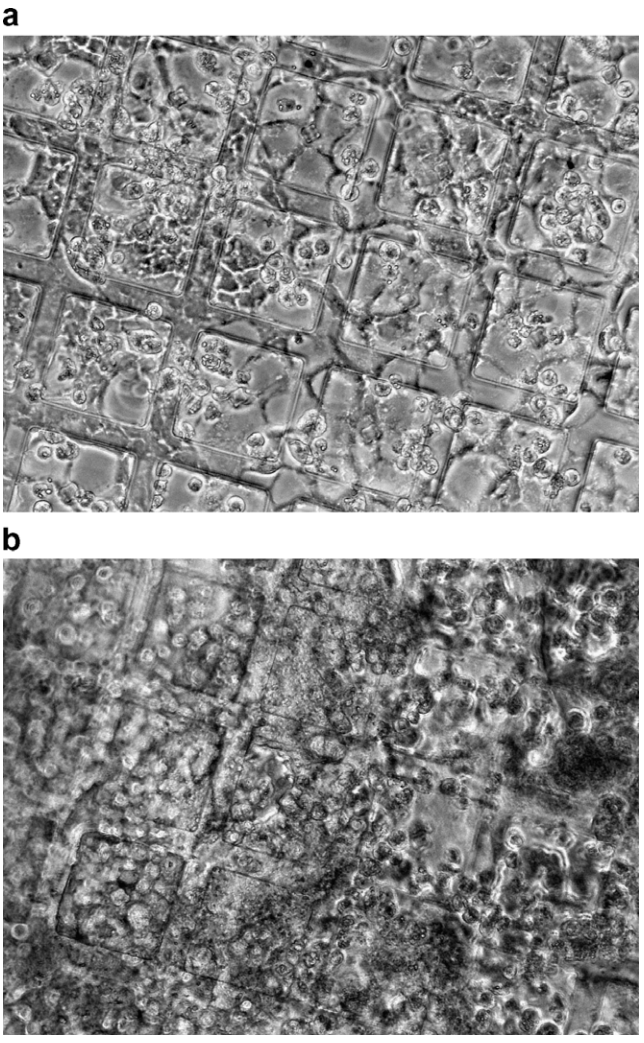

Fig. 3. Cell distribution comparison between "treated" and "un-treated" irradiation dishes. (a) The "treated" irradiation dishes were lifted off using NH_3:H_2O (1:1) + 3% H_2O_2. Cells are attached to the surface and are growing. (b) The "un-treated" irradiation dishes were lifted off using deionised water. There are a lot of dead cells floating in the medium.

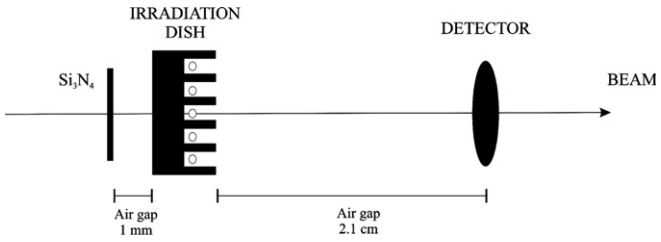

Fig. 4. The set up used to test the performance of the irradiation dishes. Three settings were used: "vacuum", "air" and "cells". The first two were performed in the respective environment and without cells in the dish. The "cells" setting was performed in air and with cells in the dish.

As mentioned above, the horizontal arrangement of the beam line forces the vertical positioning of the cells. The culture medium is removed from the dish prior to

Table 1
SRIM simulations comparison between energy loss and amount of medium remaining before irradiation

Incident proton energy (MeV)	Energy loss (MeV)				
	SU-8 bottom layer (5 μm) + cells (10 μm)	SU-8 bottom layer (5 μm) + cells (10 μm) + medium (1 μm)	SU-8 bottom layer (5 μm) + cells (10 μm) + medium (2 μm)	SU-8 bottom layer (5 μm) + cells (10 μm) + medium (5 μm)	SU-8 bottom layer (5 μm) + cells (10 μm) + medium (10 μm)
2.50	0.23 ± 0.01	0.24 ± 0.01	0.26 ± 0.02	0.30 ± 0.01	0.38 ± 0.02
2.25	0.25 ± 0.01	0.26 ± 0.01	0.28 ± 0.01	0.33 ± 0.01	0.42 ± 0.02
2.00	0.27 ± 0.01	0.29 ± 0.01	0.31 ± 0.01	0.36 ± 0.01	0.46 ± 0.02
1.75	0.30 ± 0.02	0.32 ± 0.01	0.34 ± 0.01	0.40 ± 0.02	0.51 ± 0.03
1.50	0.34 ± 0.01	0.36 ± 0.01	0.39 ± 0.01	0.46 ± 0.02	0.58 ± 0.02
1.25	0.39 ± 0.01	0.41 ± 0.01	0.44 ± 0.01	0.52 ± 0.02	0.68 ± 0.02
1.00	0.48 ± 0.02	0.50 ± 0.02	0.54 ± 0.02	0.66 ± 0.02	—

Table 2
Comparison between the experimental and simulated energy for the different settings: "vacuum", "air" and "cells"

Setting	SRIM simulations		Experimental results	
	Energy peak (MeV)	Energy loss (MeV)	Energy peak (MeV)	Energy loss (MeV)
"Vacuum" – SU-8 walls (10 μm)	2.40 ± 0.01	0.10	2.41 ± 0.02	0.09
"Vacuum" – SU-8 bottom layer (5 μm)	2.47 ± 0.01	0.03	2.47 ± 0.01	0.08
"Air" – SU-8 walls (10 μm)	2.07 ± 0.06	0.43	2.08 ± 0.03	0.42
"Air" – SU-8 bottom layer (5 μm)	2.16 ± 0.02	0.33	2.15 ± 0.02	0.35
"Cells" (simulated 10 μm culture medium remaining)	*2.04 ± 0.02*	*0.46*	*2.13 ± 0.03*	*0.37*

irradiation to ensure proton detection in the post-cell detector. However, a variable thin culture medium layer always remains. Furthermore, the culture medium may evaporate. These facts can affect the cell survival forcing the irradiation procedure to be accomplished as fast as possible. SRIM simulations [19] were performed to analyse the viability of the irradiation dishes for different remaining thicknesses of culture medium. Table 1 presents the results. Since different doses and LETs are intended to be delivered to the cells, several energy values have been used for the simulations. At energies below 1.25 MeV, it is not possible to detect protons after passing the dish, the cells and the 10 μm remaining culture medium. At the same conditions, the energy loss for 2.5 MeV protons is noticeable but still, there is a sufficient margin for proton detection.

The measured proton energy was analysed and compared to SRIM simulations. The results are shown in Table 2. The energy loss of the beam with the different settings and the corresponding simulation is very similar. However, Hepatoma cells were not available for the simulations and hence, Mammalian glands were used. The major differences between these two cell lines are their differentiation state and their size. The Mammalian glands are larger but the cells have similar density for the selected layer thicknesses. The density of exposed SU-8 (2005) was taken from the manufacturer [15]. Attending to the "cells" setting in Table 2, the experimental results give a value of 2.13 MeV, similar to the simulated value in Table 1 for 10 μm of remaining medium. However, the simulations results in Table 2 take into account the air gap that the protons pass before they reach the detector, resulting in a lower simulated value. The simulations present a reasonable evaluation of the beam scattering after passing the irradiation set up. The SRIM simulations allow us to evaluate the beam scattering and the air and medium thicknesses when the dish is mounted in the sample holder. The presented data leads to the conclusion that the unavoidable culture medium remaining in the dish during the irradiation procedure is approximately 10 μm thick.

The energy of the protons after passing through the dish in the three cases mentioned above is displayed in Fig. 5. The widest FWHM occurred for the settings "air" and "cells" due to energy scattering of the proton beam in air. It is assumed that the beam loses energy differently when the protons pass the walls (or the cross of each square) and the bottom of the irradiation dish. In addition,

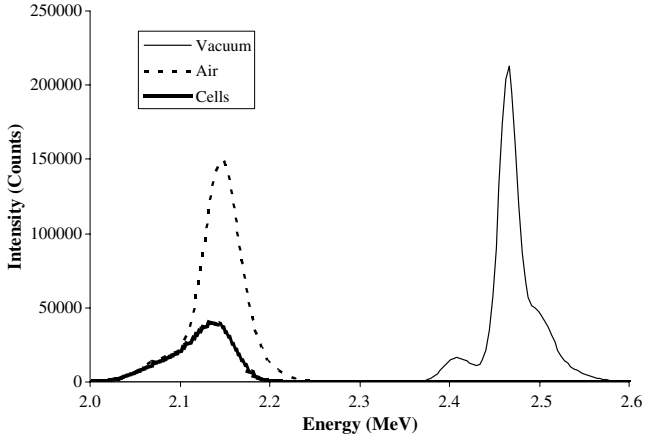

Fig. 5. Proton energy spectra for the different settings used in order to test the performance of the irradiation dishes.

beam size makes it possible that the protons pass at the same time through different thickness areas. Besides, areas with different amount of remaining medium will also result in different energy losses of the protons. The SU-8 structure deposited into the polystyrene cup is not always fully stretched, resulting in a non-flat irradiation dish (*cf.* Fig. 2). The measured proton energy loss presents different values along the irradiation dish. Thus, the tail in the peaks observed, especially noticeable in the "vacuum" case, *cf.* Fig. 5, can be produced by the situations explained above, giving proton detection for different thicknesses simultaneously. This fact might affect the calculation of the dose received by the cells. However, flatness is not a vital requirement if the cells keep on growing and the protons can be transmitted and detected.

5. Conclusions

A new cell irradiation dish has been developed for cell irradiation experiments at the Lund Nuclear Probe. It has been designed attending the requirements for a horizontal irradiation facility, implying a vertical positioning of the irradiation dish. Furthermore, due to the detector configuration used for these experiments at the Lund Nuclear Probe, the only special feature that has to be controlled is the thickness of the irradiation dish.

SRIM simulations have been done to test the irradiation configuration. After exiting into air through a thin Si_3N_4 vacuum window, the beam passes an air gap, the irradiation dish containing the cells in culture medium and finally a second air gap before being registered in a particle detector. Since the comparison between simulations and experimental result are in concordance, the simulations have been validated experimentally. Thus, the configuration ensures the detection of each proton which has passed through the successive layers.

The SU-8 irradiation dishes are flexible, biologically compatible and have a long life time. The major advantage of these irradiation dishes is that the cells grow on them without special treatment except for the hydrophilization. The dishes can be used to incubate the cells but also to hold them during the irradiation procedure. Additionally, the irradiation dishes can be sterilized and used several times. The designed and fabricated irradiation dish has successfully been tested for cell compatibility and its functionality during the irradiation procedure is more than adequate.

Acknowledgements

We would like to thank to Mariusz Graczyk at the Solid State Physic Department at Lund Institute of Technology for his help during the fabrication process.

This work is supported by Marie Curie Research Training Network, MRTN-CT-2003-503923 and Crafoordska Stiftelsen No. 20041003.

References

[1] M.A. Kadhim, S.R. Moore, E.H. Goodwin, Mutat. Res. 568 (2004) 21.
[2] <http://cellion.ifj.edu.pl>.
[3] C.S. Chen, M. Mrksich, S. Huang, G.M. Whitesides, D.E. Ingber, Biotechnol. Prog. 14 (1998) 356.
[4] G. Liu, Y. Tian, Y. Kan, Microsyst. Technol. 11 (2005) 343.
[5] Gwo-Bin Lee, Che-Hsin Lin, Guan-Liang Chang, in: The 15th IEEE International Conference on Micro Electro Mechanical Systems, 2002, p. 503.
[6] A.P. Gadre, J.A. Garra, A.J. Nijdam, A.H. Monica, M.C. Cheng, C. Luo, T.W. Schneider, T.J. Long, R.C. White, J.F. Currie, in: Twelfth International Conference on Transducers, Solid-State Sensors, Actuators and Microsystems, I, 2003, p. 806.
[7] L.J. Guerin, M. Bossel, M. Demierre, S. Calmes, P. Renaud, in: International Conference on Solid State Sensors and Actuators, Transducers '97 Chicago, 2, 1997, p. 1419.
[8] C. Jensen-McMullin, S. Ng, M. Bachman, C. Sims, N. Allbritton, G.P. Li, in: Third IEEE/EMBS Special Topic Conference on Microtechnology in Medicine and Biology, 2005, p. 34.
[9] T. Reinert, A. Fiedler, J. Škopek, J. Tanner, J. Vogt, T. Butz, Nucl. Instr. and Meth. B 219&220 (2004) 77.
[10] A. Shariff, C. Nilsson, V. Auzelyte, M. Elfman, P. Kristiansson, K. Malmquist, J. Pallon, M. Wegdén, Nucl. Instr. and Meth. B 231 (2005) 7.
[11] M. Elfman, J. Pallon, V. Auzelyte, P. Kristiansson, K. Malmquist, C. Nilsson, A. Shariff, M. Wegdén, Nucl. Instr. and Meth. B 231 (2005) 14.
[12] N. Arteaga-Marrero, J. Pallon, M.G. Olsson, V. Auzelyte, M. Elfman, P. Kristiansson, K. Malmqvist, C. Nilsson, M. Wegdén, Nucl. Instr. and Meth. B 260 (2007) 91.
[13] R. Feng, R.J. Farris, J. Mater. Sci. 37 (2002) 4793.
[14] V. Auzelyte, M. Elfman, P. Kristiansson, J. Pallon, M. Wegdén, C. Nilsson, K. Malmqvist, B.L. Doyle, P. Rossi, S.J. Hearne, P.P. Provencio, A.J. Antolak, Nucl. Instr. and Meth. B 242 (2006) 253.
[15] <www.microchem.com>.
[16] M. Nordström, M. Calleja, A. Boisen, Ultramicroscopy 105 (2005) 281.
[17] M. Nordström, R. Marie, M. Calleja, A. Boisen, J. Micromech. Microeng. 14 (2004) 1614.
[18] H.W. Lu, Q.H. Lu, W.T. Chen, H.J. Xu, J. Yin, Mater. Lett. 58 (2003) 29.
[19] <http://www.srim.org/>.

Nuclear Instruments and Methods in Physics Research B 267 (2009) 2117–2121

Contents lists available at ScienceDirect

Nuclear Instruments and Methods in Physics Research B

journal homepage: www.elsevier.com/locate/nimb

Applications of SU-8 in the development of a Single Ion Hit Facility

N. Arteaga-Marrero [a,*], G. Astromskas [b], M.G. Olsson [c], M. Elfman [a], P. Kristiansson [a], E.J.C. Nilsson [a], C. Nilsson [a], J. Pallon [a]

[a] Division of Nuclear Physics, Department of Physics, Lund University, Professorsgatan 1, Box 118, SE-22100 Lund, Sweden
[b] Division of Solid State Physics, Department of Physics, Lund University, Professorsgatan 1, Box 118, SE-22100 Lund, Sweden
[c] Department of Infection Medicine, Lund University, Sölvegatan 19, B14, SE-22184 Lund, Sweden

ARTICLE INFO

Available online 12 March 2009

PACS:
81.05.Lg
87.56.bd
85.40.Hp

Keywords:
Single Ion Hit Facility (SIHF)
Cell irradiation
SU-8
PMMA
EBL

ABSTRACT

The Lund Nuclear Microprobe (LNM) has been adapted to be used as a Single Ion Hit Facility (SIHF) for proton cell irradiation experiments at low dose.

In order to test the capabilities of the system, Ni dot arrays and artificial cells have been fabricated with the photopolymer SU-8 and common lithographic techniques. The primary purpose of the Ni dot arrays was to determine the targeting accuracy of the beam in vacuum and in air. Additionally, this sample was employed to evaluate the system performance during cell target irradiation experiments. The Ni dot arrays were also used for beam characterization.

The artificial cells were originally fabricated to test the software for cell recognition and localization, developed and implemented at the LNM. However, this sample became very functional to make small adjustments at the irradiation chamber for cell irradiation experiments.

A description of the samples, fabrication procedure and applications are presented in this paper.

1. Introduction

The Lund Nuclear Microprobe (LNM) has been equipped with a Single Ion Hit Facility (SIHF) for studying cellular response to low dose radiation. The LNM is a horizontal facility with a post-cell detection system which can provide focused beams of 2.5 MeV protons and alpha particles [1]. The system is operative regarding non-targeted irradiation since July 2007. The final modifications have been done lately to get a full operational state, i.e. targeted irradiation.

The technical development of the system requires control of the target position with high precision since subcellular targets are intended to be irradiated. The spatial targeting accuracy of the system, that is, the displacement between the coordinates selected by the software and the exact coordinates where the ions hit has to be evaluated. The accuracy depends on the beam size, the beam positioning system, and the implemented software for cell localization (CELLION). In principle, the system function can be described in two basic steps:

1. The desired target is selected using the CELLION software.
2. The output coordinates from the software are input coordinates for the scanning system for positioning the ion beam at the cell position.

The uncertainty in position arises from the combination of these two steps and is added to the uncertainty caused by the beam size.

Large area dot arrays fabricated by Electron Beam Lithography (EBL) have been previously used for microscope parameters calibration [2]. Presently, Ni dot arrays have been fabricated in order to test the system targeting accuracy during cell irradiation. Additionally, a first estimate of the beam size can be performed by Scanning Transmission Ion Microscopy (STIM) measurements since the Ni dots can only be observed if the beam size is comparable to or smaller than the dot size.

For the cell irradiation experiments, the cultured cells have to be vertically positioned due to the system arrangement. Therefore, the cell culture medium has to be removed just before irradiation to ensure the detection of the particles after passing through the cells. Living cells, however, do not survive very long outside a controlled environment regarding temperature, CO_2 concentration and nutrients. In approximately 10 min time scale, cells start to die and detach from the surface where they have been seeded, making difficult to work with living cells for the system development.

* Corresponding author. Tel.: +46 46 2227630; fax: +46 46 2224709.
E-mail address: natalia.arteaga@nuclear.lu.se (N. Arteaga-Marrero).
URL: http://www.pixe.lth.se/cellion/ (N. Arteaga-Marrero).

0168-583X/$ - see front matter © 2009 Elsevier B.V. All rights reserved.
doi:10.1016/j.nimb.2009.03.009

The CELLION software can be evaluated with the Ni dot arrays but in this case the cell shape geometry is oversimplified. In addition, no cell stain is used to visualize transparent living cells at the LNM. Since the Ni dots are not transparent, the illumination system required for cell irradiation experiments cannot be tested. Consequently, the lack of the required specific properties of the Ni dots and the difficulty to work with living cells implies the necessity to design a new sample to adjust and evaluate the system performance. Therefore, an innovative approach has been adopted which consists of an artificial cell sample simulating a real live cell scenario.

The Ni dot arrays and the artificial cell sample have been fabricated with SU-8 and conventional lithographic techniques. This paper presents a description of the created samples, their fabrication and applications testing the system for cell irradiation experiments.

2. Fabrication

The fabrication of the Ni pattern and the artificial cell sample was performed in several steps. In both cases, the initial substrate used for the fabrication was an optical glass. This substrate was spin-coated with SU-8(2005), soft baked and flood exposed with UV-light as recommended by the resist manufacturer [3]. The resulting layer was a 5 μm thick SU-8 layer on top of the glass. SU-8 is a versatile epoxy-based photopolymer widely used for device fabrication: from adhesive layer for bonding [4] to high dielectric nanocomposite material [5]. In addition, SU-8 is a cell friendly material, that is, cells attach and grow on it, especially after oxygen plasma treatment [6]. A large number of SU-8 biological applications are dedicated to microfluidic devices such as an integrated microlens array for cell counting [7]. SU-8 was chosen previously as a seat layer at the LNM to fabricate custom Petri dishes suitable for cell incubation and irradiation [8]. A similar design has been used for time-tracking living cells after X-rays irradiation [9]. Since the fabrication of the artificial cell sample requires a cell friendly material, SU-8 was chosen once more.

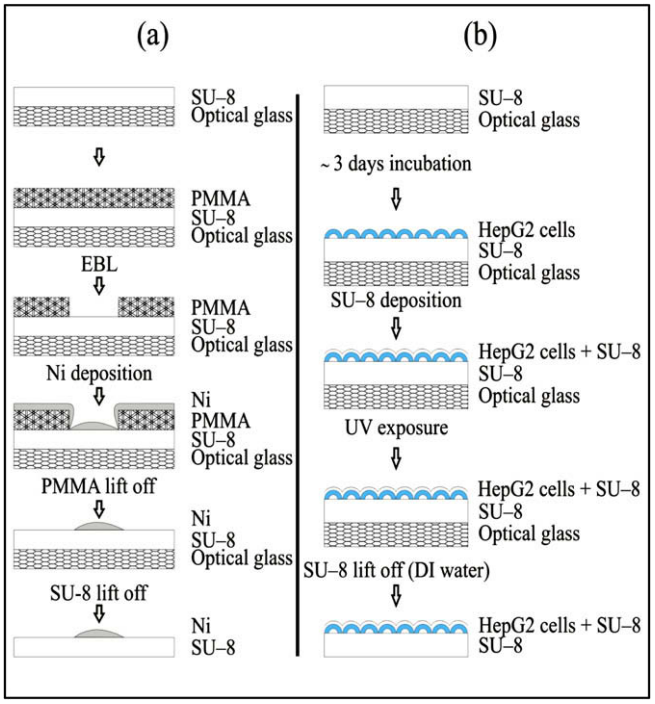

Fig. 1. Sketch of the different steps of the fabrication processes. (a) Ni dots sample fabrication. (b) Artificial cell sample fabrication.

2.1. Ni dot array

A double layer of polymethyl methacrylate (PMMA 950 k A6) was spin-coated on top of the SU-8 coated glass substrate forming a layer of 890 nm thickness. The PMMA polymer is a positive electron sensitive resist which has to be spin-coated twice in order to reach the desired thickness. The PMMA layer was patterned using the EBL system Raith 150. The following structures were exposed:

- Periodical array of 5 μm diameter dots with 50 μm spacing in between.
- Periodical array of 2 μm diameter dots with 10 μm spacing in between.
- A cross formed by 70 μm × 20 μm lines to facilitate the localization of the patterns through the sample.

After EBL exposure with a fluence of 300 $\mu C/cm^2$, the structures were developed for 90 s in a methyl isobutyl ketone (MIBK):isopropanol (1:3) solution.

In the next step, a Ni metal layer was deposited onto the patterned surface using the thermal metal evaporation system model AVAC. Finally, the PMMA resist layer was dissolved using acetone, lifting the residual Ni layer from the sample. Only the Ni structures with the shape of the exposed PMMA pattern remained on top of the SU-8 layer. The thickness of the fabricated Ni structures was 530 nm.

Fig. 1(a) displays a sketch of the different steps through the Ni dot array fabrication process.

2.2. Artificial cells

Human hepatoma cells (HepG2) were seeded on the 5 μm thick SU-8 layer. The cells were cultured in RPMI 1640 with GlutaMAX™I

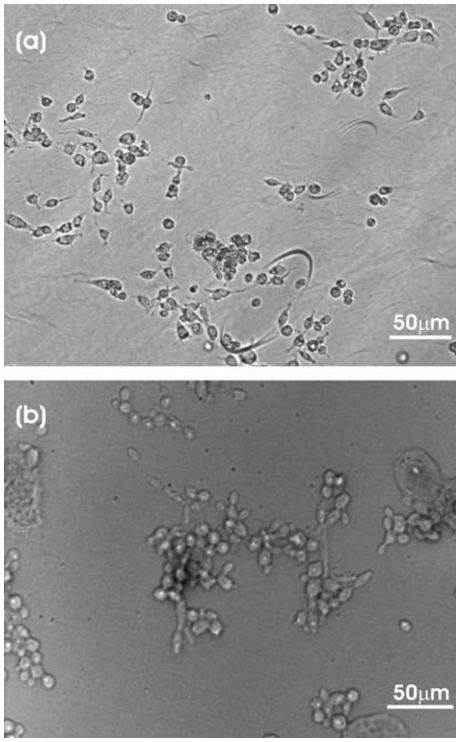

Fig. 2. Fabricated artificial cell sample in comparison with living cells. (a) Differential Interference Contrast (DIC) image of human hepatoma cells (HepG2) incubated in a standard polystyrene Petri dish. (b) Artificial cell sample fabricated using the photopolymer SU-8. The irregular living cell distribution as well as the differences in cell shape is kept in the fabricated sample.

medium (Life Technologies AB, Täby, Sweden) containing 10% fetal bovine serum (FBS) (Life Technologies AB, Täby, Sweden) and 100 μg/ml antibiotics (penicillin and streptomycin) and antimycotics. The cells were incubated at 37 °C in an atmosphere of 5% CO_2, and the medium was changed regularly.

After approximately three days, the cells reached a confluent state close to 100%. Then, the cell medium was removed and a second layer of SU-8 was spin-coated on top of the cells burying them in the resist. The samples were then flood exposed with UV-light and post-baked. Fig. 1(b) displays a sketch of the different steps through the artificial cell fabrication.

The rotation speed during the resist spin-coating determines the thickness of the deposited layer. Several velocities were tested in order to obtain samples showing the smallest differences in shape between the embedded and the living cells. The optimal conditions were found for a spin velocity of 2500 rpm which normally provides a layer thickness of approximately 5 μm. Nevertheless, no soft bake procedure was performed during the artificial cell sample fabrication aiming to maintain the cell integrity before the UV exposure. Since the soft bake temperature influences the resist properties [10], a larger resist thickness may result.

Fig. 2(a) displays the HepG2 cells cultured on a standard polystyrene Petri dish and Fig. 2(b) shows the artificial cell sample. As can be seen, the cells embedded in SU-8 (artificial cells) preserve the size and shape of the living cells and even small cell colonies can be distinguished. Furthermore, the artificial cell sample fulfils two essential requirements which are irregular cell shape and random cell distribution. Consequently, this sample was considered to provide the desired properties for testing the software.

In order to use the Ni dot array and the artificial cell sample, they are lifted off the optical glass by immersion in a deionised water bath and mounted in a standard holder.

3. Applications

The main advantage of the fabricated samples is that the formed structures are thicker than the bottom SU-8 layer that supports them. Consequently, the ions passing through the patterned regions suffer higher energy loss than the ions passing outside these regions. This energy difference can be visualized using STIM.

The advantage provided by the difference in energy loss has been previously utilised at the LNM [1]. A copper grid was used to rapidly test online the targeting accuracy of the system before cell irradiation experiments. Presently, the method has been improved by the fabrication of the Ni dot array. STIM images of the Ni dots were taken using focused 2.5 MeV protons. These images were introduced into the CELLION software. The program recognized the Ni dots as probable cells and selected the coordinates of the centre of each dot as desired target. These coordinates were uploaded into the LNM scanning system and the ion beam was directed to the selected Ni dots delivering a previously established number of protons. This procedure was used in combination with the beam deflecting system [11] to ensure that the beam only hits the Ni dots and not the SU-8 layer when travelling in between dots. Therefore, this method allowed us to detect the targeted region attending to the differences in proton energy loss between the Ni dots and the surrounding SU-8 surface.

3.1. Ni dot array

Fig. 3 shows the STIM image of the 5 μm diameter dots and the obtained energy spectra after targeting the sample in vacuum environment. The energy shift suffered by the protons after passing the different layers in the sample (the Ni dots and the SU-8 background) can be clearly observed confirming that targeting was successful. Furthermore, since the energy shift was clearly observable for the 5 μm diameter dots, we can consider that the spatial targeting accuracy of the system was within the 5 μm range.

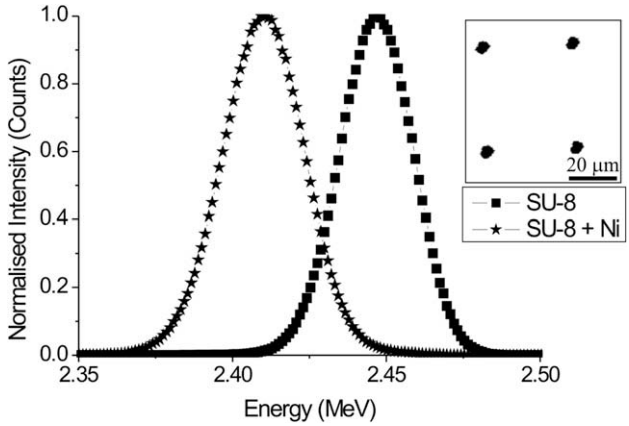

Fig. 3. Energy spectra comparison in vacuum. The square symbol line corresponds to the energy spectrum after targeting the background SU-8 surface. The star symbol line corresponds to the energy spectrum after targeting only the central coordinates of the Ni dots. The inset shows the STIM image of the 5 μm diameter Ni dots with 50 μm separation in between.

Since the main purpose of this sample was to test the spatial targeting accuracy of the system, stability in energy loss for a reduced area was a vital requirement. Thus, the thickness of the Ni dots should be the same between the inner and the outer areas. Fig. 4 shows the STIM energy spectra comparison between four randomly chosen 5 μm diameter Ni dots. In order to obtain the different curve parameters a Gaussian fit procedure was performed with Origin 7.0 [12]. The energy loss (2.41 MeV) as well as the FWHM values remained constant for all the analysed dots even if the Ni dot shape slightly varies along the array. The deviation between the data and the Gaussian fit quantify the tail observed in the high energy part of the spectrum of some of the analysed dots. This deviation was calculated to be approximately 3%. Accordingly, the efficiency hitting inside the Ni dots corresponded to a value of 97%.

Similarly, the SU-8 substrate layer should be stable regarding energy loss. Fig. 4 also shows a comparison between the energy spectra of four different SU-8 regions within the array. The energy loss value (2.44 MeV) was constant for all the analysed regions. Thus, equally to the Ni dots case, thickness fluctuations are negligible regarding energy loss.

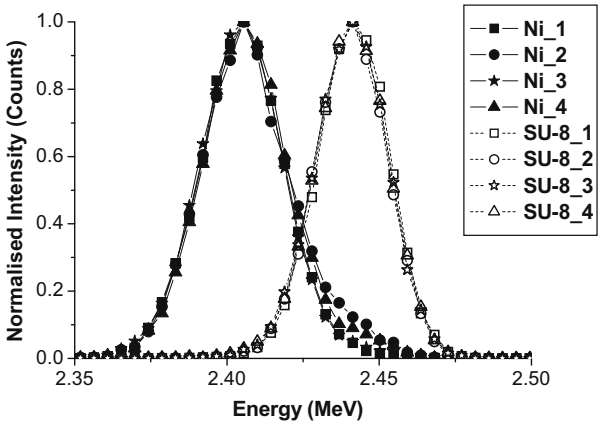

Fig. 4. Normalised energy spectra of four randomly chosen 5 μm diameter Ni dots and four different SU-8 regions within the periodical array.

The beam size during these experiments was 3.8 μm in X and 2 μm in Y direction. Therefore, the spatial targeting accuracy of the system using the 2 μm diameter Ni dots has not been studied since the beam size during this run was slightly larger than the Ni dots size.

Based on the presented data, it can be concluded that the thickness (530 nm) of the 5 μm diameter Ni dots and the corresponding energy loss (30 keV) was large enough for structure identification at the LNM.

3.2. Artificial cells

Fig. 5 shows the collected energy spectrum after STIM measurement of the fabricated artificial cell sample. Two peaks, whose energy values were obtained by a Gaussian fit procedure, can be observed. The peak at higher energy (2.33 MeV) corresponds to the substrate and the cover layer while the peak at low energy (2.27 MeV) corresponds to the two SU-8 layers with the embedded cells in between.

SRIM [13] simulations were run in order to determine the thickness of those two layers: SU-8 only and the SU-8 with the embedded cells. The energy that the protons have after passing the sample can be compared to the energy value obtained in the simulations giving an account of the layers thicknesses. Therefore, the thickness of the SU-8 layers without cells was considered to be 12.5 μm while the thickness of the SU-8 with embedded cells layer thickness was 16.1 μm. That result in a thickness of the cell layer of 3.6 μm.

The HepG2 cell line forms monolayer cultures which implies that the cells attach to the surface where they are grown and expand against the surface. In order to determine the cell thickness and size, a population of approximately 200 cells was analysed using a Nikon Eclipse TS100 microscope. The average cell thickness value was 3.8 ± 1.7 μm and the average cell size 139 ± 42 μm^2. Therefore, the thickness value obtained in the simulations for the artificial cells is in good agreement with the living cell thickness considering that during the spin procedure the cells may be stretched.

As mentioned above, the spatial targeting accuracy of the system is also controlled by the online CELLION software implemented at the LNM for cell recognition. The Ni dot array was used previously to test this program by targeting only the central coordinates of the Ni dots. However, the artificial cell sample provides a more realistic scenario to evaluate the performance of CELLION software.

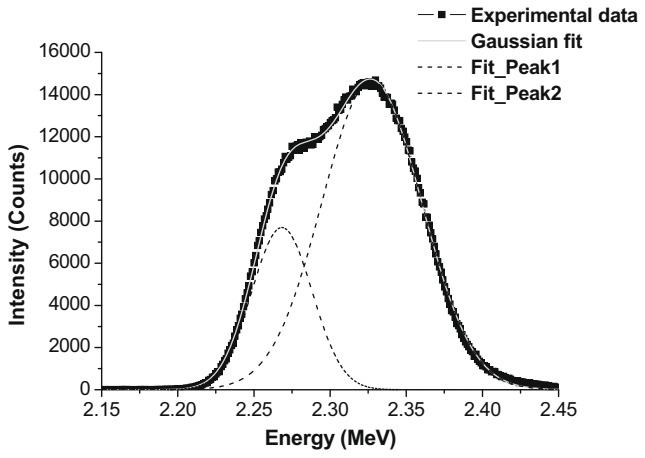

Fig. 5. STIM energy spectra of the fabricated artificial cell sample.

In addition, the artificial cells are also useful for the mechanical development of the facility. Optically, the simulated cells appear as transparent as the real cells due to the resist properties. Therefore, the movable illumination system can be tested and optimized at the irradiation chamber.

Furthermore, the LNM uses selectable objectives mounted in a translation stage for target visualization. Large magnification objectives are needed in order to select the targeted cells before irradiation due to the reduced HepG2 cell area. The position calibration of these objectives (20X, 50X) relative to the normal mounted objective (5X) can be carried out by the fabricated artificial cell sample.

Finally, the artificial cell sample was also employed to test the electronics set up for achieving single ion irradiation based on a post-cell detection system.

4. Conclusion

The LNM technical development can be investigated by means of the newly fabricated Ni dot array and artificial cell sample, which were manufactured with the photopolymer SU-8 using EBL and large UV exposure techniques.

The main advantage of these samples is their reduced thickness which allows the post-cell detection system to be employed for cell irradiation experiments. Also, the energy loss difference between the fabricated structures and the supporting layer allows proper structure identification.

The Ni dot array is appropriate for testing the implemented online cell recognition software (CELLION) and principally, the spatial targeting accuracy of the system during cell irradiation experiments. In addition, preliminary beam size estimate can also be performed.

The artificial cell sample fabricated provided a more suitable scenario to test the CELLION software in comparison with the Ni dot array. The artificial cell sample is particularly useful since it has similar properties as living cells regarding size, shape, transparency, irregularity and random distribution. In addition, the artificial cell sample presents other functionalities for the technical development of the system, for instance illumination and objective adjustment, and electronics set up for single cell irradiation tests.

Acknowledgements

The authors truly appreciate the support offered by Audrius Čečys during data collection and image processing. Also, the authors gratefully acknowledge Nataliya Lutay at the Bio Medical Centre in Lund for the HepG2 cell line measurements at the Nikon Eclipse TS100 microscope.

This work is supported by Crafoordska Stiftelsen No. 2004100 and Marie Curie Research Training Network MRTN-CT-2003-503923.

References

[1] N. Arteaga-Marrero, J. Pallon, M.G. Olsson, V. Auzelyte, M. Elfman, P. Kristiansson, K. Malmqvist, C. Nilsson, M. Wegdén, Nucl. Instr. and Meth. B 260 (2007) 91.
[2] A. Pérez-Junquera, J.I. Martín, J.M. Alameda, Microelectron. Eng. 84 (5–8) (2007) 845.
[3] Manufactured by MicroChem Corporation, <http://www.microchem.com>.
[4] Liming Yu, C. Iliescu, F.E.H. Tay, Bangtao Chen, Int. Semiconduct. Conf. 1 (2006) 189.
[5] J. Xu, C.P. Wong, J. Appl. Polym. Sci. 103 (3) (2007) 1523.
[6] M. Hennemeyer, F. Walther, S. Kerstan, K. Schurzinger, A.M. Gigler, R.W. Stark, Microelectron. Eng. 85 (2008) 1298.
[7] J.N. Kuo, C.C. Hsieh, S.Y. Yang, G.B. Lee, J. Micromech. Microeng. 17 (2007) 693.
[8] N. Arteaga-Marrero, V. Auzelyte, M.G. Olsson, J. Pallon, Nucl. Instr. and Meth. B 263 (2007) 523.

[9] T. Kuchimaru, F. Sato, Y. Aoi, T. Fujita, T. Ikeda, K. Shimizu, Y. Kato, T. Iida, Radiat. Environ. Biophys. 47 (2008) 535.
[10] T.A. Anhoj, A.M. Jorgensen, D.A. Zauner, J. Hübner, J. Micromech. Microeng. 16 (2006) 1819.
[11] V. Auzelyte, M. Elfman, P. Kristiansson, K. Malmqvist, L. Wallman, C. Nilsson, J. Pallon, A. Shariff, M. Wegdén, Nucl. Instr. and Meth. B 219–220 (2004) 77.
[12] OriginLab Corporation, Origin 7.0 SR0, <http://www.originlab.com>.
[13] J.F. Ziegler, SRIM 2006, <http://www.SRIM.org>.

SeACell: Cell Recognition Software for a Single-Ion Hit Facility

N. Arteaga-Marrero[1]*, M.G. Olsson[2], P. Kristiansson[1] and J. Pallon[1]
[1] *Division of Nuclear Physics, Department of Physics, LTH, Lund University, Professorsgatan 1, PO Box 118, SE-221 00 Lund, Sweden*
[2] *Clinical and Experimental Infection Medicine (BMC), Sölvegatan 19, B14, SE-221 84, Lund, Sweden*

Submitted to Review of Scientific Instruments

Abstract

An in-house software, SeACell, formerly referred as CELLION [1], has been improved in order to adapt the Lund Nuclear Microprobe for biological applications developing a Single-Ion Hit Facility (LNM-SIHF). SeACell allows the irradiation system to automatically recognise cells and localize their position.

A new cell validation algorithm enabled SeACell to provide high efficiency for subcellular target localization without the use of cell staining dyes. In addition, a user-friendly interface has been implemented containing a manual cell target selection, and an enhancement filter and colour display applications, to improve the quality of the input image.

Furthermore, the cell validation algorithm provides a dynamic cell targeting feature specially implemented for bystander studies allowing automatic selection of specific cells. The new interface makes SeACell more versatile and it has been proved to be efficient as a cell counter for cell damage evaluation after alpha source irradiation.

A description of SeACell software and its performance is presented in this paper.

1 Introduction

Microprobe facilities using light or heavy ions are currently being exploited for radiation research. Single-Ion Hit Facilities (SIHFs) are a microprobe tool developed to study cellular response at low dose radiation. These SIHFs are used to irradiate single living cells with an ultimate dose limit of a single ion, track the targeted cell and study its response and the response of the neighbouring cells to radiation.

SIHFs are particularly interesting because they have revealed the existence of anomalous effects after low-dose irradiation where the cells respond to ionizing radiation through pathways other than direct DNA damage. These denominated non-targeted effects include the bystander effect [2], adaptive responses, genomic instability [3], gene expression [4], inverse dose-rate effect [5], low-dose hypersensitivity [6] and the death-inducing effect [7]. The existence of such effects put into question the validity of established models for estimating low-dose radiation risks. Further studies are thus needed to estimate the real low-dose radiation risk and to determine how this non-targeted effect can be used to improve the cancer treatment by radiotherapy.

For routine use, SIHF systems must be fully automated due to technical issues related

*Contact information: Tel. +46-46-2227630, Fax. +46-46-2224709, e-mail address: natalia.arteaga@nuclear.lu.se, URL: http://www.pixe.lth.se/cellion/

to the use of living cells. In order to aim at subcellular compartments, high throughput and precise targeting accuracy are required throughout the irradiation process: target identification, beam adjustment and cell irradiation. In addition, cells are extracted from their normal growing environment during the procedure; thus the irradiation has to be performed within a very short time to preserve cell viability. Automated systems such as the one at the Gray Cancer Institute in U.K. can achieve 100% efficiency of particle detection, resolution approaching 1 μm and throughput approaching 10000 cells per hour [8].

The automation of the irradiation procedure starts with target identification, most commonly using nuclear and/or cytoplasmic stains to image cells or cell nuclei. However, the use of stains can change the nature of the analysed element, and the fluorescence observation by UV radiation damages living cells [9]. The isolation of radiation effects is thus vital for continuing the research into low-dose radiation techniques. Consequently, better imaging systems are being developed which are able to distinguish cultured cells from the surface without the use of stains. For instance, Quantitative Phase microscopy (QPm) and phase-shifting interferometry (PSI) are under testing at the microbeam facility at Columbia University [10].

There are several methods to track non-stained small spherical particles in optical microscope images. Unfortunately, they tend to fail if the background is complicated or when particles are large or non-spherical. An accurate method has been previously reported where the recognition is based on the fitting of each intensity peak in the image to a two-dimensional Gaussian function [11]. Moreover, there are commercially available algorithms to perform the cell recognition. However, they are not compatible with microprobe control software and therefore, in-house code has to be developed [12, 13].

The present work describes the automatic system developed for the SIHF at the Lund Nuclear Microprobe (LNM-SIHF), which can be carried out in a short time with a high efficiency in any computer equipped with an IDL [14] virtual machine. The paper focuses mainly on SeACell software implemented in-house for cell recognition and localization. No cell stains are used at the LNM-SIHF for imaging purposes and common image processing routines have been used to develop this unique SeACell algorithm.

2 Methods and Algorithms

2.1 Image samples: living and embedded human hepatoma cells (HepG2)

In order to facilitate the testing of the cell recognition procedure in a semi-realistic scenario, a special sample was fabricated [15]. It was created by UV large exposure to embed HepG2 cells in SU-8 photopolymer. Images of embedded cells were then taken using an optical microscope.

HepG2 cells were seeded on a commercial polystyrene Petri-dish. The cells were cultured in RPMI 1640 with GlutaMAX I medium (Invitrogen, Täby, Sweden) containing 10% fetal bovine serum (FBS) (Invitrogen) and 100 g/ml antibiotics (penicillin and streptomycin) and antimycotics. The cells were incubated at 37°C in an atmosphere of 5% CO_2, and the medium was changed regularly. Differential Interference Contrast (DIC) images of the HepG2 living cells were acquired using an optical microscope.

2.2 The SeACell algorithm

LNM-SIHF cell recognition software SeACell, was developed to localize cell coordinates and subsequently irradiate the selected cells for an input image, therefore, adapting the in-house process for cell imaging with the in-house beam-scanning system. SeACell was implemented using IDL 6.2 and it is based on a set of linked procedures which automatically perform the cell recognition. These linked procedures consist on the application of a se-

quence of morphological filters commonly applied in imaging processing [16]. The output image at each step is an input image for the next.

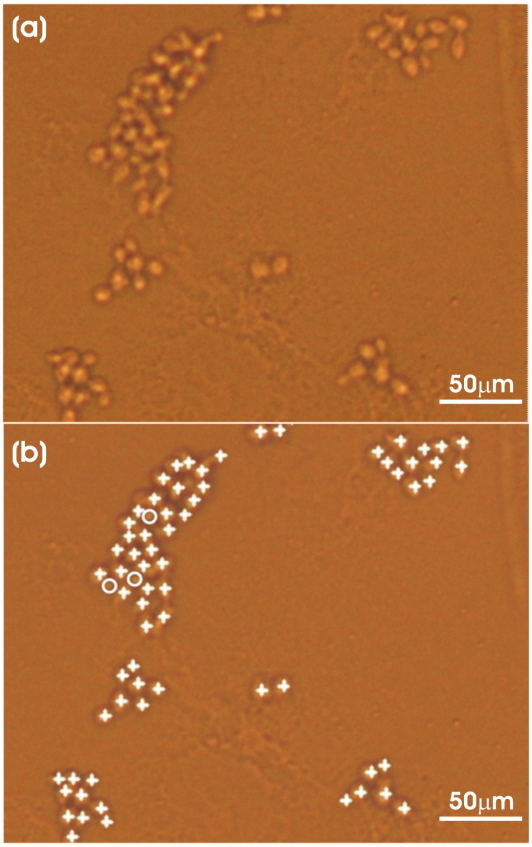

Figure 1: (a) Input image of the embedded human hepatoma cells. (b) Analysed image performed by the rough automatic cell recognition (without the cell validation algorithm). The crosses represent the localised cells. The circles show the preliminary recognition errors where clustered cells cannot be resolved.

2.2.1 Image segmentation: Threshold and scaling filter

The object of interest is extracted from the background by global thresholding. This process can select either bright or dark regions and the threshold value is chosen according to the intensity histogram of the image. Image pixels with an intensity value larger (or smaller) than the selected threshold value are rescaled creating a greyscale image.

2.2.2 Particle identification and localization

An erode morphological operator is used to eliminate specific image details smaller than the chosen structuring element [17]. The cell shape has been simulated choosing a disc shape structuring element.

Then, SeACell provides the central coordinates of the localised probable cells by a simple and fast calculation that does not depend on the structuring element. However, the method has two major disadvantages: overlapped objects are considered as single ones and some noise can be considered as target.

To deal with these problems, the structuring element is chosen a priori as accurately as possible to match the cell size of the cell line used for irradiation experiments. Figure 1 shows the analysis of the embedded cells, original image (a) in comparison with the processed one (b). Several clusters of cells have been analysed by the preliminary cell recognition. The localised cells have been marked with crosses while the circles indicate the software errors which correspond to clustered cells that cannot be resolved. For this image (412 x 318 pixels), the localization time was 0.4 s and the calculated software efficiency 96% $\pm$ 4%. As can be seen, only missed cells appear and not double targeting or noise particles. However, these errors must be prevented.

Thus, the automatic procedure for cell recognition is completed by a cell validation routine. The method disadvantages are solved by further image processing where area, diameter, cell shape and separation are used as parameters to eliminate the unwanted elements. Cell debris, cell fragments or other elements but cells can be considered probable cells. Furthermore, cell colonies matching the size of the structuring element gives a single central coordinate for a cluster of cells and dismiss several cells within the culture. Additionally, if a cell is localised twice, the beam-scanning system delivers an extra amount of ions to the same cell. These facts may compromise the biological endpoint under study.

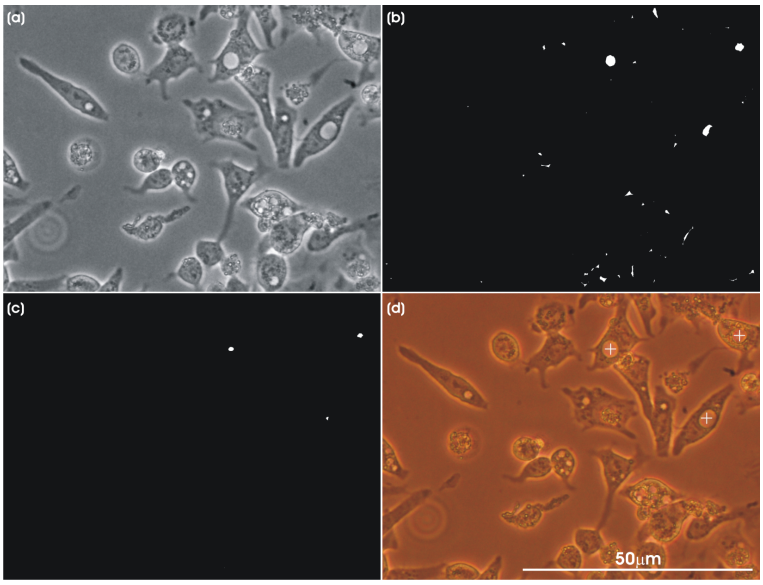

Figure 2: Steps of the SeACell recognition algorithm for analysing the living HepG2 cells. (a) Image segmentation: Thresholding. (b) Particle identification and localization (c) Cell validation algorithm: only cells with the required nucleus size and separation are selected from the identification performed in the previous step. (d) Final result where large size nuclei have been localised and marked with a cross.

2.2.3 Particle discrimination: cell validation algorithm

The cell validation algorithm consists of two erosion operators. One operator is applied to the input image using a hit structuring element. The second is applied to the inverse of the input image with a miss structuring element. The intersection of the two operators provides the desired target. The hit structuring element is chosen to match the cell (or subcellular compartment) size and shape, while the miss structuring element is used to control the separation between cells and the number of selected targets per cell. The matching image elements contain the hit structure and are contained by the miss structure. Consequently, specific shapes can be identified.

Figure 2 shows the steps of the SeACell recognition algorithm for analysing the living HepG2 cells. In this case, large area cell nuclei have been identified by the software and marked with a cross. In those cells, the nucleus is in the same plane as the cell border. Other nuclei appear smaller since they are in a different plane, because the cell is preparing for cell division or for cell death. The image (1280 x 960 pixels) was analysed in 1.8 s with a program efficiency of 100%.

The cell validation algorithm can be applied multiple times if required for a particular image. Since the algorithm is very sensitive to shape, size and rotation of the structuring elements, extracting specific image regions may require multiple applications of different hit and miss structures.

2.3 Dynamic cell targeting for bystander effect studies

Non-targeted cell irradiation is mandatory for bystander effect studies since only a few cells within the culture are irradiated. The bystander effect can be triggered by nucleus and cell cytoplasm irradiation [18, 19, 20], and they provide different pathway studies depending on the differences in the responses of irradiated and non-irradiated cells [8]. The automatic

cell recognition algorithm described above provides the coordinates of all the cells within the input image. Therefore, the analysis of the response of non-irradiated cells requires the possibility to select the desired target (i.e., certain cells or subcellular compartments in the culture).

The program is equipped with a manual target selection option for bystander studies. This option can be time-consuming in cases where the cell culture image is complicated, since an expert may be required, or the desired amount of cells to target is numerous.

The automatic cell validation algorithm thus provides a clear advantage over manual recognition. In addition, it can also be exploited for bystander studies by modifying the size parameter of the hit and miss structuring element in the algorithm.

The automatic non-targeted cell targeting is a dynamic feature that provides a 3D map of irradiated cell compartments. It can be achieved by two approaches:

i Sample movement - Since the cell compartment size is known when the cells are in focal plane, all cells in the culture can be targeted by moving the sample and focusing, in regular steps and different planes, in the focal plane. In this case, the coordinates of the targeted cells must be stored to avoid targeting the same cell twice. The main drawback is the need for mechanical sample movement, which is time-consuming.

ii Size criteria modification (fully automated) - The cell validation algorithm can be modified to match subcellular compartments. This allows the system to target without modifying the sample location. In addition to the cell coordinates storage, a new restriction is added to avoid additional dose deposition. Consequently, a single subcellular compartment per cell is selected for targeting.

Figure 3 shows the recognition performed by SeACell. For comparison purposes, the same input image used in Figure 2 was analysed using a smaller compartment-size parameter. The cell compartments were located in 1.3 s with a program efficiency of 100%. Furthermore, SeACell computing time is decreased by reducing the compartment-size parameter. As can be observed, some of the selected cells present other compartments which fulfil the searching parameter but only one of them has been chosen for ion deposition. Therefore, any cell can be targeted twice, as it is shown in both figures.

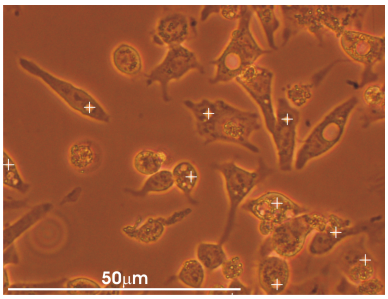

Figure 3: Microscopic image of the living HepG2 cells processed by SeACell using the cell validation algorithm for small size nucleus. For comparison purposes, Figure 2 input image results in Figure 3 by selecting a different size parameter.

2.4 Image enhancement

Enhancement filters and colour display have been added to SeACell through drop-down menus. No cell stain is used at the LNM-SIHF for imaging purposes. Therefore, the transparent cells are visualized at the irradiation chamber by an optical microscope with dark field illumination. This illumination affects the quality of the input image since it is tuneable in direction. The image quality can improve by the application of these filters during the segmentation step. The standard cell recognition procedure at the LNM-SIHF does not include any filter application. However, other SIHFs use several filters within their cell recognition procedure to remove noise and enhance edges [12]. The available filters can be divided as follows regarding their enhancement properties.

i Edge detection - Image edges are detected

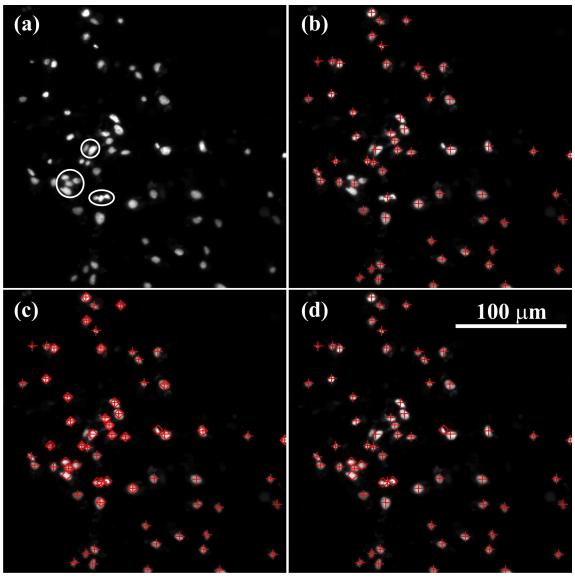

Figure 4: Analysis of PI stained cells. (a) Input image. The circles indicates cell clustered within the image (b) Cells localised using a high threshold value (cross symbol). This step is performed in 0.59 s. (c) Cells localised using a low threshold value (diamond symbol). This process takes 0.58 s. (d) Final amount of cells counted after discarding double counts. The complete image analysis is performed in 1.7 s. Attending at the cluster formed by two cells, it can be observed that one cell within the image has not been localised.

when a steep gradient occurs between adjacent pixel values and can be measured calculating the first derivative of an image [16].

ii Sharpening - Contrast is enhanced between adjacent joining areas with little variation in brightness or darkness. Basically, a high-pass filter is applied to the image.

iii Smoothing - The disparity between pixel values is decreased by averaging nearby pixels [16]. Smoothing consists on the application of a low-pass filter to an image.

iv Noise removal - The application of these filters is done to retain the low frequency information of an image.

2.5 Other application: a cell counter

SeACell is also suitable for other biological applications. Oxidative effects in bystander HepG2 cells were studied by alpha source irradiation at the Biomedical Center (BMC) at Lund University [21]. Cell damage evaluation was checked using the cell probes Hoechst 33342 and Propidium Iodine (PI). Hoechest stain is used to determine the number of living cells within the cell colony and nucleus-staining dye PI is used to count the number of dead cells. The proportion of dead cells is calculated as the ratio between the cells stained with PI and the cells stained with Hoechst.

The program versatility also allows the user the localization of stained cells. Basically, the program is used to count the number of living and dead cells. Therefore, an image of each cell culture using the different stains was taken and analysed.

Stained cells are easily located by SeACell but the intensity of the signal is not homogeneous. Therefore, the image segmentation step has to be applied twice. Then, SeACell compares the localised cells and discards double counts.

Figure 4 shows the procedure to analyse

an image of PI stained cells. Usually, damaged cells are clustered and several clusters have been marked with a circle. As can be seen, only one cluster of cells present an unresolved cell. Therefore, SeACell efficiency is quite high.

3 Summary

A cell validation algorithm has been developed and included into SeACell to investigate cells without using stain or fixation, thus allowing the study of living cells. The implemented program has been shown to fulfil the requirements needed at the LNM-SIHF regarding microprobe software compatibility, automation, recognition time and efficiency. Subcellular compartments can be recognised and localised with an efficiency of 100% using the new cell validation algorithm and no less than 96% for rough cell recognition [1]. The recognition time depends on the image size and the target size parameter. Standard computing times are less than 1.8 s and decreases with smaller target size.

A new procedure was also developed for automated dynamic cell targeting. This procedure can be used as an alternative to the implemented manual selection for non-targeted irradiation experiments, and therefore, providing more automation to the program performance.

The program performance appears independent of the surface where the cells are cultured, the microscope used and the subsequent illumination system. Polypropylene, polystyrene and SU-8 have been regularly used for cell culture at the LNM-SIHF. The program function and efficiency has been shown for images of cells cultured in various surfaces and taken at several facilities.

The software versatility allows other users to localise stained cells and obtain statistical data for specific biological experiments.

SeACell has also been updated with a new user-friendly interface. It includes the application of image enhancement filters and colour display for improvement of the input image.

Future work at the LNM-SIHF requires further development in instrumentation in order to obtain high quality input images for cell recognition, this is, continuous automatic focusing methods are necessary to preserve subcellular resolution [22].

References

[1] N. Arteaga-Marrero, J. Pallon, M.G. Olsson, V. Auzelyte, M. Elfman, P. Kristiansson, K. Malmqvist, C. Nilsson, and M. Wegdén. The new Cell Irradiation Facility at the Lund Nuclear Probe. *Nuclear Instruments and Methods in Physics Research B 260, 91*, 2007.

[2] W.F. Morgan. Non-targeted and delayed effects of exposure to ionizing radiation: radiation- induced genomic instability and bystander effects in Vitro. *Radiation Research 159, 567*, 2003.

[3] S. Wolff. The adaptive response in radiobiology: Evolving insights and implications. *Environmental Health Perspectives 106, 277*, 1998.

[4] S.A. Amundson, K.T. Do, and A.J. Fornace Jr. Induction of stress genes by low doses of gamma rays. *Radiation Research 152, 225*, 1999.

[5] M.M. Vilenchik and A.G. Knudson Jr. Inverse radiation dose-rate effect and germline mutations and DNA damage. *Proceedings of the National Academy of Sciences USA 97(10), 5381*, 2000.

[6] K.M. Prise, O.V. Belyakov, H.C. Newman, S. Patel, G. Schettino, M. Folkard, and B.D. Michael. Non-targeted Effects of Radiation: Bystander Responses in Cell and Tissue Models. *Radiation Protection Dosimetry 99, 223*, 2002.

[7] L. Huang, P.M. Kim, J.A. Nickoloff, and W.F. Morgan. Targeted and Nontargeted Effects of Low-Dose Ionizing Radiation on

Delayed Genomic Instability in Human Cells. *Cancer Research 67, 1099*, 2007.

[8] K.M. Prise, G. Schettino, M. Folkard, and K.D. Held. New insights on cell death from radiation exposure. *The Lancet Oncology 6, 520*, 2005.

[9] J. Cadet, E. Sage, and T. Douki. Ultraviolet radiation-mediated damage to cellular DNA. *Mutation Research 571, 3*, 2005.

[10] G.J. Ross, A.W. Bigelow, G. Randers-Pehrson, C.C. Peng, and D.J. Brenner. Phase-based cell imaging techniques for microbeam irradiation. *Nuclear Instruments and Methods in Physics Research B 241, 387*, 2005.

[11] S.S. Rogers, T.A. Waigh, X. Zhao, and J.R. Lu. Precise particle tracking against a complicated background: polynomial fitting with a Gaussian weight. *Physical Biology 4, 220*, 2007.

[12] O. Veselov, W. Polak, J. Lekki, Z. Stachura, K. Lebed, J. Styczen, and R. Ugenskiene. Automatic system for single ion/single cell irradiation based on Cracow microprobe. *Review of Scientific Instruments 77, 055101*, 2006.

[13] P. R. Barber, G.P. Pierce, S.M. Ameer-Beg, D.R. Matthews, L.M. Carlin, M. Keppler, M. Kelleher, F. Festy, C. Gillett, R. Springall, T.C.Ng, and B. Vojnovic. Towards high-throughput FLIM for protein-protein interaction screening of live cells and tissue microarrays. *5^{th} IEEE International Symposium on Biomedical Imaging: From Nano to Macro, 356*, 2008.

[14] Information available at www.ittvis.com/productservices.

[15] N. Arteaga-Marrero, G. Astromskas, M.G. Olsson, M. Elfman, P. Kristiansson, E.J.C. Nilsson, C. Nilsson, and J. Pallon. Applications of SU-8 in the development of a Single Ion hit Facility. *Nuclear Instruments and Methods in Physics Research B 267, 2117*, 2009.

[16] R.C. Gonzalez and R.E. Woods. *Digital Image Processing.* Prentice-Hall, Inc., 2002.

[17] R.M. Haralick, S.R. Sternberg, and X. Zhuang. Image analysis using mathematical morphology. *IEEE Transactions on Pattern Analysis and Machine Intelligence, Vol. PAMI-9 (4), 532*, 1987.

[18] L.J. Wu, G. Randers-Pehrson, A. Xu, C..A. Waldren, C.R. Geard, Z. Yu, and T.K. Hei. Targeted cytoplasmic irradiation with alpha particles induces mutations in mammalian cells. *Proceedings of the National Academy of Sciences USA 96, 4959*, 1999.

[19] C. Shao, M. Folkard, B.D. Michael, and K.M. Prise. Targeted cytoplasmic irradiation induces bystander responses. *Proceedings of the National Academy of Sciences USA 101, 13495*, 2004.

[20] J.F. Ward. The radiation-induced lesions which trigger the bystander effect. *Mutation Research 499, 151*, 2002.

[21] M.G. Olsson, E.J.C. Nilsson, J. Paczesny, S. Rutardottir, J. Pallon, and B. Åkerström. Bystander cell death and stress response is inhibited by the radical scavenger α_1-microglobulin in irradiated cell cultures. *Submitted to Radiation Research*, 2010.

[22] B. Vojnovic. Application of novel imaging techniques of early clinical trials. *European Journal of Cancer Supplements 5 (9), 19*, 2007.

Oxidative effects studies and updated technical description of the Lund Nuclear Microprobe Single-Ion Hit Facility

N.Arteaga-Marrero[1]*, P. Kristiansson[1], M.G. Olsson[2], S. Rutardóttir[2], C. Nilsson[1], J. Pallon[1] and Bo Åkerström[2]

[1] *Division of Nuclear Physics, Department of Physics, LTH, Lund University, Professorsgatan 1, PO Box 118, SE-221 00 Lund, Sweden*

[2] *Clinical and Experimental Infection Medicine (BMC), Sölvegatan 19, B14, SE-221 84, Lund, Sweden*

Manuscript

Abstract

The Single Ion Hit Facility developed at the Lund Nuclear Microprobe (LNM-SIHF) is fully operational for cell irradiation. As a first application oxidative effects on bystander cells after non-targeted proton irradiation have been studied. The preliminary biological results using the human hepatoma cell line (HepG2) show that protons can initiate the production of Reactive Oxygen Species (ROS), and the subsequent damage to the surrounding bystander cells.

In addition to the biological results, properties and capabilities of the system regarding instrumentation are also described.

1 Introduction

Nowadays, custom-build Single Ion Hit Facilities (SIHFs) have become a very powerful tool for biological applications. The main advantage offered by a SIHF is the high precision of the irradiation procedure which allows targeting subcellular compartments of living cells using a minimum delivered dose of a single ion. Therefore, low-dose radiation effects on living cells can be studied.

Non-targeted irradiation occurs in conditions where all the cells in a particular sample have not been directly irradiated or have not been exposed uniformly to radiation. The common way to achieve non-targeted irradiation consists of irradiating the particles forming a pattern across the cell culture.

Oxidative products formed and released by cells exposed to radiation have the ability to oxidise the intracellularly loaded probe 2´,7´-dichlorodihydrofluorescein diacetate (H_2DCFDA). Consequently, the probe sends out fluorescent light that can be detected by fuorescence microscopy.

The present work describes the biological application of the LNM-SIHF in which non-targeted proton irradiation was used to investigate the importance of reactive oxygen species (ROS) on bystander human hepatoma (HepG2) cells. Also, an update of the instrumental properties of the system are presented.

*Contact information: Tel. +46-46-2227630, Fax. +46-46-2224709, e-mail address: natalia.arteaga@nuclear.lu.se, URL: http://www.pixe.lth.se/cellion/

2 Materials and Methods

2.1 Outline of the microbeam irradiation system

The details of the LNM have already been described [1]. Briefly, the development of the LNM-SIHF has been made at the sub-micron beamline. Ion beams (proton and α particles) are focused in a two stage system with a quadrupole doublet at each stage. Three sets of collimating slits along the beamline are used to shape the beam and to reduce the beam current. The beam-deflection system consists of two parallel metal plates connected to a high voltage, which are used to deflect the beam off the sample on demand. A 200 nm thin Si_3N_4 membrane (1.5 mm x 1.5 mm), purchased at Silson company [2], is used as exit window to extract the beam into air. The beam-scanning system, situated at the irradiation chamber supply beam positioning along the sample in the X and Y direction. Any predefined pattern of pixels (maximum size 4096 x 4096) can be uploaded into the system and subsequently used to irradiate the sample. The LNM-SIHF employs a post-cell detection system which consists of a windowless photodiode detector(Hamamatsu S1223-01N 7139) [3] and, in combination with the beam-deflection system, controls the applied dose.

2.2 Custom-designed dishes

The LNM-SIHF has a horizontal configuration which requires a vertically positioned Petri dish containing the cell culture. The displacement of the cells due to gravity effects can be minimized using monolayer cell cultures which are attached to the surface on which they are cultivated. Additionally, the vertical arrangement requires the removal of the cell culture medium prior to irradiation. However, a layer of cell culture medium remains, the thickness of which is approximately the same as the diameter of the cells.

The custom-designed irradiation dishes developed at the LNM-SIHF have the advantage of being suitable for both cell incubation and holding the cells during irradiation. The cells are thus grown and irradiated on the same surface, which is an important technical advantage.

2.2.1 SU-8 irradiation dishes for targeted irradiation

This Petri-type dish allows the position of cell growth to be controlled to a certain degree by fabricating very small structures on the floor of the dish. The epoxy-based photopolymer SU-8 [4] was employed as a fabrication material in combination with UV lithography as previously described [5]. In order to supply the cell with the necessary culture medium, the SU-8 film is glued onto a polystyrene cup forming an effective area of approximately $\pi/4$ cm^2.

2.2.2 SU-8 irradiation dishes for non-targeted irradiation

These 5 μm thin films were also fabricated with SU-8 and UV large exposure but without any pattern or barriers. The film is glued as well onto a polystyrene cup providing an effective culture area of approximately $\pi/4$ cm^2.

2.2.3 Polypropylene irradiation dishes for non-targeted irradiation

An 8 μm thick polypropylene layer, purchased from Goodfellow (England) [6], was used to culture the cells. This layer is attached by heat treatment to a polypropylene holder offering an effective culture area of $\pi/2$ cm^2.

2.3 Experimental validation of the system: coordinates transfer

The LNM-SIHF uses in-house software, SeACell [7], for on-line cell recognition and localization which allows identification of non-stained cells in a short time with high efficiency. The transference of ion-beam coordinates between SeACell and the LNM-SIHF control software was tested.An on-line image of the living HepG2 cells was acquired prior to irradiation and analysed by SeACell which

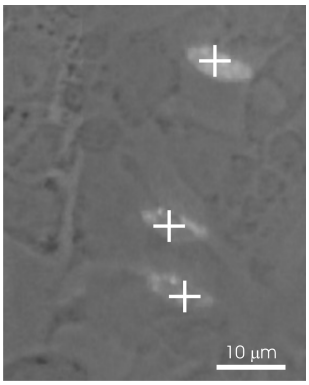

Figure 1: Overlapped images showing the coordinates transfer between SeACell and the LNM-SIHF control software: the input image of living HepG2 cells, the selected SeACell coordinates (cross symbols) and the CR-39 etched film.

searches for cells having a nucleus size within specified limits. The coordinates provided by the software were then used to create an irradiation pattern, which was subsequently uploaded into the beam-scanning system controlling the ion beam position. CR-39 track etch film was irradiated in vacuum, following the defined pattern, using 2.5 MeV protons and an average beam current of 60 pA. The beam-deflection system was employed during the irradiation procedure to guarantee exposure only in the selected pixels. The CR-39 film was than etched for approximately 10 minutes in 12N KOH at 80°C. Therefore, the irradiated pattern was visible in the CR-39 etched film. Figure 1 shows the on-line image of the living cells overlapped with the image of the CR-39 etched film. The crosses indicates the coordinates to be irradiated as determined by SeACell. As can be seen, the crosses indicating the transferred coordinates match with the beam position demonstrating the capability of the system for a reliable coordinates transfer.

3 Preliminary biological results

3.1 Sample preparation

Thin film SU-8 irradiation dishes were used to study the effects of non-targeted irradiation on HepG2 cells. The dish surface does not have any barrier and the cells can therefore interact over the entire surface. Cells in the exponential growth phase were seeded in the irradiation dishes and cultured for approximately 24 hours in 0.5 ml medium until they reached a confluent state. One hour prior to irradiation, the cells were loaded with the redox-sensitive probe H_2DCFDA (3 μM concentration), incubated at 37°C for 30 minutes, washed and resuspended in fresh medium.

3.2 Irradiation procedure

All irradiation was carried out in the absence of medium for the technical reasons discussed above.

The non-targeted irradiation pattern consisted of three spots in a row separated by approximately 2 mm. HepG2 cell cultures were exposed to 2.5 MeV focused protons, including a range of low doses, from 0.1 to 0.5 Gy. Two irradiation dishes were irradiated at each dose and a third one was used as a control sample. The control sample was exposed to the same protocol but no protons were deposited in this sample.

After irradiation, the cells were resuspended in fresh culture medium. The induction of oxidation of the H_2DCFDA probe was analysed using a Nikon Eclipse TE300 in-

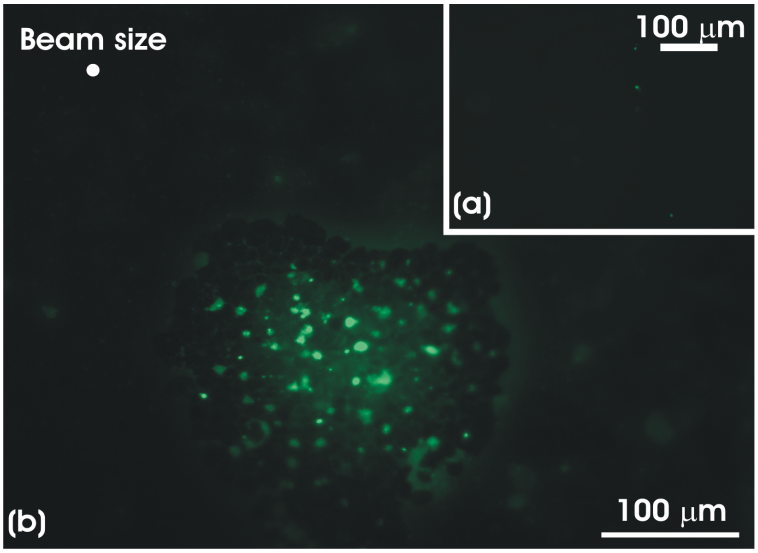

Figure 2: Oxidation levels approximately 3 hours after irradiation. (a) Control sample. (b) Irradiated sample: 0.1 Gy/spot, 3 spots in a row. Note that the scale of the image only allows the observation of a single spot.

verted fluorescence microscope.

3.3 Oxidative effects in bystander cells

Figure 2 shows the control (a) and irradiated sample (b) at the time at which oxidation was detected, i.e., approximately 3 h after irradiation. The control sample shows a few green spots, each corresponding to approximately one cell ($\sim$ 11 μm [8]). Much greater fluorescence was seen in the irradiated cells indicating oxidation. Protons can thus initiate the production of ROS, and subsequent damage to the surrounding bystander cells, as can be observed in Figure 2 (b), where a large amount of bystander cells were damaged due to oxidation. The beam size during these experiments was approximately 10 μm and a beam size reference has been added to this figure. As can be seen, the damaged area in the cell culture was larger than the beam size area and larger than a few cells.

The mechanism underlying the radiation-induced bystander response is controversial. Whether the bystander cells were damaged through nuclear or cytoplasmic irradiation is unknown, although evidence has been reported for both cases [9]. Furthermore, the mutagenicity of cytoplasmic irradiation indicates a dependence of intercellular generation on ROS [10]. One hypothesis considered is that, at low doses and under bystander conditions, repair processes are not fully activated. These cells are thus more sensitive to radiation exposure. Single Strand Breaks (SSBs) or base damage lesions produced by ROS lead to the accumulation of damage that cannot be properly repaired, increasing the probability of Double Strand Breaks (DSBs). A similar hypothesis has been suggested to be behind low-dose hypersensitivity and the inverse dose-rate effect [11]. In addition, it has been proposed that cell culture medium irradiation could cause DNA damage via soluble extra-cellular mediators [10].

Regardless of the mechanism causing the damage, the cells in the culture die a few hours after oxidation. The cell killing mechanism is not fully understood and further experiments are needed. DNA damaging effects of excessive ROS can activate cell cycle checkpoints,

induce a senescence-like state, or cause cells to undergo apoptosis and even necrosis *in vitro* [12].

Until now, the experiments carried out at the LNP-SIHF have not shown any relationship between the bystander response and the applied dose. This is in agreement to the previous results obtained at the GCI, in England, showing that the bystander response is independent of the number of particles traversing the cell [13, 14]. Furthermore, it has also been reported that the bystander response is not correlated with distance. In other words, the cells respond to the bystander signal whatever its distance from the irradiated cells. However, the damaged cells shows a tendency to form clusters [15], as observed in Figure 2 (b).

4 Summary and outlook

The LNM-SIHF fully operational for cell irradiation experiments. Targeted and non-targeted irradiation has been demonstrated using CR-39 track etch film and living HepG2 cells respectively. Future technical improvements of the system requires a fine tunning of the beam-focusing system in order to achieve irradiation of subcellular compartments.

Non-targeted proton irradiation has been performed at the LNM-SIHF showing that the production of ROS can cause damage to the surrounding bystander cells. However, further experiments are required to understand which processes lead to cell dead after irradiation. Data from several replicate experiments did not show cell damage concentrated in one spot, but a high background was observed in all the samples including the control one. This fact indicates the existence of some mechanism, independent of the irradiation procedure, which produces extra oxidation. Additionally, alternative cell-staining probes will be employed to determine the irradiation damage as well as larger cell lines in order to generalize the results.

References

[1] N. Arteaga-Marrero, J. Pallon, M.G. Olsson, V. Auzelyte, M. Elfman, P. Kristiansson, K. Malmqvist, C. Nilsson, and M. Wegdén. The new Cell Irradiation Facility at the Lund Nuclear Probe. *Nuclear Instruments and Methods in Physics Research B 260, 91*, 2007.

[2] Information available at www.silson.com.

[3] M. Elfman, P. Kristiansson, K. Malmqvist, and J. Pallon. The layout and performance of the Lund nuclear microprobe trigger and data acquisition system. *Nuclear Instruments and Methods in Physics Research B 158, 141*, 1999.

[4] Information available at www.microchem.com.

[5] N. Arteaga-Marrero, V. Auzelyte, M.G. Olsson, and J. Pallon. A SU-8 dish for cell irradiation. *Nuclear Instruments and Methods in Physics Research B 263, 523*, 2007.

[6] Information available at www.goodfellow.com.

[7] N. Arteaga-Marrero, M.G. Olsson, P. Kristiansson, and J. Pallon. SeACell: Cell Recognition Software for a Single-Ion Hit Facility. *Submitted to Review of Scientific Instruments*, 2010.

[8] N. Arteaga-Marrero, G. Astromskas, M.G. Olsson, M. Elfman, P. Kristiansson, E.J.C. Nilsson, C. Nilsson, and J. Pallon. Applications of SU-8 in the development of a Single Ion Hit Facility. *Nuclear Instruments and Methods in Physics Research B 267, 2117*, 2009.

[9] C. Shao, M. Folkard, B.D. Michael, and K.M. Prise. Targeted cytoplasmic irradiation induces bystander responses. *Proceedings of the National Academy of Sciences USA 101, 13495*, 2004.

[10] B.E. Lehnert and E.H. Goodwin. Extracellular Factor(s) following Exposure to α particles can cause Sister Chromatid Exchanges in Normal Human Cells. *Cancer Research 57, 2164*, 1997.

[11] K.M. Prise, O.V. Belyakov, H.C. Newman, S. Patel, G. Schettino, M. Folkard, and B.D. Michael. Non-targeted effects of radiation: Bystander responses in cell and tissue model. *Radiation Protection Dosimetry 99, 223*, 2002.

[12] R. Iyer and B.E. Lehnert. Effects of Ionized Radiation in Targeted and Nontargeted Cells. *Archives of Biochemistry and Biophysics 376, 14*, 2000.

[13] K.M. Prise, S. Burdak-Rothkamm, M. Folkard, G. Kashino, C. Shao, and L. Tartier. New insights on radiation-induced bystander signalling and its relationship to DNA repair. *International Congress Series 1299, 121*, 2007.

[14] K.M. Prise, M. Folkard, and B.D. Michael. A review of the Bystander Effect and its implications for low-dose exposure. *Radiation Protection Dosimetry 104, 347*, 2003.

[15] G. Schettino, M. Folkard, K.M. Prise, B. Vojnovic, K.D. Held, and B. D. Michael. Low-Dose Studies of Bystander Cell Killing with Targeted Soft X Rays. *Radiation Research 160, 505*, 2003.